6-9-2016

Quantum Information in Rydberg-Dressed Atoms

Tyler Emerson Keating

Candidate

Department

This dissertation is approved, and it is acceptable in quality and form for publication:

Approved by the Dissertation Committee:

, Chairperson

Quantum Information in Rydberg-Dressed Atoms

by

Tyler Emerson Keating

B.A., Physics, Carleton College, 2009
M.S., Physics, University of New Mexico, 2013

DISSERTATION

Submitted in Partial Fulfillment of the
Requirements for the Degree of

Doctor of Philosophy in Physics

The University of New Mexico

Albuquerque, New Mexico

May, 2016

Dedication

To my family,

Mom, Dad, Sarah, & Mega

Acknowledgments

First and foremost, I would like to thank my advisor, Ivan Deutsch. Beyond his numerous direct contributions to the work in this dissertation, his guidance and mentorship over the last several years have been invaluable. I also want to thank my collaborators at Sandia National Labs, Grant Biedermann and Yuan-Yu Jau, whose experimental perspectives have kept my theoretical musing grounded in reality. Thanks as well to my undergraduate research advisor, Arjendu Pattanayak, for showing me how fun quantum mechanics can be.

Over the course of my research, I have had the good fortune to work with a variety of talented co-authors, each of whom brought a unique background that enriched my own understanding of physics. Thanks to Krittika Goyal, Andrew Landahl, Rob Cook, Aaron Hankin, Charlie Baldwin, Joe Slote, Gopi Muraleedharan, and Zeke Carrasco for their contributions to the research contained herein. I also thank Carlos Riofrío and Hector Soza-Martinez for generous use of their MATLAB code, which formed templates for many a simulation. More broadly, thanks to all the members of CQuIC for maintaining such a friendly and collaborative work environment. Poul Jessen and his group deserve particular recognition in this regard; Ch. 5 of this dissertation relies heavily on their shared expertise.

Beyond the physics community, I would like to thank my parents, Rose and Kim, for igniting my interest in science and then giving me the lifelong support to pursue that passion. Finally, a special thank-you to my wife, Sarah. Over the course of graduate school, she has given me love, patience, excellent cooking, and the Doppler-free scheme at the heart of Ch. 4, without any of which this work would not have been possible.

Quantum Information in Rydberg-Dressed Atoms

by

Tyler Emerson Keating

B.A., Physics, Carleton College, 2009
M.S., Physics, University of New Mexico, 2013
Ph.D., Physics, University of New Mexico, 2016

Abstract

In any physical platform, two ingredients are essential for quantum information processing: single-qubit control, and entangling interactions between qubits. Neutral atoms can be individually controlled with high fidelity and are resilient to environmental noise, making them attractive candidates for implementing quantum information protocols. However, achieving strong interactions remains a major obstacle. One way to increase the interaction strength between neutral atoms is to excite them into high-lying Rydberg states, which exhibit large electric dipole moments (and by extension, strong electric dipole-dipole interactions). By slowly ramping up the Rydberg level coupling in a system, one can "dress" the atomic ground states with some Rydberg character; this maps the Rydberg dipole interaction to an effective interaction between ground states. Such Rydberg-dressed interaction is the focus of this dissertation.

After describing the physics of the Rydberg-dressed interaction, we propose three protocols that demonstrate its versatility and provide a framework for considering some of the details of realistic implementation. In all three cases, Rydberg dressing — along with

some form of single-atom control — is used to generate highly entangled states of interest. Our first proposal relates to the adiabatic model of quantum computing, in which solutions to problems are encoded in the ground states of carefully engineered Hamiltonians. The Rydberg-dressed interaction can provide nonlinear Hamiltonian terms, allowing us to encode NP-hard and other interesting problems. We model this protocol in the presence of decoherence, and find that computational fidelities of ~ 0.98 for four atoms should be possible with currently realistic experimental parameters.

Our second proposal is also related to quantum computing, this time in the circuit model. The Rydberg-dressed interaction can be used to generate a controlled-NOT logic gate which, when interwoven with single-qubit gates, can perform universal quantum computation. Experimentally, noise due to atomic thermal motion has been a primary limitation on the fidelities of these gates. We show that a Doppler-free setup, with counterpropagating lasers, effectively suppresses this type of noise, allowing simulated fidelities of up to ~ 0.998 per gate. Such strong suppression is only possible because the Doppler-free configuration can harness the natural robustness of adiabatic dressing; other gate schemes using, e.g., resonant pulses, do not exhibit the same degree of improvement.

Finally, we consider exploiting the many-body character of the Rydberg-dressed interaction to generate collective entanglement in mesoscopic ensembles of neutral atoms. An atomic ensemble uniformly illuminated by a single Rydberg-exciting laser is isomorphic to the well-known Jaynes-Cummings model. In addition to adapting generic Jaynes-Cummings entanglement protocols developed in other platforms, one can apply microwaves to drive entanglement in a way that is unique to the atomic platform. We prove that by allowing the microwave phase to vary in time, one can generate arbitrary symmetric states of the ensemble. While this method compares favorably with other entanglement protocols in many ways, the required frequency of phase switching presents a fundamental limitation on its effectiveness. To mitigate this, we propose a variant scheme in which parameters are chosen to only allow excitations within the system's dressed-ground sub-

space; this effectively cuts phase switching demands in half. All three protocols serve to illustrate the power of the Rydberg-dressed interaction and suggest directions for future study.

Contents

List of Figures

List of Tables

Chapter 1

Introduction

The essential structure of a quantum computer is relatively straightforward and platform-independent. Arbitrary control of single qubits, along with any one of a wide range of entangling two-qubit operations, is sufficient for universal quantum computation [4]. Especially since multi-qubit unitaries are typically more challenging to implement than their single-qubit counterparts, a primary goal in the development of any quantum computer is to generate entanglement between qubits with high fidelity and scalability. Substantial progress toward this goal has been made with a variety of physical implementations. Atomic ions are currently the most advanced platform in this regard [5]; accomplishments include entanglement between as many as eight ions [6, 7] and over significant spatial distances [8]. However, substantial entanglement has also been achieved in superconductors [9], quantum dots [10, 11], and linear optical systems [12]. In this dissertation, we focus on entanglement generation in neutral atom qubits.

Compared with most other platforms, neutral atoms tend to interact weakly, both with each other and with their environments. While this low interaction strength can be beneficial in terms of minimizing errors from environmental noise, it makes entanglement especially difficult to produce. Multi-atom trapping/addressing [13] and single-atom uni-

taries [14]—both critical ingredients in a scalable computer—can be performed with very high fidelities. On the other hand, while several methods for producing entangling interactions have been attempted, including collisional interactions [15] and coupling via optical cavity modes [16], high-fidelity entanglement is an outstanding challenge.

One promising path to entanglement is through dipole interactions. If two neutral atoms are brought close enough together, the electric dipole-dipole interaction (EDDI) between them can be harnessed to perform quantum computation [17]. While this technique was originally proposed for use with atoms of low principle quantum number n, the EDDI between such atoms is very weak. With such weak interactions, it is infeasible to produce entanglement faster than decoherence effects such as photon scattering destroy it, so the scheme cannot work in a realistic setting. The situation is much more promising, however, if we use Rydberg states: high-lying atomic orbitals (typically $n \gtrsim 20$) with exaggerated physical properties [18]. The most noticeable of these properties is their size: the diameter of a Rydberg atom's valence electron cloud scales as n^2, growing far larger than the distances normally associated with single atoms. Such large electron clouds are highly sensitive to electromagnetic fields, making them useful for fine manipulation of atomic positions [19] and non-demolition photon counting in cavities [20, 21]. When allowed to interact with other, ground-state atoms, they can generate large and exotic bound states such as "trilobite molecules", so-called for the striking shapes of their wavefunctions [22, 23].

When multiple Rydberg atoms are brought together, these same properties boost the effectiveness of the EDDI between them [18]. As noted above, a Rydberg atom's size — and therefore electric dipole moment — scales as n^2; the EDDI depends on the *product* of both atoms' dipole moments, and so scales as n^4. Rydberg electron clouds are also more "malleable" than their low-n counterparts and respond more readily to the presence of nearby atoms; for reasons we discuss in Chap. 2, the EDDI boost from this effect also scales as n^2. As an added benefit, the rate of spontaneous emission from Rydberg levels

drops off as n^{-2}, so even a fixed EDDI will have less decoherence to compete with as n grows. Taken together, these properties suggest that using Rydberg levels can boost the efficacy of EDDI entanglement by as much as n^8. Such a Rydberg-enhanced EDDI is at the heart of two pioneering proposals for neutral atom quantum computing, which lay out schemes for entangling individual trapped atoms [24] and cold atomic ensembles [25].

While we discuss the details of the Rydberg EDDI in Chap. 2, its usefulness can be understood with the qualitative "blockade" picture. Generally, a blockade interaction is an interaction that is used to prevent multiple, simultaneous excitations in a system. Almost any kind of multi-particle interaction can be used to generate a blockade. Notable examples include anti-bunching in electrical currents [26] and sub-poissonian loading of atom traps [27]. In our case, the EDDI can generate a large energy penalty for states with multiple Rydberg atoms, blockading the excitation of such states. If the EDDI energy is much larger than the other energy scales in a system, the blockade becomes essentially perfect, and the effect of the EDDI reduces to a heuristic: "only one atom at a time can be in a Rydberg state." Fig. 1.1 shows an illustrative example of how the Rydberg EDDI blockade has been used to generate entanglement [28]. The strengths and weaknesses of the Rydberg EDDI mesh especially well with those of a blockade. Suppressing Rydberg excitations helps limit sensitivity to stray fields, and a blockade is much more robust to fluctuations in atomic position than a raw EDDI. For this reason, the blockade has been a staple element of Rydberg-based quantum computing protocols since they were first proposed [24, 29].

Beyond the entangling operations that are the focus of this dissertation, multi-atom Rydberg systems exhibit a variety of interesting physics that is well-described by the blockade picture. A blockade can generate non-classical statistics such as antibunching of Rydberg excitations [30]. Clusters of mutually blockaded atoms tend to share collective excitations; this can lead to entanglement over mesoscopic ensembles [29], or quantum logic that is robust against fluctuations in the number of atoms present [31], not to mention the kind of collective state control we explore in Chap. 5. By exploiting the strong coupling be-

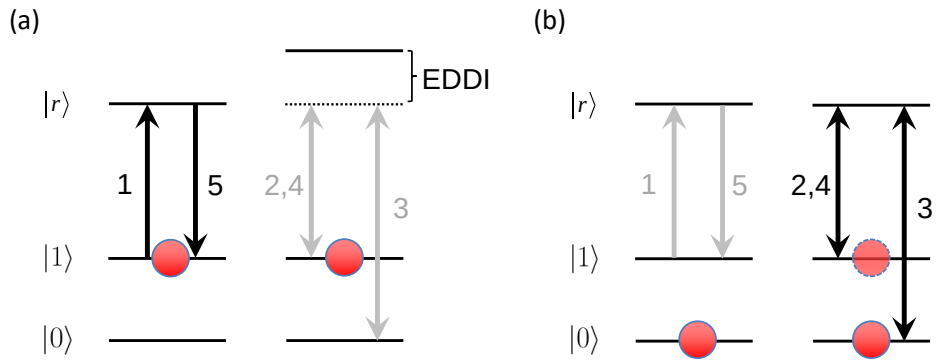

Figure 1.1: Schematic of a method to entangle two atoms via the Rydberg blockade, using a sequence of five resonant π-pulses. Each atom has two ground "logical" states, $|0\rangle$ and $|1\rangle$, and a Rydberg state $|r\rangle$. (a) If the left atom is in the $|1\rangle$ state, pulse 1 excites it to $|r\rangle$. The presence of a Rydberg atom induces an EDDI in the right atom's $|r\rangle$ state, shifting it off resonance and blockading excitation. Pulses 2–4 therefore have no effect, and pulse 5 returns the system to its initial state. (b) If the left atom is in $|0\rangle$, pulses 1 and 5 have no effect. The pulse sequence 2–4 on the right atom now maps $|0\rangle$ to $|1\rangle$, and vice-versa, via the Rydberg state. The right atom's logical state thus changes conditioned on the left atom being in $|0\rangle$; this is a maximally entangling operation.

tween Rydberg atoms and electromagnetic fields, one can expand the toolbox to include electromagnetically tuned interaction strengths [32] and coupling between the Rydberg atoms' electronic and spatial degrees of freedom [33]. The Rydberg atoms can also act as mediators for entanglement in the electromagnetic field itself, leading to a photon-photon blockade [34, 35] and other strongly nonlinear optics [36].

Despite this wide and growing range of higher-level applications, the basic task of entangling Rydberg atoms with high fidelity is an ongoing project. To make quantum computing in neutral atoms a reality, we need to be able to generate high-fidelity entanglement, even in the face of such noise sources as incoherent photon scattering and coupling to noisy environmental fields. Recent experiments have pushed the fidelities of entangling gates into the $\sim 80\%$ range [37, 38, 39], although substantial improvements are still needed to approach thresholds for fault tolerance [40]. In parallel with this, progress has

been made in producing specific entangled states in ensembles [41, 42] and addressing the experimental challenges that will come with scaling up a neutral atom system [43, 44].

To further the goal of strong and precise Rydberg interactions in noisy circumstances, we turn to another versatile technique in neutral atom physics, adiabatic excitation. By slowly changing the parameters of a coupling field from weak- to strong-coupling, it is possible to drive excitations that are robust against a range of noise sources and experimental imperfections [45]. It is natural to consider the application of this technique to Rydberg excitations, and theoretical studies indicate that robust excitations can give rise to similarly robust interactions [46]. The heart of this dissertation is an exploration of the advantages of Rydberg entanglement through adiabatic excitation, as applied in three different protocols.

The remainder of this dissertation is organized as follows. In Chap. 2, we review the details of the interaction between Rydberg atoms, particularly in the context of adiabatic dressing. In Chap. 3, we show how this interaction can be directly applied to solve problems of interest through adiabatic quantum computation. In Chap. 4, we consider the use of Rydberg-dressed interactions in gate model computation, paying special attention to their advantages when realistic noise is considered. In Chap. 5, we combine Rydberg-dressed interactions with techniques from quantum control to produce a more general class of entangled states in neutral atom ensembles. Finally, in Chap. 6, we offer some concluding remarks and directions for future study. The published works associated with this dissertation are given in Table 1.1.

Chapter	Publication
3	T. Keating, K. Goyal, Y.-Y. Jau, G. W. Biedermann, A. J. Landahl, and I. H. Deutsch. *Adiabatic quantum computation with Rydberg-dressed atoms*, Phys. Rev. A **87**, 052314 (2013).
4	T. Keating, R. L. Cook, A. Hankin, Y.-Y. Jau, G. W. Biedermann, and I. H. Deutsch. *Robust quantum logic in neutral atoms via adiabatic Rydberg dressing*, Phys. Rev. A **91**, 012337 (2015).
5	T. Keating, C. H. Baldwin, Y.-Y. Jau, G. W. Biedermann, and I. H. Deutsch. *Arbitrary Dicke-state control of symmetric Rydberg ensembles*, in preparation. Y.-Y. Jau, A. M. Hankin, T. Keating, I. H. Deutsch, and G. W. Biedermann. *Entangling atomic spins with a Rydberg-dressed spin-flip blockade*, Nature Physics **12**, 71–74 (2016).
B	T. Keating, J. Slote, G. Muraleedharan, E. Carrasco, and I. H. Deutsch. *On the Scalability of Boson Sampling with Noise*, in preparation.

Table 1.1: List of publications and associated chapters. Appendix B contains some preliminary results regarding the role of noise in the Boson Sampling problem; this work is unrelated to the Rydberg-dressed interaction, but was done in parallel with the research for this dissertation.

Chapter 2

The Rydberg Dipole-Blockade Interaction

The unique physics of Rydberg atoms come from a range of exaggerated physical properties, which have been explored in detail in a number of works including [18] and [47]. Most of these properties stem from their remarkably large sizes; the diameter of an excited electron's orbital scales with its principal quantum number as n^2, and can be on the order of microns for sufficiently large n [18]. By exciting valence electrons into states so far-removed from their atomic cores, we can induce significant electric dipole moments in the atom, allowing for strong electrostatic interactions at longer ranges than are normally associated with neutral atoms. In this chapter, we outline the nature of the electric dipole-dipole interaction (EDDI) in Rydberg atoms and describe how this interaction can be used to produce entanglement. In particular, we focus on using the EDDI to generate a "dipole-blockade" interaction, in which the excitation of one Rydberg atom prevents subsequent excitations of nearby atoms. The dipole-blockade interaction holds several advantages over the raw EDDI, and will play a central role in the protocols discussed in subsequent chapters.

2.1 Rydberg Wavefunctions

The same large sizes that give Rydberg atoms their interesting properties make their orbitals comparatively easy to analyze. Following [18], we begin with the Schrödinger equation for the valence electron of an alkali atom, in atomic units,

$$\left(-\frac{\nabla^2}{2}+V(r)\right)\Psi = E\Psi, \tag{2.1}$$

where V is an element-dependent potential energy function, r is the electron's distance from the center of the atom, and E is its energy. For hydrogen, $V(r) = -\frac{1}{r}$ in atomic units. For other alkali species, core penetration effects modify the potential inside the radius of the atomic core r_0, and in general $V(r \leq r_0) < -\frac{1}{r}$. Outside this radius, the core looks – to good approximation – like a positive point charge, and $V(r > r_0) = -\frac{1}{r}$. In either case, the equation is separable into radial and angular components, leaving the partial solution

$$\Psi_{n\ell m}(r,\theta,\phi) = \frac{\rho_{n\ell}(r)}{r} Y_{\ell m}(\theta,\phi), \tag{2.2}$$

$$\frac{\partial^2 \rho_{n\ell}}{\partial r^2} + \left(2E - 2V(r) - \frac{\ell(\ell+1)}{r^2}\right)\rho_{n\ell} = 0, \tag{2.3}$$

where $Y_{\ell m}$ are the (species-independent) spherical harmonics and $\rho_{n\ell}$ are the radial wavefunctions.

This equation admits a simple, exact solution only for hydrogen. However, since the vast majority of a Rydberg atom's wavefunction lies far from the atomic core, we can restrict ourselves to finding a solution for $r > r_0$, where the Hamiltonian is hydrogenic. For such a solution, the extra potential depth inside the core will shift the energy and phase of the overall wavefunction, but leave it otherwise unchanged. The phase shift τ and energy are given by

$$\tau = \int_0^{r_0} \sqrt{2}\left(\sqrt{E+V(r)} - \sqrt{E_H + V_H(r)}\right) dr, \tag{2.4}$$

$$E = -\frac{1}{2(n-\delta_\ell)^2}, \tag{2.5}$$

ℓ	Li	Na	K	Rb	Cs
s	0.40	1.35	2.19	3.13	4.06
p	0.04	0.85	1.71	2.66	3.59
d	0.00	0.01	0.25	1.34	2.46

Table 2.1: Quantum defects for low-ℓ Rydberg states of Alkali atoms, from [3]. At higher ℓ, so little of the valence electron's wavefunction penetrates the core that quantum defects become negligible.

where a subscript H denotes the solution for hydrogen and δ_ℓ is the "quantum defect", an effective reduction in principal quantum number that captures the reduced energy inside the core. Inside this region, an electron will have far more kinetic than binding energy, so δ_ℓ depends strongly on atomic species and ℓ but only weakly on n. Specifically, δ_ℓ is n-independent up to a correction term that scales with the binding energy, $\sim n^{-2}$ [48]. For high-n Rydberg states, this correction can be ignored entirely, leaving the empirical values shown in Table 2.1. These values allow us to easily map out the Rydberg spectrum, which will prove essential to calculating the strength of the EDDI below.

2.2 Electric Dipole-Dipole Interactions

Because the separation between a Rydberg atom's valence electron and its core is so large compared to the core itself, such an atom's electric character is dominated by its dipole moment. The electric dipole moment of a single Rydberg atom given by $-e\mathbf{x}$, where e is the electron charge and $\mathbf{x}$ is the vector displacement of the electron from the core. The dipole moments of two nearby (but non-overlapping) Rydberg atoms will produce an EDDI, shifting the system's energy by

$$V_{DD} = \frac{e^2}{R^3}(\mathbf{x}^{(1)} \cdot \mathbf{x}^{(2)} - 3x_1^{(1)}x_1^{(2)}), \tag{2.6}$$

where R is the distance between atoms, x_1 is the component of $\mathbf{x}$ along the interatomic axis, and superscript (i) indicates an operator on the i^{th} atom. The valence electron contributes only a tiny fraction of an atom's total mass, so we can apply the "frozen atom" approximation and treat R as a fixed, classical parameter. In this approximation, V_{DD} acts on the atoms' electron degrees of freedom to produce an effective dipole potential as a function of interatomc distance. The total, two-atom Hamiltonian (ignoring fine- and hyperfine-structure) is then

$$H = \sum_{n,\ell,m} E_{n\ell m}(|n\ell m\rangle \langle n\ell m|^{(1)} + |n\ell m\rangle \langle n\ell m|^{(2)}) + V_{DD}, \tag{2.7}$$

where $E_{n\ell m}$ is the energy given in Eq. (2.5).

Note that the position operators $\mathbf{x}$, and thus V_{DD} itself, have odd parity. The eigenstates of the single-atom Hamiltonian, by contrast, are eigenstates of parity due to spherical symmetry, so the expected value of V_{DD} is zero for all its eigenstates; that is, V_{DD} has zero diagonal matrix elements in the $|n\ell m\rangle^{(1)} \otimes |n\ell m\rangle^{(2)}$ basis. Instead, V_{DD} couples pairs of atomic eigenstates to other, nearby eigenstates with $\ell' = \ell \pm 1$. Typically, we are concerned with how this coupling modifies the single-atom eigenstates, especially how the interaction shifts their energies. To characterize this effect, we first consider the total Hamiltonian projected onto the subspace consisting of some arbitrary state of interest $|\Psi\rangle$ and one other state $|\Psi'\rangle$ that couples to $|\Psi\rangle$ to first order in the interaction. For concreteness, we consider a high-lying s-orbital with principle quantum number $n = 100$, and two nearby p-orbitals to which it is coupled by the dipole-dipole interaction,

$$\begin{aligned}
&|\Psi\rangle \equiv |100, s, 0\rangle^{(1)} \otimes |100, s, 0\rangle^{(2)}, \\
&|\Psi'\rangle \equiv \frac{1}{\sqrt{2}} \left(|99, p, -1\rangle^{(1)} \otimes |101, p, 1\rangle^{(2)} + |101, p, 1\rangle^{(1)} \otimes |99, p, -1\rangle^{(2)} \right), \\
&H \to 2E_{100s} |\Psi\rangle \langle\Psi| + (E_{99p} + E_{101p}) |\Psi'\rangle \langle\Psi'| + \left(\frac{c_3}{R^3} |\Psi'\rangle \langle\Psi| + h.c \right),
\end{aligned} \tag{2.8}$$

where $c_3 \equiv R^3 \langle\Psi'| V_{DD} |\Psi\rangle$ is the EDDI coupling strength between Ψ and Ψ'. This sub-

Hamiltonian can be diagonalized analytically; its two-atom eigenvalues are shifted to

$$E_\Psi, E_{\Psi'} \to \frac{2E_{100s} + E_{99p} + E_{101p}}{2} \pm \frac{1}{2}\sqrt{\delta^2 + \frac{c_3^2}{R^6}}, \qquad (2.9)$$
$$\delta = 2E_{100s} - E_{99p} - E_{101p},$$

where δ, sometimes referred to as the "Förster defect", is the base energy difference between Ψ and Ψ'. If the EDDI is small compared to the energy difference between the states, $c_3/R^3 \ll \delta$, the states are only weakly mixed and the energy shift takes the form of a van der Waals interaction, scaling as $\delta^{-2}R^{-6}$ [49]. In the opposite limit of $c_3/R^3 \gg \delta$, the levels are mixed more strongly and the shift takes the form of a resonant dipole-dipole interaction, scaling as R^{-3}. This is illustrated in Fig. 2.1. If a state is especially close in energy to its coupled state, such resonance can make the energy shift both stronger and longer-range than would otherwise be expected.

In the complete Hamiltonian of Eq. (2.7), each state $|\Psi\rangle$ is coupled not just to a single $|\Psi'\rangle$, but to every other state with $\ell' = \ell \pm 1$. The resulting energy shift can be calculated similarly to the simpler Eq. (2.9), except that instead of diagonalizing a 2×2 Hamiltonian, one must diagonalize a larger Hamiltonian containing a range of levels that contribute significantly to the shift. As in Eq. (2.9), each state asymptotes to an unshifted state at large R and becomes increasingly shifted as R shrinks. When the EDDI strength is small compared to the base splitting between levels ($R \gtrsim 10\,\mu$m for typical Rydberg atoms), most couplings are well within the van der Waals regime. Since the van der Waals shift scales as δ^{-2}, the total energy shift is dominated by a few states with energies very close to the state in question. In this case, one only needs to diagonalize H within a small subspace to closely approximate the energy shift. As R decreases and the EDDI grows stronger, more couplings are brought into the resonant dipole-dipole regime, and so more states must be included to accurately calculate the total shift. If enough states are brought into resonance in this way, finding the spectrum can become computationally infeasible. When the EDDI becomes large compared to the energy separation between adjacent n ($R \lesssim$ a few μm for typical Rydberg atoms), perturbation theory breaks down. The very idea of calculating an

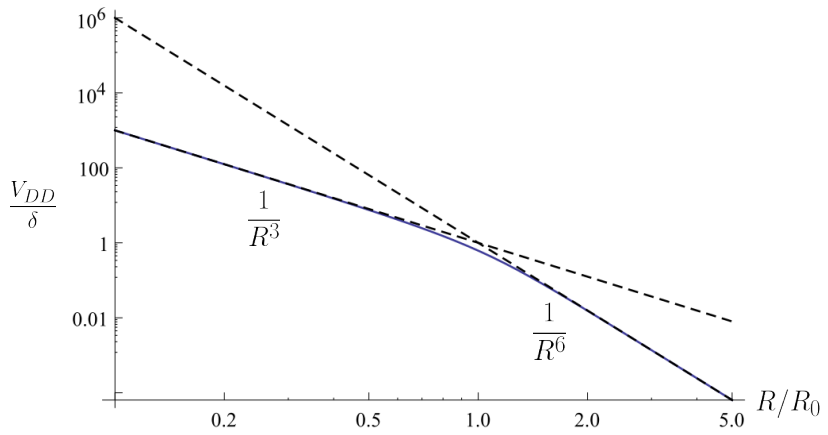

Figure 2.1: Log-log plot of interaction energy V_{DD} as a function of interatomic distance R, for the simplified two-level model. R is given in units of a characteristic distance, $R_0 \equiv (c_3/\delta)^{1/3}$. V_{DD} behaves as an R^{-3} dipole-dipole interaction below R_0, and as an R^{-6} van der Waals interaction above R_0. Dotted lines show pure dipole-dipole and van der Waals scaling, for comparison.

"energy shift" stops being useful, as $\{n, \ell, m\}$ are no longer good quantum numbers; the collective states are more molecular than atomic in character [50].

In addition to shifting the energies of Rydberg states, the EDDI also affects coupling between states. When a ground state $|g\rangle$ is coupled via laser to a Rydberg state $|\Psi\rangle$, the coupling strength depends on two things: the power of the laser, and a dimensionless "oscillator strength" $f_{\Psi,g}$, which is related to the geometries of the states in question. As the EDDI combines bare atomic states into dressed states, it similarly combines their oscillator strengths,

$$f_{\Psi',g} = \sum_{\Psi} \langle \Psi | \Psi' \rangle f_{\psi,g}. \tag{2.10}$$

If a given Rydberg state has especially high oscillator strength, the EDDI will tend to weaken it by diluting the dressed state with other, more weakly coupled levels. Conversely,

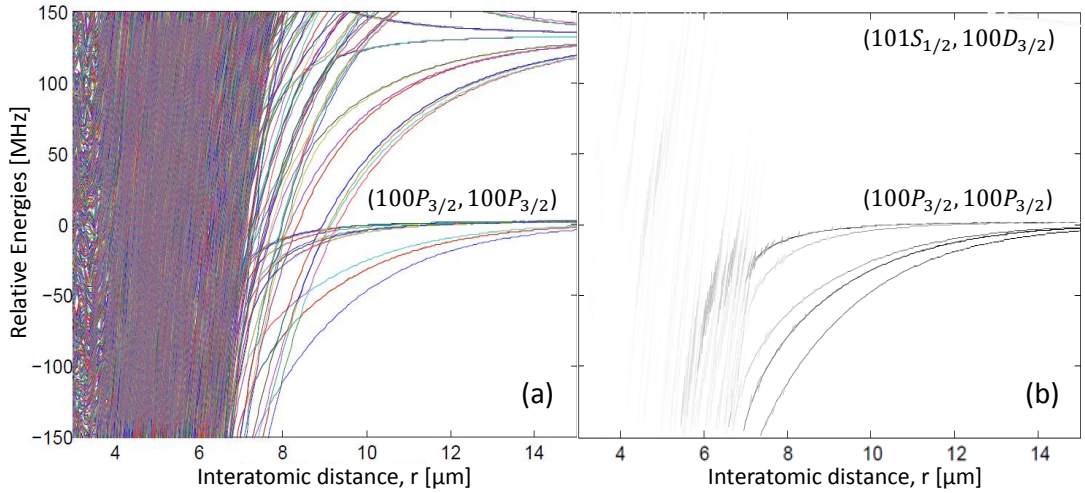

Figure 2.2: Section of the EDDI-shifted Rydberg spectrum for two ^{133}Cs atoms [1]. (a) Doubly excited levels as a function of distance between atoms that asymptote near the atomic pair $|100P_{3/2}, 100P_{3/2}\rangle$. As R decreases, the EDDI grows from a perturbative shift to the dominant term in the Hamiltonian. (b) Weighting of the levels in (a) by their oscillator strengths to couple to the two-atom ground state. In the very strongly coupled regime of $R < 7$ μm, coupling to the ground state is spread out among many shifted states.

states with low or no oscillator strength become more strongly coupled as they are mixed with higher-strength states. Between these two effects, the EDDI tends to "spread out" the available coupling strength, broadening the range of levels with significant coupling to the ground state. In practice, the essential physics can often be captured by considering only a single Rydberg level at a time, but multiple couplings must be taken into account when the precise interaction strength is important. Both the EDDI-induced energy shift and its effect on coupling strengths can be seen in Fig. 2.2, which shows the spectrum of a few shifted states calculated by Yuan-Yu Jau [1].

2.3 The Dipole Blockade

The EDDI is a two-body effect and so can be used to produce entanglement directly, but a few of its properties make it unwieldy for this purpose. For one, the EDDI only acts on states with two (or more) Rydberg atoms, so a strong EDDI goes hand in hand with a high Rydberg population. The same properties that give Rydberg atoms their strong interactions make them highly sensitive to external electromagnetic fields, so demanding a high Rydberg population makes a system more susceptible to environmental noise. For another, the effective EDDI potential scales as R^{-k} (where k varies between 3 and 6), so its gradient scales even more strongly with R, as $R^{-(k+1)}$. For small R, where the EDDI is at its strongest, its gradient is also large, and the interaction strength varies sharply with position. Not only does this magnify the impact of any experimental imprecision in the atoms' locations, it results in an interatomic force that can produce unwanted entanglement between the atoms' positional and electronic degrees of freedom.

To avoid these effects, we would prefer a protocol that can harness the entangling power of the EDDI without actually exciting multiple Rydberg atoms simultaneously. This suggests a blockade-type interaction, in which we generate entanglement by *suppressing* double-excitation rather than driving it. In Chapter 1 and Fig. 1.1, we briefly described a way to accomplish this using sequential pulses. We now outline a method that relies on adiabatic dressing and is more directly applicable to the protocols in later chapters. Consider the arrangement shown in Fig. 2.3. One of two ground states of a neutral alkali atom, denoted as the "logical states" $|0\rangle$ and $|1\rangle$, is coupled to a high-lying Rydberg state $|r\rangle$ by a laser with Rabi frequency Ω_r and detuning Δ_r. (For concreteness, we show a cesium atom with logical states encoded by the hyperfine "clock states", $|1\rangle = |6S_{1/2}, F = 4, m_F = 0\rangle$, $|0\rangle = |6S_{1/2}, F = 3, m_F = 0\rangle$, and coupled to a $100P$ Rydberg state.) In a frame rotating at the laser frequency and in units where $\hbar = 1$, the Hamil-

tonian describing one such atom is

$$H^{(i)} = -\Delta_r \left|r\right\rangle \left\langle r\right|^{(i)} + \frac{\Omega_r}{2}\left(\left|r\right\rangle \left\langle 1\right|^{(i)} + \left|1\right\rangle \left\langle r\right|^{(i)}\right) - E_{HF}\left|0\right\rangle \left\langle 0\right|^{(i)}, \tag{2.11}$$

where E_{HF} is the hyperfine splitting energy between $|0\rangle$ and $|1\rangle$ and we have set $|1\rangle$ to zero energy to simplify subsequent expressions. For two such atoms, the total Hamiltonian consists of two copies of $H^{(i)}$ plus the EDDI:

$$H = H^{(1)} + H^{(2)} + V_{DD}\left|rr\right\rangle \left\langle rr\right|. \tag{2.12}$$

By treating V_{DD} as a scalar, we are making the approximation from section 2.2 that the EDDI gives two Rydberg atoms an effective R-dependent potential. Since both atoms need to be in $|1\rangle$ for the system to be coupled to $|rr\rangle$, the states $|00\rangle$, $|01\rangle$, and $|10\rangle$ are unaffected by the EDDI and behave only according to their single-body dynamics. To understand the blockade, then, we can project the Hamiltonian onto the subspace where both atoms are in $|1\rangle$ or $|r\rangle$,

$$H \to -\Delta_r\left(\left|1r\right\rangle \left\langle 1r\right| + \left|r1\right\rangle \left\langle r1\right| + 2\left|rr\right\rangle \left\langle rr\right|\right) + \frac{\Omega_r}{2}\left(\left(\left|1r\right\rangle + \left|r1\right\rangle\right)\left\langle 11\right| + h.c.\right) + V_{DD}\left|rr\right\rangle \left\langle rr\right|. \tag{2.13}$$

Because of this Hamiltonian's symmetry, it can be simplified by rewriting it in a two-atom basis, with the single-Rydberg states expressed in terms of a symmetric "bright" state $|B\rangle$ and an antisymmmetric "dark" state $|D\rangle$,

$$\begin{aligned} &\left|B\right\rangle \equiv \frac{\left|1r\right\rangle + \left|r1\right\rangle}{\sqrt{2}}, \quad \left|D\right\rangle \equiv \frac{\left|1r\right\rangle - \left|r1\right\rangle}{\sqrt{2}}, \\ &H = -\Delta_r(\left|B\right\rangle \left\langle B\right| + \left|D\right\rangle \left\langle D\right|) - (\Delta_r - V_{DD})\left|rr\right\rangle \left\langle rr\right| + \frac{\sqrt{2}\Omega}{2}(\left|B\right\rangle \left\langle 11\right| + \left|rr\right\rangle \left\langle B\right| + h.c.). \end{aligned} \tag{2.14}$$

The $|11\rangle$ state is coupled to the bright state, and from there to the double-Rydberg state, with a Rabi rate enhanced by a factor of $\sqrt{2}$ over the original Ω_r. The EDDI changes the detuning of the $|B\rangle \leftrightarrow |rr\rangle$ transition to $\Delta_r - V_{DD}$ while leaving the detuning of $|11\rangle \leftrightarrow$

$|B\rangle$ at Δ_r. The dark state is uncoupled from all other states and so can be ignored when considering the ideal case, but it will become important when analyzing errors below.

If $V_{DD} \gg \Delta_r$, the $|11\rangle \leftrightarrow |B\rangle$ transition can be much closer to resonance than the $|B\rangle \leftrightarrow |rr\rangle$ transition, especially if Δ_r is chosen to have the same sign as V_{DD}. This allows strong excitation of a single Rydberg atom while suppressing excitation of the second atom; Rydberg excitations beyond the first are blockaded. In the perfect blockade limit where $V_{DD} \to \infty$, $|rr\rangle$ drops out entirely and the collective Hamiltonian is reduced to two-level coupling between $|11\rangle$ and $|B\rangle$. Like the EDDI that gave rise to it, this Hamiltonian can produce entanglement. Most straightforwardly, a π-pulse turns the separable $|11\rangle$ into the maximally entangled $|B\rangle$. But unlike the raw EDDI, it functions without driving multiple, simultaneous Rydberg excitations, and so avoids many of the disadvantages listed above. In particular, when V_{DD} is large enough that the blockade is essentially perfect,

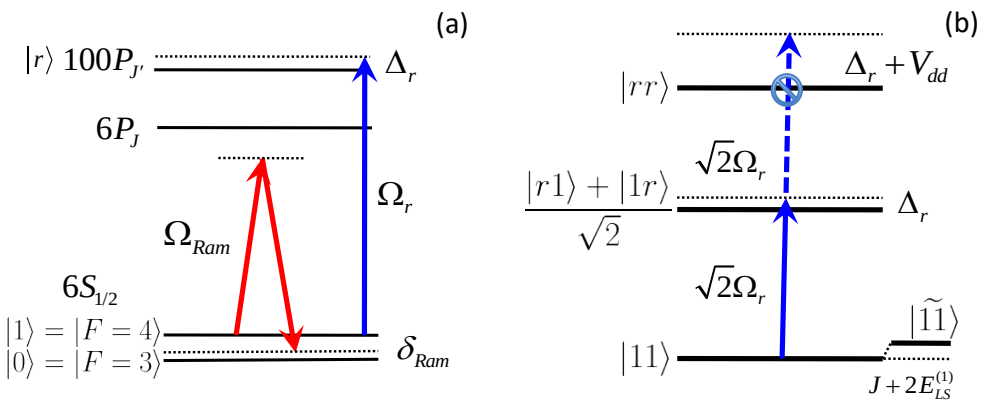

Figure 2.3: (a) Schematic of relevant energy levels and laser couplings in cesium atoms: Qubits are encoded in the hyperfine clock states, controlled by two-photon Raman lasers. Interactions between qubits are mediated by off-resonant excitation near a highly excited Rydberg state $|100P_{J'}\rangle$, tuned to dress either $|0\rangle$ or $|1\rangle$. (b) Dressed Rydberg interaction for two atoms: The logical state $|x_1x_2\rangle$, $x \in \{0,1\}$, is dressed by the bright state, with one atom in the Rydberg level; the doubly excited state is blockaded. The result is a two-atom light shift with an entangling component κ.

the blockade interaction becomes independent of its exact value. Thus, at small R where the EDDI is at its strongest, the blockade interaction is robust to fluctuations in the atoms' positions.

The dipole blockade is also easily generalized to systems of more than two atoms. In a system of N atoms, all within a blockade radius of one another, any one Rydberg atom will blockade the excitations of all other atoms. The blockade becomes a many-body effect, in which the laser drives a single, collective Rydberg excitation throughout the ensemble. The singly-excited bright state for N atoms is a so-called W-state:

$$|B_N\rangle = \frac{1}{\sqrt{N}} \sum_{i=1}^{N} |1\rangle^{(1)} \otimes |1\rangle^{(2)} \otimes \ldots |r\rangle^{(i)} \otimes \ldots |1\rangle^{(N)}. \tag{2.15}$$

The ground state $|1\rangle^{\otimes N}$ is coupled to $|B_N\rangle$ by N copies of $H^{(i)}$, each acting on a different atom. A given $H^{(i)}$ couples the ground state to the i^{th} term of the sum in $|B_N\rangle$ with Rabi rate Ω_r; including the normalization factor, this means $\langle B_N| H^{(i)} |1\rangle^{\otimes N} = \Omega_r/(2\sqrt{N})$. Multiplying this by the N copies of $H^{(i)}$ gives

$$\langle B_N| \sum_{i=1}^{N} H^{(i)} |1\rangle^{\otimes N} = \frac{\sqrt{N}}{2} \Omega_r, \tag{2.16}$$

i.e. the N-body Rabi rate is enhanced by a "superradiant" factor of $\sqrt{N}$. In some sense, the entire ensemble becomes a single, two-level qubit with N-dependent laser coupling. This makes blockaded atoms a natural platform for exploring symmetric many-body dynamics, e.g. in Bose-Einstein condensates [51]. We discuss such dynamics further in Chap. 5.

As a final aside, Eq. (2.13) also exhibits interesting properties when $\Delta_r \approx V_{DD}/2$. Under these conditions, the blockade is replaced by an "anti-blockade": single Rydberg excitation is far off resonance, but double excitation becomes a near-resonant, two-photon process. This regime also exhibits entangling dynamics, as $|B\rangle$ is not strongly excited and Rydberg states tend to be created in pairs. All the protocols here avoid this regime because it is subject to the same drawbacks of double-Rydberg population as the raw EDDI, and because many-body resonances make analysis considerably more complicated beyond two

atoms if the second excitation is not strongly suppressed [52]. However, the anti-blockade has been used to generate neutral atom entanglement in, e.g., [53].

2.4 Blockade Dressing

Even though the Rydberg blockade involves excited states beyond the ground subspace, our final goal is to produce ground-state entanglement. Some Rydberg population will necessarily be excited over the course of any entangling protocol, but we are ultimately interested in Rydberg dynamics only insofar as they lead to effective interactions in the ground manifold. Motivated by this, we now treat the dipole blockade as a ground state dressing interaction, similarly to our treatment of the Rydberg-dressing EDDI above. This leads us to a picture in which the effect of Rydberg excitation is reduced to an interaction between dressed ground states.

2.4.1 Ideally Blockaded Dressing Interactions

We begin by returning to the Hamiltonian for a single, Rydberg-coupled atom. In Eq. (2.11), this Hamiltonian is expressed in terms of the bare states, i.e. the eigenstates of the atomic Hamiltonian without interaction with a laser field. In this basis, the laser couples bare states together. We can also diagonalize the Hamiltonian exactly, taking us to a basis in which the bare ground states are dressed by some admixture of Rydberg character, and vice-versa. In this basis, the states are not coupled but have energies dependent on the laser parameters,

$$H^{(i)} = -\frac{\Delta_r}{2}\mathbf{1} - \frac{\mathrm{sign}(\Delta_r)}{2}\sqrt{\Delta_r^2+\Omega_r^2}\left(|\tilde{r}\rangle\langle\tilde{r}|^{(i)} - |\tilde{1}\rangle\langle\tilde{1}|^{(i)}\right) - (E_{HF} - \frac{\Delta_r}{2})\,|0\rangle\langle 0|^{(i)}, \quad (2.17)$$

where $\mathbf{1}$ denotes the identity and tildes denote the dressed states that connect to their corresponding bare states when the laser coupling is adiabatically returned to zero with red

detuning. The dressed states are superpositions of the original states with their coupled counterparts, according to a mixing angle θ_m that depends on the coupling strength:

$$\theta_m = -\arctan\left(\frac{\Omega_r}{\Delta_r}\right) \tag{2.18}$$

$$|\tilde{1}\rangle = \cos\left(\frac{\theta_m}{2}\right)|1\rangle + \sin\left(\frac{\theta_m}{2}\right)|r\rangle \tag{2.19}$$

$$|\tilde{r}\rangle = \sin\left(\frac{\theta_m}{2}\right)|1\rangle - \cos\left(\frac{\theta_m}{2}\right)|r\rangle\,. \tag{2.20}$$

If the laser coupling is weak, $\Omega_r \ll \Delta_r$, each state is dressed by a small admixture of the other, and the system is well-described by a laser-driven "light shift" (ΔE_{LS1}) of the bare states' energies. Taking the lowest-order expansion of Eq. (2.17) in $\frac{\Omega_r}{\Delta_r}$ gives the well-known weak dressing light shift, $E_{LS1} \approx \pm\frac{\Omega_r^2}{4\Delta_r}$. For strong laser coupling, each dressed state has substantial population in both bare states, and so can no longer be considered as a shifted bare state. Regardless, the essential physics is the same in both regimes, so we will use the terms "dressed ground" and "dressed Rydberg" states to refer to any eigenstates of the coupled Hamiltonian, regardless of coupling strength.

A single atom in $|1\rangle$ is dressed according to Eq. (2.17), and we take the laser detuning to be small compared to the ground state hyperfine splitting so that atoms in $|0\rangle$ are not dressed at all. Therefore, two-atom states with at most one atom in the $|1\rangle$ state behave simply: $|00\rangle$ exhibits no light shift, while $|01\rangle$ and $|10\rangle$ are shifted by E_{LS1} as defined above. Absent the EDDI, $|11\rangle$ would experience two independent light shifts, for a total of $2E_{LS1}$. The presence of the Rydberg blockade, however, modifies the dressing interaction, leading to a two-body light shift $E_{LS2} \neq 2E_{LS1}$. The magnitude of this new shift can be easily seen from Eq. (2.14), at least in the perfect blockade limit. If $|rr\rangle$ is completely blockaded, then $|11\rangle$ and $|B\rangle$ form a two-level system analagous to $|1\rangle$ and $|r\rangle$ in the single-atom case. The only difference is that Ω_R has been enhanced by a factor of $\sqrt{2}$ for two atoms, so Ω_r^2 is replaced by $2\Omega_r^2$ in the dressed energy formula. Knowing this, we can

write the dressed ground Hamiltonian,

$$E_{LSn} = -\frac{1}{2}\left(\Delta_r - \text{sign}(\Delta_r)\sqrt{\Delta_r^2 + n\Omega_r^2}\right) \tag{2.21}$$

$$\hat{P}_{\tilde{g}} H \hat{P}_{\tilde{g}} = -2E_{HF}\,|00\rangle\langle 00| + (E_{LS1} - E_{HF})(|\widetilde{01}\rangle\langle\widetilde{01}| + |\widetilde{10}\rangle\langle\widetilde{10}|) + E_{LS2}\,|\widetilde{11}\rangle\langle\widetilde{11}| \tag{2.22}$$

where $\hat{P}_{\tilde{g}}$ is the projector onto the dressed ground subspace. To distill the interacting element of this Hamiltonian, we can separate out the single-atom Hamiltonians $H^{(i)}$, giving

$$\hat{P}_{\tilde{g}} H^{(i)} \hat{P}_{\tilde{g}} = -E_{HF}\,|0\rangle\langle 0|^{(i)} + E_{LS1}\,|\widetilde{1}\rangle\langle\widetilde{1}|^{(i)} \tag{2.23}$$

$$\hat{P}_{\tilde{g}} H \hat{P}_{\tilde{g}} = \hat{P}_{\tilde{g}}\left(H^{(1)} + H^{(2)}\right)\hat{P}_{\tilde{g}} + \kappa|\widetilde{11}\rangle\langle\widetilde{11}|, \quad \kappa \equiv (E_{LS2} - 2E_{LS1})\,. \tag{2.24}$$

The *differential light shift*, κ,[1] describes the two-body component of H that is nonseparable, and thus encapsulates the interaction's entangling power between the dressed ground states [46]. The $H^{(i)}$ do not affect the system's entanglement and so can be largely ignored for our purposes. More formally, any action by $H^{(i)}$ can be reversed through an appropriate single-body operation on the i^{th} atom, during or after the entangling process. Experimentally, this could be accomplished via a single-atom light shift. What remains is a simple yet powerful picture: the blockade-dressed interaction shifts the energy of $|\widetilde{11}\rangle$ by κ compared to all other dressed ground states. According to the Schrödinger equation, a state's energy determines the rate at which it accumulates phase. Heuristically, the *two-body* energy of $|\widetilde{11}\rangle$ determines the rate at which it accumulates an *entangling* phase. Based on this intuition, we might guess that a full "rotation" from separable to entangled states requires an entangling phase of π, so the Blockade-dressed interaction should be able to produce maximal entanglement in time π/κ. Indeed, this speed limit plays a central role in all the protocols described below.

In general, the value of κ for given laser parameters does not simplify beyond the difference between two square root factors. Two particularly illustrative limits, though,

[1] The differential light shift is often denoted J in the literature [54] but we reserve J to denote collective spin in Chap. 5.

deserve special mention. For weak dressing, κ can be Taylor expanded to lowest order in $\frac{\Omega_r}{\Delta_r}$. As noted above, the single-atom light shift scales as Ω_r^2 for weak dressing, but the quadratic term for two atoms is exactly twice that for a single atom, and they cancel out in κ. Instead, we must expand to the next order to find a nonvanishing term, giving $\kappa \approx \pm\frac{\Omega_r^4}{8\Delta_r^3}$. For weak dressing, then, the entangling interaction is much weaker than the single-atom energies. In the opposite limit, where the laser is on resonance and dressing strength is at maximum, $E_n = \sqrt{n}\Omega_r$. This gives $\kappa = \pm(2-\sqrt{2})\Omega_r \approx \pm.6\Omega_r$, meaning κ is linear in the laser's Rabi rate and comparable in strength to the single-atom shift. Because of this huge discrepancy in strength between the two regimes, we typically find that strong dressing parameters are preferable, both in theory and in experiment [39]. This is especially true in the context of decoherence. Any experiment with laser-excited neutral atoms will suffer some decoherence due to photon scattering, i.e. absorption of a photon followed by spontaneous emission, and minimizing its impact is an important concern. In the weak dressing regime, the photon scattering rate γ scales as Δ_r^{-2}. The single-atom light shift scales more weakly with Δ_r (as Δ_r^{-1}), so increasing Δ_r causes γ to drop off more sharply than light shift strength. As a result, increasing the laser detuning is an effective way to reduce the impact of photon scattering in experiments that are speed-limited by the single-atom light shift. By contrast, κ drops off more sharply than γ, as Δ_r^{-3}. In experiments that are speed-limited by κ, increased laser detuning suppresses the useful interaction more than it does the photon scattering rate, and minimum scattering decoherence is achieved at or near resonance.

2.4.2 Effects of Imperfect Blockade

The above analysis provides an especially clean and intuitive picture of Rydberg dressing in the perfect blockade limit. When the blockade is imperfect, the overall structure of the interaction remains the same, although calculation of its quantitative strength becomes more complicated. For laser detunings we consider, the $|\widetilde{11}\rangle$ state is always the only

one that experiences any kind of entangling interaction, so the concept of an "entangling energy" κ holds in all regimes, as does the identity $\kappa = E_{LS2} - 2E_{LS1}$. The effect of an imperfect blockade is to modify E_{LS2} from the value given in Eq. (2.21). Here we describe some mechanisms by which this occurs.

The simplest type of blockade imperfection is one in which the scalar blockade approximation holds, but is small enough to allow some double-Rydberg excitation, i.e. $\Omega_r \ll V_{DD} \ll \infty$. In this case, the blockade-dressed interaction is weakened compared to its ideal value, and regains some explicit dependence on V_{DD}. Since the Hamiltonian acts on the 3-dimensional $\{|11\rangle, |B\rangle, |rr\rangle\}$ subspace, its eigenvalues are roots of cubic polynomials, and κ always admits an analytic form. However, the general solution is complicated and offers little insight, so we instead focus on two illustrative limits. If V_{DD} is large enough that $|rr\rangle$ population remains small, we can find the effect on κ by treating $\langle rr| H |B\rangle$ as a second-order perturbation. This gives a correction to the light shift of $\Delta\kappa \approx \frac{|\langle B|\widetilde{11}\rangle|^2}{2V_{DD}}\Omega_r^2$; the exact value depends on both V_{DD} and the dressing strength, but it is generally small and quadratic in Ω_r. If the EDDI is very weak, then V_{DD} itself can be treated as a first-order perturbation, giving $\kappa \approx |\langle rr|\widetilde{11}\rangle|^2 V_{DD}$. In this limit, the interaction is no longer blockade-based in any meaningful sense. Rather, double-Rydberg dressing is mediating a van der Waals interaction between dressed ground states. Both of these regimes are exemplified by the blue dotted curve in Fig. 2.4, which shows κ as a function of R for typical laser parameters; the interaction initially grows as R^{-6}, like a van der Waals interaction, with decreasing R, then tapers off to a V_{DD}-independent plateau as the blockade becomes nearly perfect.

The V_{DD}-dependence of κ further complicates matters for non-ideal blockades because V_{DD} is not constant. Even when the treatment of V_{DD} as a single scalar is a good one, it varies with the distance between the atoms R. Gradients in V_{DD} then lead to an interatomic force, which entangles the atom's electronic state with its motional state and causes decoherence. These forces scale with $|rr\rangle$ population, providing a strong incentive to minimize

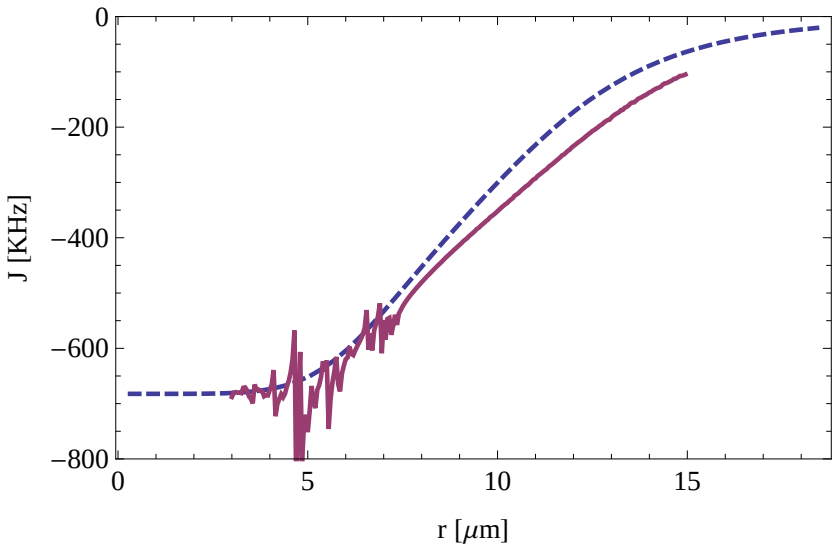

Figure 2.4: Ground-state interaction strength $J(R)$ as a function of distance between the two cesium atoms in $F = 4$ clock states, for $\Omega_r = 10$ MHz and $\Delta_r = 8$ MHz. Calculated using all $l \leq 6$ atomic orbitals $(s, p, d, f, g, h, i$; purple solid line) and more approximately using only the nearest $l \leq 2$ orbitals $(s, p, d$; blue dashed line). As seen in the more exact calculation, below $r = 8$ μm there are resonances whose exact positions cannot be predicted without taking higher-l states into account.

blockade-breaking, even beyond the desire to maximize the blockade-dressing strength. This effect is examined in more detail in Chap. 4.

Finally, the blockade may exhibit imperfections that do not respect the approximation of V_{DD} by a scalar, and require consideration of the richer multi-level dynamics that gave rise to the EDDI in the first place. Recall from Sec. 2.2 that the effect of the EDDI can be calculated by finding the set of levels that couple significantly to the level of interest, then (numerically) diagonalizing the dipole-dipole Hamiltonian in the subspace spanned by those levels. The EDDI strength determines how many levels are coupled strongly enough to be included, which in turn affects the complexity of the multi-level dynamics. At large R, the EDDI is dominated by a few levels that shift away from resonance in "well behaved" ways, and such imperfections are not a major error source. At smaller R, on the other hand, increasingly many states come into play, so multi-Rydberg-level errors

must be considered. Looking at the left-hand side of Fig. 2.3a, we see that the number of level crossings becomes truly daunting. Fortunately, most of these crossings are not cause for concern because they are only weakly coupled to $|1\rangle$. As the EDDI increases at shorter distances to couple the target Rydberg state with more and more nearby states, the target state's population is spread out among all of them, and the Rydberg laser's coupling strength to $|1\rangle$ is effectively diluted. Fig. 2.3 shows the same level diagram weighted by said coupling strength; we see that coupling drops off sharply in the very regime where the number of crossings skyrockets. Nevertheless, it is expected that at least some of these crossings are coupled strongly enough to cause atom loss and other decoherence [55].

What's more, the many-level character of these errors makes them difficult to predict precisely. Both curves in Fig. 2.4 show κ, calculated as in Sec. 2.2 by numerically diagonalizing the EDDI Hamiltonian with one ground and multiple Rydberg states[2]. The blue curve was calculated using just a few Rydberg levels most strongly coupled to the ground state, while the red curve includes hundreds of levels of various n and ℓ. We see that the *overall* shape of the curves match fairly well, especially in the strong-blockade regime. However, the more exact curve shows a cluster of resonances that do not appear in the calculation with fewer levels. Since perturbation theory breaks down at short distances, the locations of these resonances vary strongly with the number of levels included, and they do not show signs of converging before computational limits are reached. Therefore, it seems likely that care must be taken when driving Rydberg excitations at small R, but exactly how multi-level resonances will affect a given protocol will likely have to be answered through laboratory experiment.

[2]Calculation by Yuan-Yu Jau [1].

Chapter 3

Adiabatic Quantum Computation

The solutions to certain mathematical problems can be encoded in the ground states of many-body systems, e.g., an Ising model on a graph [56]. One method of solving such problems is quantum annealing (QA), in which one continuously deforms a system's Hamiltonian to transform some easy-to-prepare initial state into the final, solution-encoding ground state [57, 58]. QA has been studied extensively in a variety of platforms, and is reviewed in, e.g., [59, 60]. Recently, interest in QA has been sparked by the work of the D-Wave corporation, who claim to have produced annealing devices with 100+ superconducting qubits [61, 62].

In this chapter, we consider QA in neutral atom systems, using the Rydberg-dressing interaction to generate Hamiltonians with computationally interesting ground states. More specifically, we consider adiabatic quantum computation (AQC), a subclass of QA in which the system remains in its ground state at all times [63]. AQC is implemented by continuous transformation of the Hamiltonian from an initial form whose ground state is easy to prepare to the final form whose ground state encodes the output of the algorithm; in effect, the entire computation is performed by going from the bare- to the dressed-basis. If the energy gap between the ground and excited states is sufficiently large, the transition

from initial to final Hamiltonian can be accomplished efficiently. AQC is particularly attractive because the existence of an energy gap can make the system inherently robust to certain types of errors [64].

In contrast to quantum circuit implementations where atoms are excited to the Rydberg state with a resonant π-pulse [24, 65, 66], here we base our proposal on adiabatic Rydberg dressing of the atomic ground state. Far off-resonance dressing of this sort has been studied previously in the context of dipolar gases [46, 67]. This leads to an entangling mechanism that is more compatible with AQC, where interactions are always on and can be continuously changed to transfer from the initial to final Hamiltonian. Such adiabatic evolution has been employed in recent cold atom/ion experiments to study quantum simulations of Ising models [68, 69]. As a specific example, we will show how our architecture can be used to implement "quantum annealing" (QA) in an Ising spin-lattice [70] to solve an instance of the quadratic unconstrained binary optimization (QUBO) problem. We will model the physics of its implementation to benchmark the performance of a proof-of-principle realization for a few qubits with nearest-neighbor interactions.

The goal of QUBO is to find the N-tuple of binary variables, $\vec{x} = (x_1, x_2, \ldots, x_N)$, $x_i \in \{0,1\}$, that minimizes the function

$$f(\vec{x}) = \sum_{i=1}^{N} h_i x_i + \sum_{i,j=1}^{N} \kappa_{ij} x_i x_j. \tag{3.1}$$

This is equivalent to solving for the ground state of a generic Ising model, a problem that is generally NP-hard [71]. Nonetheless, specific instantiations of this problem map onto a variety of satisfiability and related algorithms which are tractable, and thus provide useful testbeds for the AQC architecture [72]. Moreover, because the algorithm can be NP-hard, it is important to have multiple architectures (ion, superconductors, Rydberg atoms, ground-state atoms, etc.) in which to cross-verify the solution [73].

To map QUBO onto a QA algorithm, each binary variable is replaced by a projector acting on a qubit, $x_i \Rightarrow (\mathbb{I} + \sigma_z^{(i)})/2$, where the Pauli matrices are defined as usual on

the qubit pseudospin, $|0\rangle = |\downarrow\rangle, |1\rangle = |\uparrow\rangle$. The solution to QUBO maps onto finding the ground state of the "problem Hamiltonian," H_P, in the Ising form

$$H_P = \sum_{i=1}^{N} \tilde{h}_i \sigma_z^{(i)} + \sum_{i,j=1}^{N} \tilde{\kappa}_{ij} \sigma_z^{(i)} \otimes \sigma_z^{(j)}, \tag{3.2}$$

where $\tilde{\kappa}_{ij} = \kappa_{ij}/4$ and $\tilde{h}_i = h_i/2 + \sum_j \tilde{\kappa}_{ij}$. Since the Hamiltonian commutes with all $\sigma_z^{(i)}$, the ground state is one of the computational basis states, which can be read out directly.

As a benchmark for performance of this architecture, we will study a class of QUBO problems corresponding to a one-dimensional spin chain with symmetric interactions, $\kappa_{<ij>} = \kappa$, where $<ij>$ denotes nearest neighbors. We choose the values h_i to be equally spaced and less than κ, $h_i = i\delta E$ with $N\delta E < \kappa$ for N qubits. The solution to this QUBO problem is the trivial antiferromagnetic ground state; minimization is achieved with the state $|1010\cdots10\rangle$ for even N or $|0101\cdots10\rangle$ for odd N, i.e. the bits alternate between 1 and 0 and the final bit is 0. Further, the gap between ground and first excited states scales as N^{-1}, so the necessary evolution time to maintain adiabaticity grows linearly. We consider this example only as a proof-of-principle of the method that can be modeled numerically for a few qubits and address the critical issue of decoherence. In practice, we can accomodate more complex Ising problems on more general graphs, as we will detail later; in particular, a two-dimensional lattice would be a straightforward but NP-hard generalization [71], and would require no qualitative changes to the protocol described here.

To implement this test-bed algorithm in a neutral-atom system, we consider cesium atoms with qubits encoded in two hyperfine magnetic sublevels in the ground-electronic state of alkali-metal atoms, e. g., the "clock states" of $6S_{1/2}$ ^{133}Cs: $|0\rangle = |F = 3, M_F = 0\rangle$, $|1\rangle = |F = 4, M_F = 0\rangle$. The atoms can be trapped in tightly focused optical tweezers with interatomic spacings on the order of 10 μm, thereby allowing individual addressing of qubits, similar to that already achieved in other neutral atom [74] and ion trap [75] experiments. Arbitrary single qubit Hamiltonians of the form $H = \mathbf{B} \cdot \sigma$ can be achieved with

stimulated two-photon Raman transitions in the standard manner, with negligible photon scattering over the duration of the evolution for sufficient detuning and intensity of the lasers. The last critical ingredient is the coupling matrix of pairwise interactions, $\tilde{\kappa}_{ij}$.

As in Chap. 2 and Fig. 2.3, we generate these interactions by dressing the single-qubit ground states with blockaded Rydberg states. The coupling constant is the difference in the light shift (LS) between blockaded and non-interacting pairs of atoms. In the perfect blockade limit with blue detuning,

$$\kappa = E_{LS2} - 2E_{LS1} \approx -\frac{1}{2}\left(\Delta + \sqrt{\Delta^2 + 2\Omega^2} - 2\sqrt{\Delta^2 + \Omega^2}\right). \tag{3.3}$$

where Ω and Δ are the Rabi frequency and detuning of the dressing laser, respectively. We assume the detuning of the Rydberg laser is small compared with the ground-state hyperfine splitting (9.2 GHz for ^{133}Cs), but allow the laser to be tuned near resonance with either $|0\rangle$ or $|1\rangle$ for each atom. This gives an effective interaction Hamiltonian of $H_{int} \approx \kappa |x_1 x_2\rangle \langle x_1 x_2|$, with $x \in \{0,1\}$. Up to single qubit terms (that can be compensated by individually addressed atomic LS), $H_{int} \Rightarrow \pm(\kappa/4)\sigma_z \otimes \sigma_z$. The positive/antiferromagnetic (negative/ferromagnetic) sign is achieved when $x_1 = x_2$ ($x_1 \neq x_2$). The ability to choose the signs of the elements of $\tilde{\kappa}_{ij}$ provides extra flexibility in this platform, even if the sign of the physical coupling is fixed in the dressing interaction.

One fundamental limitation on the fidelity of operation is the scattering of photons due to excitation of the Rydberg state at a rate $\gamma_r = N_r \Gamma_r$, where N_r is the population in the Rydberg state and $\Gamma_r/2\pi$ is its linewidth. (The trapping lasers also contribute to photon scattering, but their effect can be made negligible with blue detuned "bottle traps" [76].) While $\Gamma_r \propto n^{-3}$ points to larger principal quantum numbers, a variety of practical considerations limits the value of n, including the linewidth of the Rydberg excitation laser, the sensitivity of the Rydberg state to ambient fields, and the sheer size of the Rydberg atom. As a reasonable operating point for our architecture, we consider here the $100P_{3/2}$ state, for which $\Gamma_r/2\pi = 530$ Hz and the radius of the atom $r \approx 0.7\ \mu$m. By directly dressing the ground state with the Rydberg state using a single optical field at $\lambda = 318$ nm, we avoid

the strong photon scattering that arises in the conventional two-photon excitation scheme via an intermediate excited state and reduce the total photon scattering rate by a factor of 10 or more.

Since the rate of photon scattering depends directly on our choice of Rydberg laser detuning, finding the Δ that minimizes photon scattering is an important consideration. More precisely, we seek to maximize the figure of merit $q = \kappa/\gamma_r$ so that we achieve a large gap between the ground state and excited computational states of the problem Hamiltonian, while minimizing photon scattering over the duration of the evolution. Recall from Sec. 2.4.1 that κ drops off more quickly than γ_r with increasing Δ, so q is maximized by strong, near-resonant dressing. For this reason, one might expect that the highest fidelities could be achieved *on* resonance, i.e. at $\Delta = 0$. However, Δ is limited from below by a competing requirement: the gap between dressed-ground and dressed-Rydberg states, $\Delta E = \sqrt{2\Omega^2 + \Delta^2}$, must be sufficient to ensure adiabatic evolution at all times, even near the start and end of the protocol when $\Omega \approx 0$. The optimal detuning is thus the minimum detuning to satisfy this gap requirement.

A second fundamental limitation is the accuracy with which we can implement the QUBO Hamiltonian using the Rydberg-blockade interaction. Ideally, we would like to introduce only the desired pairwise couplings specified by the matrix κ_{ij}. In practice there will be additional perturbations due to the long-range nature of the dipole-dipole interaction and the strong blockade mechanism. For our geometry, this means that there are residual next-nearest neighbor couplings and many-body effects (see, e.g., [77]) when more than two atoms are close to the blockade radius. Both interaction types will add unwanted terms to our final Hamiltonian, potentially shrinking the minimum gap or even changing the final ground state if they are too large. However, as long as these effects can be treated as a perturbation that is sufficiently small compared to the minimum energy gap, they will not interfere with the adiabaticity of evolution, and the algorithm will still give the correct answer; this sets a minimum acceptable energy gap and, by extension,

constrains the size of problem that can be solved.

The qualitative discussion above holds only for a simplified model of participating atomic levels and for a perfect dipole-blockade, i.e. when the probability of simultaneously exciting two adjacent Rydberg atoms is zero. To obtain a more accurate description we can find the dressed-state eigenvalues by diagonalizing the two-atom system in the presence of the laser field, yielding a position dependent $\kappa(R)$ [46]. Outside the blockade radius, the result is $\kappa(R) \propto R^{-k}$, where $k = 3$ for the Förster regime or $k = 6$ for the Van der Waals regime. As we are considering direct excitation to a p-state, there may be concern that pairs of atoms would couple to noninteracting "Förster zero states" that evade the Rydberg blockade [54]. Such zeros are avoided, however, in a more complete description of the electric dipole-dipole interaction (EDDI) since mixing occurs not only between p- and s-states but also with nearby d-states and higher angular momentum orbitals. Inside the so-called blockade radius the situation becomes significantly more complex, as is discussed in Sec. 2.4.2. We will restrict our attention here to $r > 8\ \mu$m, which will give us sufficient coupling and control over the atoms without having to address many of the issues that arise at extremely short distances.

Including these limitations and the full doubly-excited spectrum shown in Fig. 2.2, the optimal detuning is found empirically. For a Rydberg laser that achieves a Rabi frequency $\Omega_r = 10$ MHz, we find that a good choice of detuning is $\Delta_r = 8$ MHz. Figure 2.4 shows a calculation of $\kappa(R)$ for these parameters, and its comparison to the simplified two-level atomic model. For tightly trapped separated atoms, $\kappa(R = 8\ \mu\text{m})/2\pi = -470$ kHz. At such a laser power and detuning, there is substantial dressing, with as much as $\sim 20\%$ of Rydberg character in the dressed ground states. The maximum photon scattering rate is $\gamma_r/2\pi \approx 100$ Hz, yielding an excellent figure of merit for AQC. Next-nearest-neighbor and three-body interactions for these parameters are smaller than the minimum gap for up to five atoms; increasing Δ_r and r could increase the maximum problem size farther at the expense of q. This requires more runs of the experiment, but as long as the fidelity is

sufficient, the probability to find the ground state can be amplified.

With these parameters we model the performance of proof-of-principle experiments to implement a simple example of QA. The basic protocol is as follows: One optically pumps the atoms into a clock state and initializes the qubits in an eigenstate of σ_x through the application of a Raman-resonant $\pi/2$-pulse. One then phase-shifts the Raman beam by $\pi/2$, leaving the atoms in the ground state of the beginning Hamiltonian, $H_B = -\Omega \sum_i \sigma_x^{(i)}$, where 2Ω is the Raman-Rabi frequency. This initializes the quantum register in an equal superposition of all computational basis states. The transition from initial to final QUBO Hamiltonian is achieved by ramping down the Raman laser power while ramping up the individual atoms' Raman detunings that create the local Hamiltonians $\tilde{h}_i \sigma_z^{(i)}$. Simultaneously, we linearly increase the Rydberg laser power that creates the coupling Hamiltonians $\kappa_{ij} \sigma_z^{(i)} \otimes \sigma_z^{(j)}/4$ with $\kappa_{ij} = \kappa \forall_{i=j\pm1}$, achieved when all atoms are arranged in an evenly spaced lattice, and negligible next-nearest neighbor interactions, as discussed above. Note, since in our problem the coupling parameter $\kappa_{<ij>}$ is positive while the physical κ is negative, we achieve the desired antiferromagnetic Ising coupling by using Rydberg laser fields that individually address the atoms, alternately dressing nearest neighbors in $|0\rangle$ and $|1\rangle$. At the final time, the answer to the algorithm can be read out using state-dependent resonance fluorescence. We consider here linear ramps. More optimal time-dependent evolution can improve adiabatic following, but will depend on the specific problem.

We take as our parameters $\Omega = \kappa_{<ij>} = 2\pi \times 470$ kHz, and $h_i = 2\pi \times (i/N) 118.5$ kHz for N qubits, achievable with the atom-laser interactions discussed above. The ramp time is taken to be 35 μs, sufficiently long to maintain adiabatic evolution, but sufficiently short compared to the photon scattering time. We treat spontaneous emission from the Rydberg level as effectively randomizing the magnetic spin state as the population cascades back to the electronic ground state. For practical reasons, the detection scheme does not distinguish between different magnetic sublevels in the same hyperfine subspace. All magnetic sublevels in $F = 4$ are treated as logical-1 and those in $F = 3$ as logical-0. Our simula-

tion for two qubits, with the correct solution to QUBO encoded in $|10\rangle$, gives a fidelity of 0.997. For larger numbers of qubits, the fidelity scales favorably. For three and four qubits, scaling up the evolution time linearly with qubit number, we find fidelities of 0.989 and 0.990.

The performance of the neutral-atom platform for AQC depends on a combination of practical and fundamental questions. The minimum gap between the ground state and first excited state determines the time scale for implementing the algorithm and thus the probability of spontaneous emission, the fundamental source of decoherenece. For a given problem size, the gap is constrained by κ arising from the Rydberg-dressing, whose optimal value for a given laser power depends on the details of the atomic level structure. We found here that for reasonable power and detuning we could achieve $\kappa = 470$ kHz and a fidelity of ~ 0.99 in a proof-of-principle solution to an Ising model with ~ 4 qubits. Modest increases in this coupling would allow us to attain high-fidelity control with larger numbers of qubits. However, unlike fault-tolerant universal quantum computation in the quantum circuit model, for the purpose of solving optimization problems by QA, such high fidelity is not necessary. One requires instead that the fidelity of finding the system in the ground state be sufficiently high that one can amplify the success probability with k independent trials. For our current parameters, this should allow us to explore the regime of $10-20$ qubits, where interesting physics beyond classical simulation is accessible.

Finally, while this initial proof-of-principle analysis focused on nearest-neighbor Ising spin lattices, in principle this atomic architecture should allow us to explore more arbitrary connected graphs associated with a general QUBO problem. For example, a complete bipartite graph is isomorphic to a square crosshatch of intersecting lines, where each line represents a vertex of the graph and their interesctions are the edges [72]. This could be achieved in our system by encoding logical qubits as Rydberg-coupled one dimensional spin chains [78]. The proximity of these spin chains to one another in a designed trapping geometry would determine the edges of the graph. Such an architecture would give sub-

stantial flexibility to explore a wide range of computationally complex Ising problems and open the door to deeper studies of QA and general AQC, as we will study in future work.

Chapter 4

Quantum Logic Gate

4.1 Introduction

In addition to directly simulating some problems of interest in AQC, the on-demand entangling interactions provided by the Rydberg blockade can be applied to gate model quantum computation [37, 79, 80]. In the gate model, unlike in AQC, the system's Hamiltonians are not adjusted to match the problem at hand. Instead, the computer has access to a small, fixed set of "logic gate" unitaries, which can be applied in various sequences to solve different problems. Here, we focus on generating a controlled-Z (CZ) gate, which imparts a phase of -1 on a pair of atoms if both are in the logical-$|1\rangle$ state. Like all entangling gates, the CZ can be combined with single-qubit gates to accomplish universal quantum computation [4]. In the standard approach of fast gates, one employs short, resonant pulses in conjunction with the Rydberg blockade to induce the requisite entangling interaction [54]. However, such a mechanism is not robust to thermal motion of the atoms, which imparts random phases on the two-atom state that vary from shot to shot. Indeed, such random phases are impediments to the direct observation of entanglement in the signature two-atom Rydberg blockade [37]. More generally, the decoherence arising from

coupling internal (electronic) and external (motional) degrees of freedom is a dominant source of error that limits the implementation of high-fidelity quantum gates [81].

Adiabatic Rydberg dressing provides an alternative approach, one which can be more resilient against errors due to atomic motion. The original proposal of Jaksch *et al.* [24] was such a dressing-based scheme, but it examined adiabatic evolution as a mechanism for relaxing the requirement of single atom addressability, and only did so for atoms cooled to the ground state of motion. Subsequent proposals have suggested various modifications, but most either ignore thermal motion in order to focus on electronic effects [82, 83] or require experimental parameters that are challenging to achieve [84]. Our motivation is to use adiabaticity to substantially improve the robustness to errors caused by atomic motion, and thereby achieve high-fidelity operation with current technology. Similar robustness was recently studied in adiabatic passage of atoms to a doubly-excited Rydberg state [85], which might be used as a mechanism to generate quantum logic gates.

Adiabatic evolution does not protect against all types of decoherence, however, and the motional errors we consider are not strongly suppressed by adiabaticity alone. In fact, motional errors have been among the main fidelity-limiting factors in recent attempts to produce an adiabatic gate [43]. The protocol we consider is compatible with a "Doppler-free" laser configuration, in which the qubits are excited by two counterpropagating beams rather than just a single beam. Such a configuration does not directly reduce the terms in the Hamiltonian that lead to motional decoherence, but it changes their form to one more amenable to adiabatic suppression. Taken together, adiabatic dressing and a Doppler-free configuration produce more than an order-of-magnitude reduction of motional decoherence that neither change achieves on its own.

4.2 Implementing a CZ gate

4.2.1 The Dressed-Blockade Interaction

As in previous chapters, we consider qubits encoded in single ^{133}Cs atoms, individually trapped in tightly focused optical tweezers, with a typical separation of 5–10 microns (see Fig. 4.1). Qubits are encoded in the clock states, $|0\rangle \equiv |6S_{1/2}; F = 4, M_F = 0\rangle$ and $|1\rangle \equiv |6S_{1/2}; F = 3, M_F = 0\rangle$. We consider direct excitation to a high-lying Rydberg level, $|r\rangle \equiv |84P_{3/2}; M_J\rangle$ by a single exciting laser at $\lambda_L \approx 319$ nm in the absence of the trap which is turned off during the duration of the interaction so the atoms undergo ballistic motion [80]. In the absence of the dipole-dipole interaction, each atom (labeled $i = a, b$) interacts with a laser propagating on the interatomic z axis. The Hamiltonian individually governing the dynamics of the two atoms is (in the two-level, rotating wave approximation, $\hbar = 1$),

$$H_i = \frac{p_i^2}{2m} - \Delta |r\rangle_i \langle r| + \frac{\Omega}{2}(e^{ik_L z_i} |r\rangle_i \langle 0| + e^{-ik_L z_i} |0\rangle_i \langle r|). \tag{4.1}$$

When including the dipole-dipole interaction of atoms in the Rydberg states, the two-atom Hamiltonian takes the form,

$$H = H_a \otimes \mathbb{1} + \mathbb{1} \otimes H_b + V_{dd}(z_b - z_a) |rr\rangle \langle rr|, \tag{4.2}$$

where $V_{dd}(z)$ is the dipole-dipole potential for two atoms excited to the Rydberg state. This form of the interaction energy is approximately correct for atoms separated by a large enough distance such that the interaction is perturbative when compared to the splitting of the atomic Rydberg levels (e.g., in the van der Waals regime). For more closely spaced atoms, the electrostatic forces will strongly mix many atomic orbitals into molecular-type orbitals, so that the double excitation is no longer of the form $|rr\rangle \langle rr|$, for a single Rydberg level [50]. Nevertheless, as long as the blockade is strong, we can obtain the essential physics by considering only one doubly-excited state with a given dipole-dipole potential.

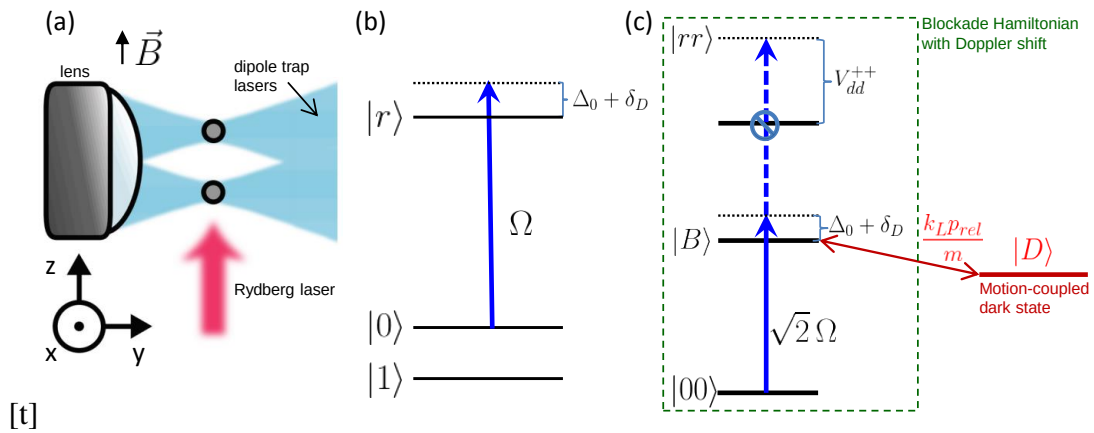

[t]

Figure 4.1: (a) Schematic for the CPHASE gate. Two cesium atoms are trapped and cooled in dipole traps, several μm apart. During the CPHASE gate, the trapping lasers are turned off and the atoms are illuminated by a 319 nm Rydberg laser. A bias magnetic field ensures that the laser's propagation axis coincides with the atomic quantization axis. (b) In each atom, the logical-$|0\rangle$ state is coupled to a $|84P_{3/2};M_J\rangle$ Rydberg state. The coupling laser has Rabi rate Ω and detuning from atomic resonance Δ_0, with a momentum-dependent Doppler shift $\delta_D \equiv k_l p/m$. (c) In the two-atom basis, $|00\rangle$ is coupled to the bright state $|B\rangle$, again with base detuning Δ_0 and Doppler shift δ_D. Excitation to $|rr\rangle$ is blockaded by the dipole-dipole interaction V_{dd}. Atomic motion further couples $|B\rangle$ to a dark state, $|D\rangle$, outside the ideal blockade subspace.

The position dependent phases $\exp(\pm ik_L z_i)$ associated with photon recoil can be removed from the Hamiltonian by moving to a frame where a Rydberg excited atom is moving with a velocity $\boldsymbol{v} = -\mathbf{k}_L/m$ with respect to the lab frame, yielding,

$$H_i \Rightarrow \frac{p_i^2}{2m} - \left(\Delta - \frac{k_L p_i}{m}\right)|r\rangle_i\langle r| + \frac{\Omega}{2}(|r\rangle_i\langle 0| + |0\rangle_i\langle r|). \tag{4.3}$$

Here we have absorbed the constant recoil energy into the standard definition of the detuning, $\Delta \to \Delta - k_L^2/2m$. In this frame, the Doppler shift, $k_L p_i/m$, is explicitly visible. The single atom laser induced light shift (LS) on the ground state at zero momentum is $\Delta E_{LS}^{(1)} = \frac{1}{2}\left(-\Delta + \text{sign}(\Delta)\sqrt{\Delta^2+\Omega^2}\right)$.

As the interaction is only a function of the relative atomic distance, it is useful to re-express the Hamiltonian in terms of the center-of-mass $\mathbf{P}_{cm} = \mathbf{p}_a + \mathbf{p}_b$ and relative $\mathbf{p}_{rel} = (\mathbf{p}_b - \mathbf{p}_a)/2$ momentum coordinates. In addition, the laser field only couples the

logical state $|00\rangle$ to a symmetric superposition of one excited and one ground state atom. Defining the bright and dark states of this two-atom system, $|B\rangle \equiv (|r0\rangle + |0r\rangle)/\sqrt{2}$ and $|D\rangle \equiv (|r0\rangle - |0r\rangle)/\sqrt{2}$, Eq. (4.2) can be rewritten as

$$\begin{aligned} H &\approx H_0 + H_1, \\ H_0 &= -\Delta\Big(|B\rangle\langle B| + |D\rangle\langle D|\Big) - \Big(2\Delta - V_{dd}(\bar{z})\Big)|rr\rangle\langle rr| \\ &\quad + \frac{\sqrt{2}\Omega}{2}\Big(|B\rangle\langle 00| + |00\rangle\langle B| + |rr\rangle\langle B| + |B\rangle\langle rr|\Big), \\ H_1 &= T + V_{grad} + V_{Dop}. \end{aligned} \tag{4.4}$$

Written in this form, H_0 is the "frozen atom" model including only the internal state dynamics, that show the usual $\sqrt{2}\Omega$ Rabi flopping between the double-ground $|00\rangle$, single-Rydberg bright $|B\rangle$, and double Rydberg $|rr\rangle$ states. The blockade energy is taken at the mean atomic separation $\bar{z}$. H_1 accounts for the effects of atomic motion according to

$$\begin{aligned} T &\equiv \frac{P_{cm}^2}{4m} + \frac{p_{rel}^2}{m}, \\ V_{grad} &\equiv \left.\frac{dV_{dd}}{dz}\right|_{\bar{z}} (z-\bar{z})\,|rr\rangle\langle rr|\,, \text{ and,} \\ V_{Dop} &\equiv \frac{k_L P_{cm}}{2m}\Big(|B\rangle\langle B| + |D\rangle\langle D| + 2\,|rr\rangle\langle rr|\Big) - \frac{k_L p_{rel}}{m}\Big(|B\rangle\langle D| + |D\rangle\langle B|\Big). \end{aligned} \tag{4.5}$$

T is the kinetic energy; this term does not entangle internal and external degrees of freedom and thus is unimportant in the perturbation to the logic gate. V_{grad} accounts for the interatomic forces due to the local gradient of the dipole-dipole potential for the doubly-excited Rydberg state and results from linearizing V_{dd} about the point $z = \bar{z}$. V_{Dop} describes the effect of the Doppler shift. This includes a term diagonal in the $\{|B\rangle, |D\rangle\}$ basis that depends on the center of mass momentum. The off-diagonal terms in V_{Dop} account for the coupling between bright and dark states due to the relative motion of the atoms, familiar in studies of coherent population trapping [86]. This term leads to random phases induced by thermal motion that cause errors and reduce the entangling action of the interaction.

The eigenstates of H_0 are completely decoupled from the motional degrees of freedom and define the adiabatic basis. The problem can be simply diagonalized; the general case

has been studied in [46]. In a strongly blockaded regime, $|V_{dd}(\bar{z})| \gg |\Delta|, \Omega$, excitation to the doubly-excited state $|rr\rangle$ is suppressed by a factor of order $(V_{dd})^2/(\Omega^2+\Delta^2)$. The ground state $|00\rangle$ and the entangled bright state $|B\rangle$ form an effective two-level system, and coupling to $|rr\rangle$ can be treated as a perturbation. The two-atom ground-state light-shift energy is then approximately, $E_{LS}^{(2)} \approx \frac{1}{2}\left(-\Delta + \text{sign}(\Delta)\sqrt{\Delta^2+2\Omega^2}\right)$ [46]. The effective atomic interaction strength κ is the difference between the two-atom light shift and that for two atoms in the absence of the dipole-dipole force, $\kappa \equiv E_{LS}^{(2)} - 2E_{LS}^{(1)}$. For weak dressing, $\Omega \ll |\Delta|$, $\kappa \approx -\Omega^4/(8\Delta^3)$. As we will see, however, the regime of the highest fidelity operation occurs for strong dressing, close to equal superpositions of ground and bright states. In our previous analysis, we found $\kappa/2\pi = 500$ kHz to be experimentally feasible [1].

4.2.2 The CZ Gate Protocol

Given an interaction of this form, it is straightforward to produce a two-qubit logic gate in a manner analogous to Jaksch *et al.* [24]. Adiabatically increasing the Rydberg laser power while decreasing the detuning creates the coupling, $\kappa(t)$. Concurrently, the instantaneous ground state of H_0 evolves from the bare $|00\rangle$ state into a "dressed" state with some admixture of Rydberg character, $|\widetilde{00}\rangle = c_0|00\rangle + c_B|B\rangle + c_{rr}|rr\rangle$, where the coefficients c_0, c_B, and c_r depend on the time-dependent parameters $\Delta(t)$ and $\Omega(t)$, as well as the static blockade $V_{dd}(\bar{z})$. Perfect adiabatic state transfer is ensured by satisfying the adiabatic condition, $|\langle e|\frac{d}{dt}H_0|\widetilde{00}\rangle| \ll |E(e)-E(\widetilde{00})|^2$, where $|e\rangle$ is any one of the instantaneous excited states of H_0. Inverting this ramp returns the system to the bare logical subspace, with the addition of nontrivial phases. When the adiabatic condition is satisfied, $\kappa(t)$ is the rate at which the dressed ground state accumulates the entangling phase. Integrating the evolution over the total time duration of the gate, $[0,T]$, gives a unitary map, $U_{LS}^{(2)}$, that, when

restricted to the two-qubit-logical subspace, takes the diagonal form,

$$\begin{aligned} U_{LS}^{(2)} &= \sum_{xy=0,1} e^{-i\phi_{xy}} |xy\rangle \langle xy|, \text{ where,} \\ \phi_{11} &= 0;\ \phi_{10} = \phi_{01} = \int_0^T dt\, E_{LS}^{(1)}(t);\ \phi_{00} = \int_0^T dt\, E_{LS}^{(2)}(t). \end{aligned} \tag{4.6}$$

Following this with the inverse of local single qubit unitaries, $U_{LS}^{(1)} = \exp(-i\phi_{10}|0\rangle\langle 0|)$, cancels the single atom light shifts, yielding the controlled phase gate, $U_{C\phi_J}$,

$$\begin{aligned} U_{C\phi_J} &= \left(U_{LS}^{(1)} \otimes U_{LS}^{(1)}\right)^\dagger U_{LS}^{(2)} = e^{-i\phi_\kappa |00\rangle\langle 00|}, \\ &\text{where } \phi_\kappa = \int_0^T dt\, \kappa(t). \end{aligned} \tag{4.7}$$

The single-atom light shifts can be compensated by, e.g., applying microwave pulses or Raman lasers. The case where $\phi_\kappa = \pi$ is of particular interest, since $U_{C\pi} \equiv U_{CZ}$ is the controlled-Z (CZ) gate, which, up to local unitaries, is equivalent to a controlled-X (CX, or CNOT) gate.

The speed of the gate is set by balancing the requirements that one adiabatically follows the dressed ground state of the Hamiltonian during the implementation of the gate while avoiding the errors that accumulate over time. One fundamental source of such errors is the finite lifetime of the Rydberg state, Γ^{-1}. Decay of $|r\rangle$ will not only dephase the qubits, but with high probability optically pump them into magnetic sublevels outside the computational space, so we treat this as loss. This effect can be described as the action of a non-Hermitian, effective Hamiltonian with an imaginary part to the detuning: $\Delta \to \Delta - i\Gamma/2$. Over the full duration T of a gate, such loss will reduce the trace of the density matrix. For a large detuning, the interaction strength scales as $\kappa \sim -\Omega^4/\Delta^3$, while the decay rate due to absorption of a photon and decay of the Rydberg state scales as $\gamma \sim \Omega^2\Gamma/\Delta^2$. This implies that it is not advantageous to remain in the large detuning limit, but to instead adiabatically sweep to resonance, where the dressing is maximum, while simultaneously avoiding, to the maximum degree possible, double excitation of two atoms into the Rydberg state.

The shape of the laser pulse can strongly influence the speed at which one can perform the gate while remaining adiabatic; finding the optimal pulse shape for a given control goal is an area of active research (see, e.g., [87]). For a sufficiently large energy gap (between the dressed ground and excited states) such that the time required to achieve the desired adiabaticity is short compared to other constraints such as finite Rydberg lifetime, one can remain adiabatic solely by rounding the edges of an essentially square-topped pulse and have minimal impact on gate time. In the opposite limit, when the energy gap is not very large compared to other decoherence rates, to achieve very high levels of adiabaticity one might require a more triangular pulse, where laser power increases slowly until half the desired phase is accumulated at which point the process is reversed. The parameter ranges we explored fell between these two extremes where adiabaticity was one of a few limiting factors on the gate's speed and fidelity. An example simulation of the time dependent Schrödinger equation in the absence of decoherence is shown in Fig. (4.2) for the following parameters: pulse rise time 1 μs, Rabi frequency sweep $\Omega/2\pi = 0 \rightarrow 3$ MHz, detuning sweep $\Delta/2\pi = 6 \rightarrow 0$ MHz, Rydberg decay rate $\Gamma/2\pi$= 3.7 kHz, and interatomic separation $\bar{z} = 5$ μm. These parameters produce a blockade shift of $V_{dd}(\bar{z})/2\pi \approx -6.4$ MHz, giving an interaction strength of $\kappa/2\pi \approx 1.8$ MHz at full power. For this example, the populations are highly adiabatic; approximately 99.5% of the original population returns to the ground state.

4.3 Motional Errors

The method described produces a high-fideity CPHASE gate when errors due to motional effects are neglected. To account for the motional degrees of freedom, we must consider the near-degenerate manifold of dressed ground states, all with the same electronic character but different momenta, $|\widetilde{00}\rangle \otimes |p_{rel}, P_{cm}\rangle$. The perturbative effects of motion are described by H_1, Eq. (4.4). For a gate performed for atoms in free flight, the finite mo-

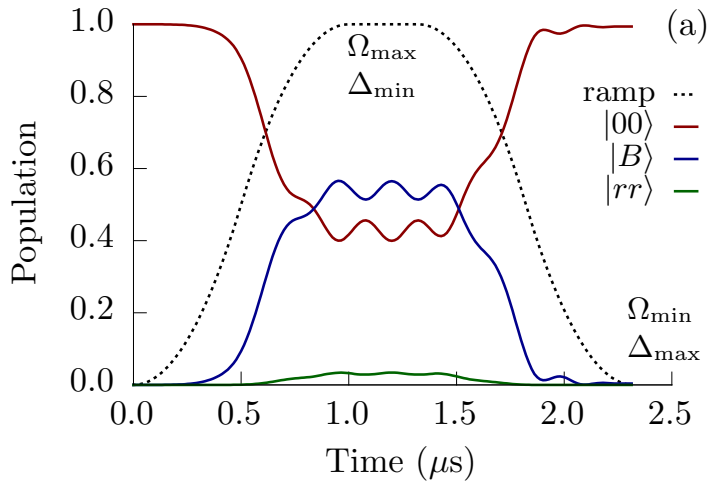

Figure 4.2: Pulse shape and bare state populations over the course of a gate with experimentally feasible parameters: pulse rise time 1 μs, Rabi frequency sweep $\Omega/2\pi = 0 \to 3$ MHz, detuning sweep $\Delta/2\pi = 6 \to 0$ MHz, Rydberg decay rate $\Gamma/2\pi$= 3.7 kHz (blackbody limited lifetime), and interatomic separation $r = 5$ μm. As the laser turns on and is tuned to resonance, the bare ground state (red) is dressed by admixing significant bright state (blue) population, while the blockaded $|rr\rangle$ state (green) remains mostly unpopulated. Adiabaticity and available interaction strength set comparable constraints in this case, so that the laser pulse shape that best achieves the desired evolution is neither square-topped nor triangular.

mentum spread of the atoms leads to two types of errors corresponding to the two terms in V_{Dop}, Eq. (4.5). First, the perturbation of the energy,

$$\langle\widetilde{00}|\, V_{Dop}\, |\widetilde{00}\rangle = \frac{k_L P_{cm}}{2m}(|c_B|^2 + 2|c_{rr}|^2), \tag{4.8}$$

leads to a momentum-dependence of the light shift. This in turn leads to a momentum-dependence of the phase accumulated over the course of the gate, which manifests as decoherence after averaging over motional degrees of freedom. Second, the off-diagonal terms, $\langle D|\, V_{dd}\, |\widetilde{00}\rangle$, transfer population from the ideal dressed ground states into electronic dark states, potentially causing qubit loss as well as decoherence.

An adiabatic gate is naturally robust against some of these motional noise sources. Specifically, the dressed ground manifold is "protected" from the excited dressed states by

an energy gap, $\Delta E \approx \sqrt{\Delta^2 + \Omega^2}$, and by design, we assume that the laser intensity is turned on slowly enough to stay adiabatic given this gap. As long as $|\langle e| H_1 |\widetilde{00}\rangle| \ll |\Delta E|$, averaged over the atomic thermal distribution and for all excited states $|e\rangle$, any time-dependent sweep of the laser parameters that is adiabatic for H_0 will also be adiabatic for $H_0 + H_1$. Since H_1 does not significantly affect adiabaticity, we can completely characterize its effects by examining its action on the dressed ground subspace. By guaranteeing that we remain in a dressed ground state, we make the gate robust against errors that couple the system to states outside the desired 3-level space, $\{|00\rangle, |B\rangle, |rr\rangle\}$. The off-diagonal bright-dark coupling is such an error, so its effects are largely suppressed. The Doppler shift, on the other hand, is not suppressed and remains a major source of error, even for cold atoms.

To ensure that Doppler errors are also suppressed, we can make use of a "Doppler-free" configuration. We can achieve this through the addition of the light-shifts from counter-propagating laser-beams on two Rydberg transitions such that the Doppler shift cancels to first order in p. Consider counter-propagating lasers with opposite helicity, σ_+/σ_-, tuned to address two different sublevels in the Rydberg manifold (see Fig. 4.3),

$$\begin{aligned}
\sigma_+ :\ & |0\rangle = |6S_{1/2}, F = 4, m_F = 0\rangle \\
& \rightarrow |r_1\rangle = |84P_{3/2}, m_J = 3/2\rangle\, |I = 7/2, m_I = -1/2\rangle \\
\sigma_- :\ & |0\rangle = |6S_{1/2}, F = 4, m_F = 0\rangle \\
& \rightarrow |r_2\rangle = |84P_{3/2}, m_J = -3/2\rangle\, |I = 7/2, m_I = +1/2\rangle
\end{aligned} \tag{4.9}$$

Note, we choose a $nP_{3/2}$ Rydberg multiplet because this has much larger oscillator strength than the corresponding $nP_{1/2}$ mutiplet [88]. We can suppress the coupling of the $m_F = 0$ ground state to the $m_J = \pm 1/2$ sublevels with a sufficiently large Zeeman shift so that those transitions remain well off resonance (e.g., $B \approx 10$ G). Because the two beams are differently detuned and orthogonally polarized, we avoid standing waves in intensity and polarization.

Given the couplings in Eq. (4.9), we can write the single-atom Hamiltonian as in Eq.

(4.1),

$$\begin{aligned} H_A =& \frac{p^2}{2m} - \Delta(|r_1\rangle\langle r_1| + |r_2\rangle\langle r_2|) \\ &+ \left(\frac{\Omega_1}{2} e^{ik_L z}|r_1\rangle\langle 0| + \frac{\Omega_2}{2} e^{-ik_L z}|r_2\rangle\langle 0| + h.c.\right). \end{aligned}$$

Including counter-propagating laser beams doubles the incident power, so in order to make a fair comparison to a single laser beam we will assume that $\Omega_1^2 = \Omega_2^2 = \Omega^2/2$. In such a configuration, there are coupled and uncoupled excited states for the each of the atoms $|r_\pm\rangle \equiv (\Omega_1|r_1\rangle \pm \Omega_2|r_2\rangle)/\Omega$. As before, we can go to a comoving frame, yielding the single atom Hamiltonian

$$\begin{aligned} H_A =& \frac{p^2}{2m} - \Delta\big(|r_+\rangle\langle r_+| + |r_-\rangle\langle r_-|\big) \\ &+ \frac{k_L p}{m}\big(|r_-\rangle\langle r_+| + |r_+\rangle\langle r_-|\big) + \frac{\Omega}{2}\big(|r_+\rangle\langle 0| + |0\rangle\langle r_+|\big). \end{aligned} \tag{4.10}$$

For this configuration, as in Eq. (4.4), we can split the two-atom Hamiltonian into H_0 for "frozen atoms" and a perturbation H_1 due to motion. Thus,

$$\begin{aligned} H_0 =& H_A \otimes \mathbb{1} + \mathbb{1} \otimes H_A + V_{dd} \\ =& -\Delta(0)\sum_{i=\pm}(|B_i\rangle\langle B_i| + |D_i\rangle\langle D_i|) \\ &+ \sum_{i,j=\pm}\Big(V_{dd}^{ij}(\bar{z}) - 2\Delta(0)\Big)|r_i r_j\rangle\langle r_i r_j| \\ &+ \frac{\sqrt{2}\Omega}{2}(|B_+\rangle\langle 00| + |r_+ r_+\rangle\langle B_+| + h.c.) \\ &+ \frac{\Omega}{2}\Big[(|r_+ r_-\rangle + |r_- r_+\rangle)\langle D_-| \\ &+ (|r_+ r_-\rangle - |r_- r_+\rangle)\langle B_-| + h.c.\Big], \end{aligned} \tag{4.11}$$

$$\begin{aligned} H_1 =& T + V = \frac{P_{cm}^2}{4m} + \frac{p_{rel}^2}{m} + \frac{k_L P_{cm}}{2m}(\sigma_x^r \otimes \mathbb{1} + \mathbb{1} \otimes \sigma_x^r) \\ &- \frac{k_L p_{rel}}{m}(\sigma_x^r \otimes \mathbb{1} - \mathbb{1} \otimes \sigma_x^r) \\ &+ \sum_{i,j=\pm}\frac{dV_{dd}^{ij}}{dz}(z - \bar{z})|r_i r_j\rangle\langle r_i r_j|. \end{aligned}$$

We have defined the Pauli-x operators acting on Rydberg states to be $\sigma_x^{(r)} \equiv |r_-\rangle\langle r_+| + |r_+\rangle\langle r_-|$ as well as the bright and dark states,$|B_\pm\rangle \equiv (|r_\pm 0\rangle + |0\, r_\pm\rangle)/\sqrt{2}$ and $|D_\pm\rangle \equiv (|r_\pm 0\rangle - |0\, r_\pm\rangle)/\sqrt{2}$. The effect of gradient forces now depends in the dipole-dipole potential for the different Rydberg states, $V_{dd}^{ij}(z) = \langle r_i|\, V_{dd}(z)\, |r_j\rangle$.

We see that for the counter-propagating σ_+/σ_- geometry, H_0 is block diagonal in the electronic degrees of freedom as well as diagonal in p. The states $|00\rangle$, $|B_+\rangle$, and $|r_+r_+\rangle$ form a block described by our desired 3-level blockade Hamiltonian, while $|B_-\rangle$, $|D_-\rangle$, $|r_+, r_-\rangle$, and $|r_-, r_+\rangle$ form a separate block; the state $|D_+\rangle$ is completely uncoupled from all other states. The terms in V arising from the Doppler shift scale as $k_L p\sigma_x^r/m$, but because this coupling is off-diagonal, its effect will manifest as a second order perturbation to the energies of $|B_+\rangle$ and $|r_+r_+\rangle$. This counter-propagating laser configuration can thus be considered as "Doppler-free" to first order. By contrast, with a single laser beam, $\langle B|\, V\, |B\rangle$ was nonzero, leading to contributions to the dressing energy that are first order in the Doppler shift. To zeroth order in p, our scheme only involves the states in the 3×3 ideal block; the other states are only included through perturbations. Restricting H_0 to this subspace leaves

$$\begin{aligned} H_0 = {} & V_{dd}^{++}(z)\, |r_+r_+\rangle\langle r_+r_+| - \Delta\Big(\, |B_+\rangle\langle B_+| + 2\, |r_+r_+\rangle\langle r_+r_+|\,\Big) \\ & + \frac{\sqrt{2}|\Omega|}{2}\Big(\, |B_+\rangle\langle 00| + |00\rangle\langle B_+| + |r_+r_+\rangle\langle B_+| + |B_+\rangle\langle r_+r_+|\,\Big), \end{aligned} \tag{4.12}$$

a Doppler-free Hamiltonian (see Fig. 4.1).

The ability to suppress motional error via this Doppler-free configuration is a key benefit of the adiabatic gate approach. For comparison, consider the effects of the same error Hamiltonians on a gate protocol based on fast pulses [54]. Such a gate involves the application of resonant lasers on one atom at a time in a series of unitary evolutions: a π-pulse excites a control qubit in one logical state to the $|r\rangle$ state followed by a 2π-pulse applied to the target qubit; the control qubit is then de-excited by another π-pulse. During its time $T = 2\pi/\Omega$ in the Rydberg state, the control qubit freely evolves, resulting in a phase accumulation due to the Doppler shift, $\exp(-2\pi i\frac{k_L p}{m\Omega})$. This error is first-order in p, as in the

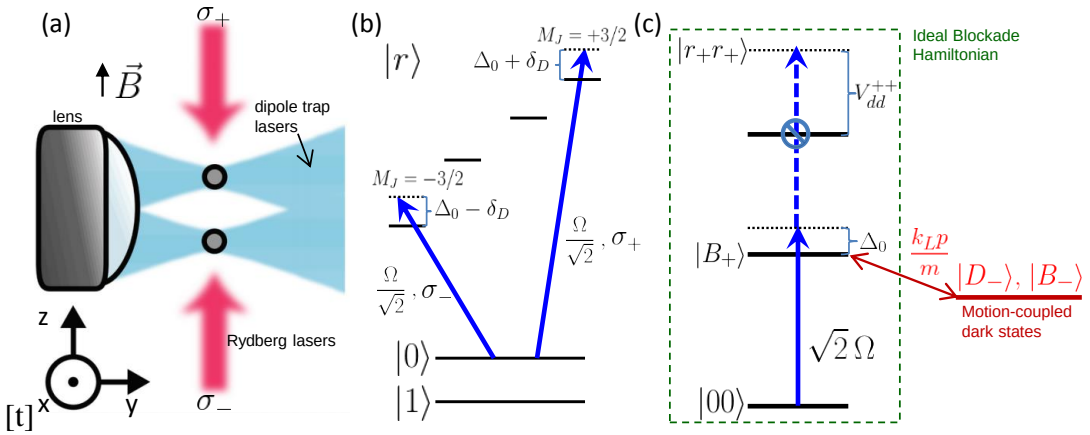

Figure 4.3: (a) Schematic for the "Doppler-free" configuration. Two cesium atoms are trapped and cooled in dipole traps, several μm apart. During the CPHASE gate, the trapping lasers are turned off and the atoms are illuminated by two counterpropagating, 319 nm Rydberg lasers. The two Rydberg lasers have opposite circular polarizations, so they couple the atoms to orthogonal magnetic sublevels of the Rydberg manifold. Both Rydberg lasers propagate along the interatomic separation axis; a bias magnetic field ensures that this coincides with the atomic quantization axis. (b) In each atom, counterpropagating lasers couple the logical-$|0\rangle$ state to the $m_J = \pm\frac{3}{2}$ magnetic sublevels of the $|84P_{3/2}\rangle$ Rydberg manifold. The two lasers have the same Rabi rate $\Omega/\sqrt{2}$ and detuning from resonance Δ_0, but experience opposite Doppler shifts, $\delta_D \equiv k_L p/m$. Zeeman splitting should be made large enough that coupling to $m_J = \pm\frac{1}{2}$ can be neglected. (c) In the two-atom basis, the states $|00\rangle$, $|B_+\rangle$, and $|r_+r_+\rangle$ are coupled by the ideal blockade Hamiltonian with no Doppler shifts. Instead, motional noise manifests as a coupling to the dark state $|D_+\rangle$. Because $|D_+\rangle$ is outside the ideal adiabatic basis, we can suppress the effects of this coupling through adiabatic evolution.

single-laser adiabatic protocol. Using the counter-propagating σ_+/σ_- laser geometry, the situation is similar, except that now each atom evolves according to the Hamiltonian H_A, Eq. (4.10). During the time T the off-diagonal terms of the Hamiltonian cause the control qubit to evolve from $|r_+\rangle$ to $\cos(2\pi\frac{k_L p}{m\Omega})|r_+\rangle + \sin(2\pi\frac{k_L p}{m\Omega})|r_-\rangle$. Any population transferred to $|r_-\rangle$ will be uncoupled from the de-exciting π-pulse, and this leads loss of probability amplitude that is first-order in p. The fast pulse scheme cannot be made "Doppler-free" to first order. In contrast, adiabatic evolution suppresses population transfer to states outside the 3×3 ideal block, so this population loss is greatly reduced; it only manifests as a

second-order energy perturbation, which leads to errors a factor of $\sim \frac{k_{LP}}{m\Omega}$ smaller.

In addition to the effect of finite momentum spread, recent work has shown that the Rydberg interaction itself can lead to further two-body decoherence when the blockade is imperfect [89]. Because the dipole-dipole energy V_{dd} varies with interatomic distance, it can produce an interatomic force when the system is in $|rr\rangle$. In our case, the effect of the force is captured by V_{grad}, Eq. (4.5), which does not change in the Doppler-free geometry. The perturbation on the dressed ground state is $\langle\widetilde{00}|\, V_{grad}\, |\widetilde{00}\rangle = |c_{rr}|^2 fracdV_{dd}dz(z-\bar{z})$, leads to a displacement on the relative momentum of atoms in this state, $\delta p_{rel} = \int_0^T |c_{rr}(t)|^2 \frac{dV_{dd}}{dz} dt$. Higher order perturbations take the system out of its dressed ground state to some excited state $|e\rangle$; as long as the evolution remains adiabatic, they are suppressed by an extra order of $|\langle e|\, V_{grad}\, |\widetilde{00}\rangle|/\Delta E$. For a near "perfect blockade," where $|V_{dd}| \gg \Delta, \Omega$, and $c_{rr} \approx 0$, this force can be neglected entirely.

4.4 Simulated Gate Fidelities

To evaluate the performance of the gate, we use as our metric the fidelity to produce the desired output given an input of all the logical states, $|\psi_0\rangle = (u_H \otimes u_H)\,|00\rangle$, where u_H is the Hadamard gate. This fidelity $\mathcal{F} = \langle\psi_{tar}|\,\rho_{out}\,|\psi_{tar}\rangle$, where $|\psi_{tar}\rangle$ is the target state obtained through a combination of local unitaries and an ideal CZ gate, $|\psi_{tar}\rangle = U_{CZ}\,|\psi_0\rangle = \frac{1}{2}(|11\rangle + |10\rangle + |01\rangle - |00\rangle)$, while ρ_{out} is the actual state in the logical space produced in the presence of the error sources described above: nonadiabatic dressing, decay of the Rydberg state, Doppler shift, and dipole-dipole forces for an imperfect blockade,

$$\rho_{out} = \mathrm{Tr}_{\mathrm{ext}}\left[e^{-i|00\rangle\langle 00|\otimes\delta p_{rel} z} U_{\mathrm{eff}} \left(|\psi_0\rangle\langle\psi_0| \otimes \rho^{\mathrm{ext}}\right) U_{\mathrm{eff}}^{\dagger} \times e^{i|00\rangle\langle 00|\otimes\delta p_{rel} z}\right]. \tag{4.13}$$

Here ρ^{ext} is the thermal state associated with the "external" (motional) degrees of freedom, δp_{rel} is the total momentum displacement caused by the dipole force, and U_{eff} is the total effective action of the gate including all decoherence sources other than the dipole-dipole

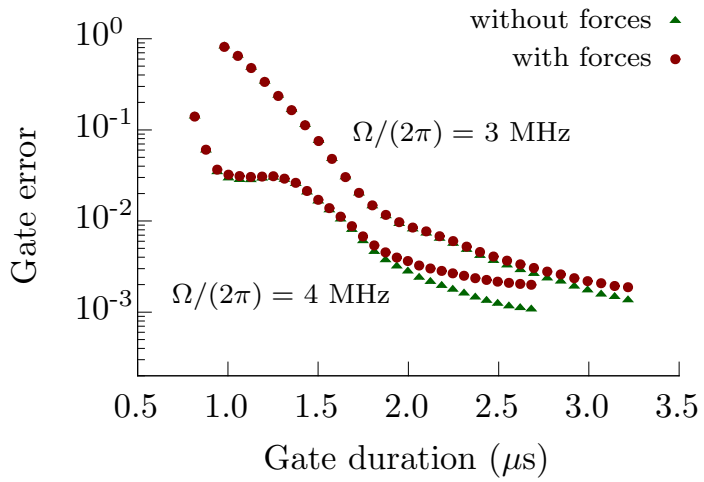

Figure 4.4: Simulated gate error rates $(1-\mathcal{F})$ as a function of adiabatic ramp time. The upper pair of curves were generated with the parameters given in Fig. 4.2, while the lower curves used a higher Rabi rate for the exciting laser. Ignoring interatomic forces but including all other errors (green triangles), the higher Rabi rate improves both gate speed and fidelity. Including interatomic forces (red circles), any gain in fidelity from the increased speed is offset by stronger forces owing to a larger $|rr\rangle$ population when the blockade is imperfect. This suggests that beyond a certain threshold, increased laser power requires a commensurately stronger blockade interaction in order to improve fidelity.

force. It is nonunitary due to the non-Hermitian Hamiltonian arising from decay of the Rydberg state and thus we treat the map as generally non-trace-preserving. We are able to separate out the effects of the dipole force through a first-order Baker-Campbell-Hausdorff expansion; since H_0 commutes with momentum displacements, all higher-order terms will scale as the products of already small error Hamiltonians and can be ignored. Because U_{eff} does not couple different logical states, it is convenient to expand $\mathcal{F}$ in the logical basis, giving

$$\mathcal{F} = \frac{1}{4} \sum_{x,y,x',y'} (-1)^{\delta_{xy,00} - \delta_{x'y',00}} \langle xy| \rho_{out} |x'y'\rangle \tag{4.14}$$

where $|xy\rangle$ are over the two-qubit logical states.

To understand the effects of atomic motion on gate errors, consider the contribution to

the fidelity from each of the matrix elements in Eq. (4.14) under the assumption of perfect adiabatic evolution of the dressed states. When both atoms are in the logical-1 state, we assume no coupling to the laser, and thus there is no error contribution from $\langle 11|\,\rho_{out}\,|11\rangle$. When both atoms are in the logical-0 state, both photon scattering and motional effects come into play. Motional dephasing has no effect on populations, only photon scattering contributes error on the diagonal terms of ρ_{out},

$$\langle\widetilde{00}|\,\rho_{out}\,|\widetilde{00}\rangle = \frac{1}{4}e^{-\gamma T}, \tag{4.15}$$

where the factor $e^{-\gamma T}$ accounts for loss due to the finite lifetime of the Rydberg state $\gamma T = \Gamma\int_0^T \left(|c_B(t')|^2 + 2|c_{rr}(t')|^2\right)dt'$. On the other hand, the off-diagonal terms are affected by both loss and dephasing, leaving

$$\begin{aligned}\langle 11|\rho_{out}\,|widetilde00\rangle &= -\frac{1}{4}e^{-\gamma T/2}\int dP_{cm}dp_{rel}\,e^{-i\phi_{Dop}} \\ &\quad\times\langle P_{cm},p_{rel}|\,\rho^{ext}\,|P_{cm},p_{rel}\rangle \\ &= -\frac{1}{4}\,e^{-\gamma T/2}\int dP_{cm}dp_{rel}\,e^{-i\phi_{Dop}}\frac{e^{-\frac{p_{cm}^2}{4\Delta p_{th}^2}}e^{-\frac{p_{rel}^2}{\Delta p_{th}^2}}}{4\pi\Delta p_{th}^2}.\end{aligned} \tag{4.16}$$

We have assumed a thermal state of motion associated with the initial trapped atom of mass m with mean vibrational quantum number $\bar{n}$, with $\Delta p_{th}^2 = (\bar{n}+1/2)m\omega_{osc}$. Since Doppler effects do not couple different velocities, this thermal state can be treated as a classical velocity distribution to obtain the above expression. The additional phase, $e^{-i\phi_{Dop}}$, is due to perturbation of the dressed ground state energy arising from the Doppler shift,

$$\begin{aligned}\phi_{Dop}(P_{cm},p_{rel}) \equiv \int_0^T \Bigg(&\langle\widetilde{00}(t')|\,V_{Dop}\,|\widetilde{00}(t')\rangle \\ &+\sum_e \frac{\left|\langle e|\,V_{Dop}\,|\widetilde{00}(t')\rangle\right|^2}{\langle\widetilde{00}(t')|\,H_0\,|\widetilde{00}(t')\rangle - \langle e|\,H_0\,|e\rangle}\Bigg)dt'.\end{aligned} \tag{4.17}$$

With a single coupling laser the correction to the light shift, Eq. (4.8), is first order in p, and Eq. (4.16) can be integrated analytically. This leads to a reduction in the fidelity of

order $e^{-(\bar{n}+1/2)\eta(\omega_{osc}T)^2}$, where $\eta = E_{recoil}/\hbar\omega_{osc}$ is the Lamb-Dicke parameter. For example, using the parameters in Fig. 4.2 and $\bar{n} = 5$, we find that the $\langle 11|\,\rho_{out}\,|00\rangle$ coherence is reduced to ~ 0.90 of its original value due to Doppler effects — an order of magnitude more decoherence than from any other source. In contrast, with the Doppler-free configuration, the first order correction vanishes, thereby strongly suppressing the effect of the Doppler shift. The $|01\rangle$ and $|10\rangle$ states experience similar Doppler perturbations to their single atom light shifts, which are generally different from the light shifts on $|00\rangle$. This implies that the coherences between $\{|01\rangle, |10\rangle\}$ and $\{|11\rangle, |00\rangle\}$ are also significantly reduced by Doppler effects, and the Doppler-free configuration likewise suppresses these decoherences.

The effect of the dipole-dipole force is seen in the coherences $\langle xy|\,\rho_{out}\,|00\rangle$, where $xy \neq 00$. Because atoms in $|00\rangle$ will experience a relative momentum kick when the blockade is imperfect and they are both excited into the Rydberg state, this local basis state will contain "which way" information relative to the other basis states. Tracing over the motional degrees of freedom, this leads to a reduction of the coherences,

$$\begin{aligned}\langle xy|\,\rho_{out}\,|00\rangle &\propto \mathrm{Tr}_{\mathrm{ext}}\left[e^{-i\delta p_{rel}z}\rho_{rel}^{\mathrm{ext}}\right] \\ &= \int dp_{rel}\,\langle p_{rel}+\delta p_{rel}|\,\rho_{rel}^{\mathrm{ext}}\,|p_{rel}\rangle = e^{-\frac{(\bar{n}+1/2)\delta p_{rel}^2}{2M\omega}}.\end{aligned} \tag{4.18}$$

Because δp_{rel} scales with $|rr\rangle$ population, this decoherence provides a strong penalty for increasing the exciting laser power beyond the point of "breaking" the blockade (see Fig. 4.4). For this reason, strong blockade interactions as well as high Rabi rates will be required to achieve very high fidelities.

Finally, the gate's fidelity is reduced by imperfect adiabatic following. Diabatic transitions during the ramps to and from resonance generally cause both population loss and dephasing for each atom's $|0\rangle$ state, so nearly every element of ρ_{out} is affected. The magnitude of the resulting fidelity loss must be found by numerical simulation, but because adiabaticity is basically independent of motional noise, the simulation can be performed quickly using only electronic degrees of freedom.

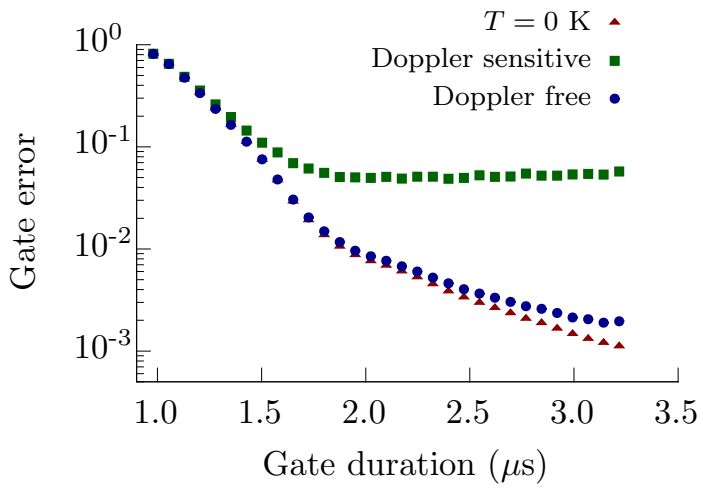

Figure 4.5: Simulated gate error rates $(1-\mathcal{F})$ as a function of adiabatic ramp time. For comparison, the red triangle curve ignores motional effects and includes errors due solely to diabatic transitions and finite Rydberg lifetime. For ramp times below ~ 1.5 μs, all curves predict low fidelities because the gate is not adiabatic. As the ramp time and adiabaticity are increased, other error sources become limiting factors. Including all error sources while using the Doppler-free configuration (blue circles), we can reach error rates of $\sim 2\times 10^{-3}$, with finite blockade strength as the primary fidelity-limiting factor. By contrast, the single-laser configuration (green squares) suffers more than an order of magnitude greater error than its counterparts.

To calculate the fidelity according to Eq. (4.14), we simulate the evolution according to the (non-Hermitian) time-dependent Schrödinger equation governed by H_{eff}. This generates the (non-trace-preserving) evolution U_{eff}, accounting for errors due to imperfect adiabatic evolution, loss of atoms due to excitation to the Rydberg state, and decoherence due to thermal spread of Doppler shifts. We use the simulated excitation to $|rr\rangle$ to calculate the relative momentum kick given to atoms due to the dipole-dipole force, and from this include the additional decoherence effect described in Eq. (4.18).

As an example, we take the parameters given in Fig. 4.2. This requires a ramp time on the order of 1 μs to stay adiabatic, so that one can perform a CPHASE gate in $\sim$ 2.3 μs. Putting together all of the error sources discussed, we calculate a gate infidelity

of $1-\mathcal{F} \sim 2\times 10^{-3}$ for the Doppler-free configuration. The gate error arises in small part from the second-order effect of Doppler shifts and finite Rydberg lifetime, but it is dominated by interatomic dipole forces owing to an imperfect blockade (see Fig. 4.5). By contrast, without the Doppler-free configuration, the same parameters give an infidelity of $1-\mathcal{F} \sim .04$, almost all of which is due to the spread in Doppler shifts.

4.5 Conclusion

We have studied a method for robustly implementing a CZ gate between neutral cesium atoms based on adiabatic dressing of the ground state via the Rydberg blockade. The main advantage of this approach is that it strongly suppresses random phases between bright- and dark-state superpositions that arise due to atomic motion. In addition, by employing two counterpropagating Rydberg lasers in a σ_+/σ_- configuration, one can eliminate the Doppler shift to first order. All effects of thermal motion then take the form of coupling to a dark state outside the ideal blockade subspace, which is suppressed by an energy gap during adiabatic evolution. When both adiabatic dressing and the Doppler-free configuration are used together, errors from thermal motion are reduced by more than an order of magnitude compared to either strategy used alone.

With motional errors reduced in this way, the main remaining source of error is entanglement between internal and external degrees of freedom due to dipole-dipole forces when the Rydberg blockade is imperfect. Such error is highly nonlinear in laser power; it can be kept small as long as the Rydberg blockade is nearly perfect, but increases rapidly when laser power is increased beyond the point of breaking the blockade. This implies that the available blockade strength sets an upper limit on useful laser power, which in turn limits both the fidelity and speed of the gate. If the blockade shift can be increased by bringing atoms into closer proximity or by the appropriate choice of Rydberg levels, the gate errors will be limited solely by finite Rydberg lifetime.

As a final note, we have considered here gates performed while atoms are untrapped and fall ballistically. Recapturing the atoms after the gate will generally cause the atoms to heat [90]. This effect is not reflected in our error estimates because it does not affect the fidelity of any one gate, but it could increase decoherence if multiple gates are performed successively with no re-cooling in between. In principle, all of these errors would be substantially reduced in a "magic trap" which traps electronic-ground-state and Rydberg atoms equivalently [91]. In that case, cooling the atoms to the vibrational ground state would completely remove Doppler shifts as well as suppress decoherence due to the dipole-dipole force in an imperfect blockade, providing a potential path to high-fidelity quantum logic.

Chapter 5

Symmetric Control

While the logic gate described above can be used as a component of a universal quantum computer, it is at its heart only a two-body operation. The dressed-Rydberg interaction can also be used in an inherently many-body context, to produce entangled ensemble states. Beyond their intrinsic interest as highly non-classical states, entangled many-body states are a valuable resource for quantum information. Premade entangled states can be used to simplify the tasks of quantum computation [92] and error correction [93]. Many-body entanglement is also a crucial ingredient in metrology beyond the standard quantum limit [94] and schemes for encoding logical qubits [95].

The group of Poul Jessen has pioneered techniques for control of high-dimensional qudits encoded in the internal hyperfine magnetic sublevels of cesium [96, 97, 98, 14]. In this chapter, we build on that work by applying the same control techniques to the collective states of atomic ensembles. Specifically, we are interested in *symmetric* control of ensembles, in which we produce some entangled state by applying a Hamiltonian that acts on every atom in the ensemble equivalently. Such restricted dynamics still allow for the creation of interesting entangled states, but have lower experimental requirements than completely arbitrary control. Symmetric many-body control has been shown in ionic [7]

and photonic [99] systems, and has been proposed for Bose-Einstein condensates [100]. Here, we describe a method for symmetric many-body control of ensembles of neutral atoms.

5.1 The Jaynes-Cummings Hamiltonian

We consider as our system a collection of N ^{133}Cs atoms, all packed within a volume whose radius is smaller than the Rydberg blockade radius. As in previous chapters, each atom's logical states are encoded in the clock states, $|0\rangle \equiv |6S_{1/2}; F = 3, M_F = 0\rangle$ and $|1\rangle \equiv |6S_{1/2}; F = 4, M_F = 0\rangle$. The ensemble is uniformly illuminated by a laser, coupling $|1\rangle$ to $|r\rangle$ in every atom with the same Rabi frequency Ω_r and detuning Δ_r. The Hamiltonian for this system is a generalization of the two-body expression in Eq. (2.12). In the frame rotating at the laser frequency and units with $\hbar = 1$,

$$H^{(i)} = E_{HF} |1\rangle \langle 1|^{(i)} + (E_{HF} - \Delta_r) |r\rangle \langle r|^{(i)} + \frac{\Omega_r}{2} \left(|r\rangle \langle 1|^{(i)} + |1\rangle \langle r|^{(i)} \right), \tag{5.1}$$

$$H = \sum_{i=1}^{N} H^{(i)} + V_{DD}, \tag{5.2}$$

where E_{HF} is the ground-state hyperfine splitting and V_{DD} is the Hamiltonian describing the EDDI-induced blockade interaction. If we assume a perfect blockade, this Hamiltonian is symmetric under the exchange of any two atoms, so we can restrict our attention to symmetric states, i.e. states that are unchanged by any permutation of atom labeling. Because a symmetric state cannot, by definition, specify which atoms are in which states, it can be described entirely by specifying *how many* atoms are in each state – that is, how many atoms are in each of $|0\rangle$, $|1\rangle$, and $|r\rangle$. Because the total number of atoms is fixed at N, the number of atoms in $|0\rangle$ is always equal to N minus the number of atoms in the other two states, and so is not an additional degree of freedom. Thus, for any given N, a basis for the symmetric subspace can be compactly denoted by two indices: the number of atoms n_r in the $|r\rangle$ state, and the number of atoms n in the $|1\rangle$ state.

The blockade Hamiltonian, V_{DD}, acts to modify the energies of states with $n_r > 1$. Following the arguments of Sec. 2.3, the effect of this is to suppress the simultaneous excitation of multiple Rydberg states. In the perfect blockade limit, second-and-higher excitations are prevented entirely, so V_{DD} can be conveniently accounted for by projecting into the subspace of states with $n_r \leq 1$. Rydberg excitation becomes a binary degree of freedom: either the ensemble has a collective Rydberg excitation, or it does not. We assume a perfect blockade for all analysis in the remainder of this chapter, so our state space of interest is indexed by n and a binary variable (here taking the values $\{r,g\}$) denoting the presence/absence of a Rydberg excitation. In any future analysis where an ideal blockade is not assumed, the state space cannot be truncated in this matter, and the precise structure of V_{DD} must be accounted for.

Explicitly, the basis states for the symmetric, perfectly blockaded subspace are

$$\begin{aligned} |g,n\rangle &\equiv \text{Sym.}\Big(|1\rangle^{\otimes n} \otimes |0\rangle^{\otimes N-n} \Big), \\ |r,n\rangle &\equiv \text{Sym.}\Big(|r\rangle \otimes |1\rangle^{\otimes n} \otimes |0\rangle^{\otimes N-n-1} \Big), \end{aligned} \tag{5.3}$$

where Sym. denotes symmetrization over all possible permutations. For example, if $N = 3$,

$$|r,1\rangle = \frac{1}{\sqrt{6}}\Big(|r10\rangle + |r01\rangle + |1r0\rangle + |10r\rangle + |0r1\rangle + |01r\rangle \Big). \tag{5.4}$$

In the literature, the symmetric ground states $|g,n\rangle$ are often referred to as the "Dicke states" for N qubits, following from Dicke's seminal work on symmetric ensembles of two-level atoms [101].

The Rydberg laser excites atoms from $|1\rangle$ into $|r\rangle$ (and vice-versa), so it couples every ground state $|g,n\rangle$ to its Rydberg counterpart $|r,n-1\rangle$. As shown in Eq. (2.16), the collective coupling of n atoms to a Rydberg state simultaneously is enhanced by a factor of $\sqrt{n}$ over the single-atom coupling strength, so the total Hamiltonian in the symmetric basis is

$$\begin{aligned} H = \sum_{n=0}^{N} & nE_{HF} \,|g,n\rangle\langle g,n| + (nE_{HF} - \Delta_r)\,|r,n-1\rangle\langle r,n-1| \\ & + \frac{\sqrt{n}\Omega_r}{2}\Big(|r,n-1\rangle\langle g,n| + |g,n\rangle\langle r,n-1| \Big). \end{aligned} \tag{5.5}$$

This expression is similar in form to the familiar Jaynes-Cummings (JC) Hamiltonian [102]; in fact, it is known [103] that the two Hamiltonians can be made isomorphic with the appropriate transformations, as we now show. In second quantized form, we take the all-atoms-in-$|0\rangle$ state, $|g,0\rangle$, to be the "vacuum" state. Let $\hat{a}_1^\dagger$ be a *bosonic* operator that creates one atom in the $|1\rangle$ state, symmetrically across the ensemble. Let $\hat{c}_r^\dagger$ be a *fermionic* operator that creates one atom in the $|r\rangle$ state, again symmetrically across the ensemble. The analog of the Pauli exclusion principle allows only one Rydberg atom at a time, enforcing a perfect blockade. Rewriting Eq. (5.5) in terms of these operators gives

$$H = E_{HF}\hat{a}_1^\dagger\hat{a}_1 + (E_{HF} - \Delta_r)\hat{c}_r^\dagger\hat{c}_r + \frac{\Omega_r}{2}(\hat{c}_r^\dagger\hat{a}_1 + \hat{a}_1^\dagger\hat{c}_r). \tag{5.6}$$

We now make the Jordan-Wigner transformation [104] from fermionic to Pauli operators; since we have one "mode", $\hat{c}_r \to \hat{\sigma}_-$, $\hat{c}_r^\dagger \to \hat{\sigma}_+$, and $\hat{c}_r^\dagger\hat{c}_r \to \hat{\sigma}_+\hat{\sigma}_- = (1+\hat{\sigma}_z)/2$. Substitution into Eq. (5.6) yields the Jaynes-Cummings Hamiltonian,

$$H_{JC} = E_{HF}\hat{a}_1^\dagger\hat{a}_1 + (E_{HF} - \Delta_r)\left(\frac{1+\hat{\sigma}_z}{2}\right) + \frac{\Omega_r}{2}(\hat{\sigma}_+\hat{a}_1 + \hat{a}_1^\dagger\hat{\sigma}_-). \tag{5.7}$$

Here, the presence or absence of a Rydberg excitation plays the role of the two-level spin in a conventional JC cavity, and atoms in $|1\rangle$ take the place of photons as the system's bosonic degree of freedom. Other aspects of the isomorphism between the JC model and the symmetric-Rydberg-coupled ensemble are given in Table 5.1.

Returning to the form of Eq. (5.5), we see that this Hamiltonian is block-diagonal, with 2×2 blocks each consisting of some $|g,n\rangle$ and its partner $|r,n-1\rangle$. Each block takes the same form as a single-atom light shift Hamiltonian, but with a $\sqrt{n}$ enhancement of the laser's effective Rabi rate. These blocks can be diagonalized exactly, giving

$$\begin{aligned} H = \sum_{n=0}^{N} &(nE_{HF} - \frac{\Delta_r}{2})(|\widetilde{r,n}\rangle\langle\widetilde{r,n}| + |\widetilde{g,n}\rangle\langle\widetilde{g,n}|) \\ &- \frac{\mathrm{sign}(\Delta_r)}{2}\sqrt{\Delta_r^2 + n\Omega_r^2}(|\widetilde{r,n}\rangle\langle\widetilde{r,n}| - |\widetilde{g,n}\rangle\langle\widetilde{g,n}|), \end{aligned} \tag{5.8}$$

where tildes denote dressed states, i.e. eigenstates of the 2×2 blocks. As in previous chapters, we quantify the entangling power of this Hamiltonian by the nonlinear light

	Cavity QED	Symmetric Atomic Ensemble
Two-level system	2-level atom, $\{\|g\rangle, \|e\rangle\}$	Presence or absence of Rydberg excitation
Bosonic mode	$\|n\rangle = n$ photons in cavity mode	$\|n\rangle = n$ atoms in logical-$\|1\rangle$
Vacuum	$\|0\rangle$ =no photons in cavity mode	$\|0\rangle^{\otimes N}$ =all atoms in logical-$\|0\rangle$
Bare states	$\|g\rangle\otimes\|n\rangle, \|e\rangle\otimes\|n\rangle$	Sym.($\|0\rangle^{\otimes N-n}\|1\rangle^{\otimes n}$), Sym.($\|0\rangle^{\otimes N-n}\|1\rangle^{\otimes n-1}\|r\rangle$)
Dressed states	$\alpha\|g,n\rangle \pm \beta\|e,n-1\rangle$	Sym.($\|0\rangle^{\otimes N-n}\|1\rangle^{\otimes n-1}[\alpha\|1\rangle \pm \beta\|r\rangle$)
Frequency scales	boson= ω_c, 2-level= ω_{eg}, Rabi= g	boson= E_{HF}, 2-level= $E_{HF}-\Delta_r$, Rabi= Ω_r
Qubit control	Rabi oscillations on 2-level atom	Rabi oscillations on collective Rydberg excitation
Boson control	Field driving cavity mode	Rabi oscillations between clock states

Table 5.1: Isomorphism between the cavity QED Jaynes-Cummings model and symmetrically controlled atomic ensembles.

shift,

$$\kappa = \langle\widetilde{g,2}|H|\widetilde{g,2}\rangle - 2\langle\widetilde{g,1}|H|\widetilde{g,1}\rangle. \tag{5.9}$$

Since we are no longer dealing with just two qubits at a time, there are further modifications to the light shift strength for $n \geq 3$; nevertheless, the two-body κ provides a good estimate of the speed at which we can perform control. In the weak dressing limit, H becomes quadratic, and its nonlinearity is fully described by κ according to

$$\langle\widetilde{g,n}|H|\widetilde{g,n}\rangle - n\langle\widetilde{g,1}|H|\widetilde{g,1}\rangle \approx (n^2-n)\frac{\kappa}{2}. \tag{5.10}$$

Depending on the system's initial state, H_{JC} by itself can generate entanglement over time. In particular, H_{JC} can turn the spin coherent state $|\Psi_{SC}\rangle = (|0\rangle+|1\rangle)^{\otimes N}/2^{N/2}$ into a highly entangled cat-like state. More precisely, we consider applying H_{JC} to the dressed counterpart $|\widetilde{\Psi}_{SC}\rangle$ of the bare state $|\Psi_{SC}\rangle$, defined by

$$\begin{aligned} |\Psi_{SC}\rangle &= \left(\frac{|0\rangle+|1\rangle}{\sqrt{2}}\right)^{\otimes N} = \sum_{n=0}^{N} c_n|g,n\rangle \\ |\widetilde{\Psi}_{SC}\rangle &\equiv \sum_{n=0}^{N} c_n|\widetilde{g,n}\rangle, \end{aligned} \tag{5.11}$$

where c_n are the expansion coefficients of $|\Psi_{SC}\rangle$ in the Dicke basis. Single-atom light

shifts can be used to cancel the linear component of Eq. (5.10), leaving $H \approx n^2\kappa/2$. Applying this H to $|\widetilde{\Psi}_{SC}\rangle$ for a time t leaves us with

$$e^{-iHt/2}|\widetilde{\Psi}_{SC}\rangle = \sum_{n=0}^{N} c_n e^{-in^2\kappa t/2}|\widetilde{g,n}\rangle, \tag{5.12}$$

that is, each $|\widetilde{g,n}\rangle$ accumulates a phase of $-n^2\kappa t/2$. If we choose $t = \pi/\kappa$, the accumulated phase becomes $-n^2\pi/2$; modulo 2π, this is zero for all even n and $-\pi/2$ for all odd n. This generates the state

$$\begin{aligned} e^{-iH\pi/(2\kappa)}|\widetilde{\Psi}_{SC}\rangle &= \sum_{\text{even } n}^{N} c_n|\widetilde{g,n}\rangle - i\sum_{\text{odd } n}^{N} c_n|\widetilde{g,n}\rangle \\ &= \frac{1-i}{\sqrt{2}}\left(\frac{1+i}{\sqrt{2}}\sum_{\text{even } n}^{N} c_n|\widetilde{g,n}\rangle + \frac{1-i}{\sqrt{2}}\sum_{\text{odd } n}^{N} c_n|\widetilde{g,n}\rangle\right) \\ &= \frac{1-i}{2}\sum_{n=0}^{N} c_n|\widetilde{g,n}\rangle + \frac{1+i}{2}\sum_{n=0}^{N}(-1)^n c_n|\widetilde{g,n}\rangle \\ &= e^{-i\pi/4}\frac{|\widetilde{\Psi}_{SC}\rangle + i\sigma_x^{\otimes N}|\widetilde{\Psi}_{SC}\rangle}{\sqrt{2}}. \end{aligned} \tag{5.13}$$

Up to phases, this state is a superposition of $|\widetilde{\Psi}_{SC}\rangle$ with its parity image formed by flipping every qubit, i.e. a cat state. Note that the time required for this method does not depend on n; maximal entanglement can be generated in time π/κ regardless of the number of qubits.

H_{JC} can also produce cat-like states when dressing is strong, although the mechanism is less obvious. When a conventional, cavity JC system is prepared in the state $|g\rangle \otimes |\alpha\rangle$, with the atom in its ground state and the field in a coherent state, the system's Rabi oscillations will exhibit collapse and revival [105], going from high- to zero-amplitude and back in time $t \approx 2\pi\sqrt{\bar{n}}/g$. Gea-Banacloche showed [106] that if the mean photon number $\bar{n} = |\alpha|^2 \gg 1$, at half the revival time the atom and field become disentangled again; their state becomes $(|g\rangle + i|e\rangle) \otimes (|\tilde{\alpha}\rangle + |-\tilde{\alpha}\rangle)$, where $|\pm\tilde{\alpha}\rangle$ are slightly squeezed coherent states. At this time, the field is a near-cat state of the cavity mode. In the context of the symmetric Rydberg ensemble, for large N, an initial preparation in $|\Psi_{SC}\rangle$ is analogous to the initial condition $|g\rangle \otimes |\alpha\rangle$. If we allow the system to undergo Rabi oscillations in the

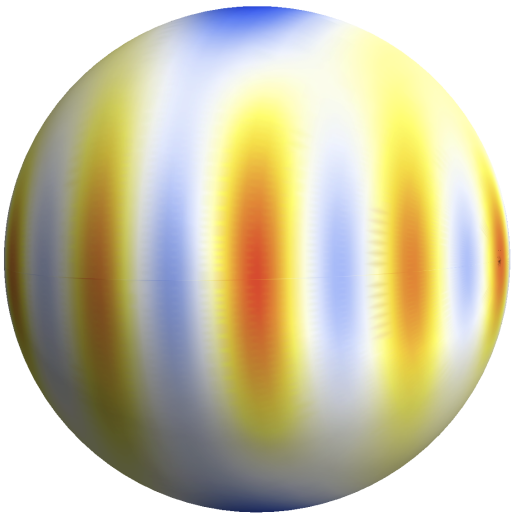

Figure 5.1: Entanglement generated in the collapse of JC Rabi oscillations. We simulate 10 atoms initially prepared in a separable state, $(|0\rangle + |1\rangle)^{\otimes 10}$, and allowed to evolve under H_{JC} with the Rydberg laser on resonance ($E_{HF} - \Delta_r = 0$). At a time $t = \pi\sqrt{5}/\Omega_r$, the system approaches a cat-like state. The spin Wigner function plotted here exhibits large interference fringes (blue positive, red negative), indicating strong entanglement.

presence of a Rydberg laser, then at half the revival time we expect the state to be close to $\text{Sym.}\big((|0\rangle + i\,|r\rangle) \otimes (|0\rangle^{\otimes N-1} + |1\rangle^{\otimes N-1})\big)$. A final pulse, with the appropriate phase, will remove the single Rydberg excitation, and return a cat-like state — such as the one shown in Fig. 5.1 — in the ground subspace. Both collapse and revival [107] and the resulting generation of cat states in a related protocol [41] have been proposed previously.

5.2 Controllability

The above protocols employed the JC Hamiltonian to generate particular entangled states. Here, we pursue the broader objective of complete control over an atomic ensemble's Dicke subspace. Most generally, a system is considered controllable if one can perform

an arbitrary quantum transformation on it through appropriate choices of the system's free parameters. We specifically consider *state-to-state* controllability; that is, we want the ability to map any given input state of our ensemble to an arbitrary but fixed output state. Other types of control, such as generating arbitrary unitary transformations [108, 109], are mostly beyond the scope of this chapter but use many of the same tools and concepts as state-to-state control.

By itself, the JC Hamiltonian only includes pairwise couplings between states, so it must be augmented with some additional "control Hamiltonian" to achieve full quantum control. This kind of control has long been studied in cavity QED [110] and ion traps [111], and more recently in circuit QED [112]. In all cases, the JC Hamiltonian itself is the same, but the nature of the control Hamiltonian can vary depending on what sorts of interactions are most straightforwardly implemented in a given system. Some of these control procedures can be directly ported over to the atomic ensemble platform. For example, Law and Eberly showed [113] how arbitrary superposition states of N photons in a cavity could be synthesized through a series of SU(2) rotations on the "carrier and red-sidebands" of the JC model, a procedure implemented in ion traps [114] and circuit QED [115]. In atomic ensembles, the carrier and red-sideband transitions, $|g,n\rangle \leftrightarrow |r,n\rangle$ and $|g,n\rangle \leftrightarrow |r,n-1\rangle$ respectively, are equivalent to lasers driving the $|0\rangle \leftrightarrow |r\rangle$ and $|1\rangle \leftrightarrow |r\rangle$ transitions respectively, in the presence of the Rydberg blockade. One can employ this protocol to create arbitrary states in the Dicke-subspace.

The mapping to symmetric atomic ensembles considered here gives also gives us a unique control option: by driving atomic ground-state transitions, we can act directly on the system's bosonic degree of freedom and perform transformations not possible with a true harmonic oscillator. For our control Hamiltonian, we consider a microwave (or Raman transition) coupling $|0\rangle$ to $|1\rangle$ in each atom. The Rabi rate and detuning are fixed at $\Omega_{\mu w}$ and $\Delta_{\mu w}$, respectively, but we allow the microwave's phase to vary as a function of time. As with the Rydberg laser, we assume the microwave illuminates the entire ensemble

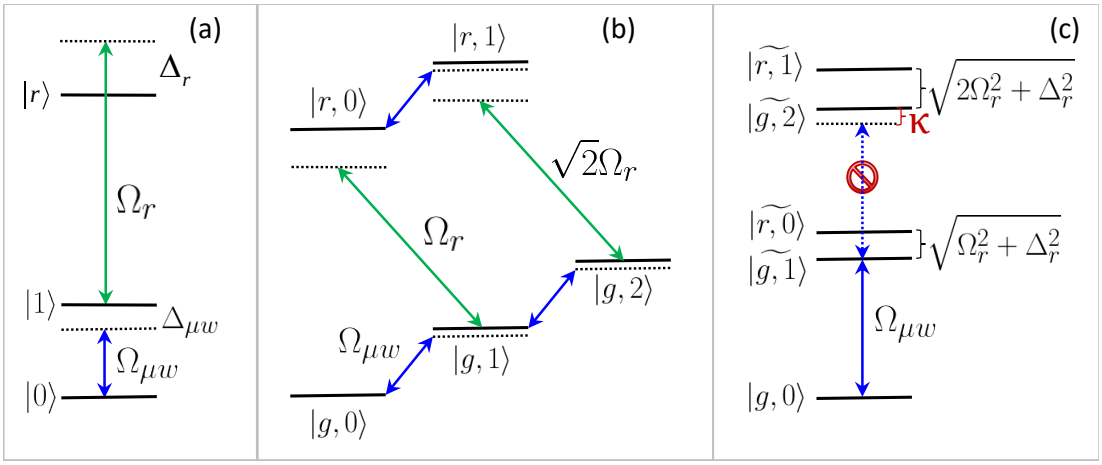

Figure 5.2: The Rydberg JC Hamiltonian for two atoms. (a) Basic level structure for the three-level atom: a qubit is encoded in the ground hyperfine states, and logical-$|1\rangle$ is optically coupled to a Rydberg state, while logical-$|0\rangle$ is far off resonance and effectively uncoupled. (b) Bare states for two atoms, symmetrically coupled, under the condition of a perfect blockade. (c) Two-atom dressed states, which exhibit the nonlinear JC ladder energy-level structure. If the microwave is tuned to resonance for flipping one qubit (in the presence of a light shift), double spin flips are blockaded by the dressing interaction κ. The microwave thus drives transitions from $|g,0\rangle$ to $|\widetilde{g,1}\rangle$, a maximally entangled state in the dressed-ground subspace.

symmetrically, so it is described by a sum of identical Hamiltonians acting on all atoms individually. In the frame rotating at the microwave frequency,

$$H_{\mu w}(t) = \sum_{i=1}^{N} \frac{\Omega_{\mu w}}{2}(e^{-i\phi(t)}\,|1\rangle\langle 0|^{(i)} + e^{i\phi(t)}\,|0\rangle\langle 1|^{(i)}) - \omega_{\mu w}\,|1\rangle\langle 1|^{(i)}, \tag{5.14}$$

where $\phi(t)$ is an arbitrary, time-dependent phase and $\omega_{\mu w} = E_{HF} + \Delta_{\mu w}$ is the microwave frequency. (The full $\omega_{\mu w}$ appears instead of $\Delta_{\mu w}$ as a coefficient because E_{HF} is already included in H_{JC}.) The full Hamiltonian, including both $H_{\mu w}$ and H_{JC} from Eq. (5.8), is illustrated for two atoms in Fig. 5.2. The effect of $H_{\mu w}$ is most easily understood in a "pseudo-spin" picture, in which we map the Dicke states to an effective spin with $J = N/2$. In this picture, the collective spin operator $\mathbf{J}$ is related to the Pauli operators on each qubit $\vec{\sigma}^{(i)}$ according to $\mathbf{J} = \sum_{i=1}^{N} \vec{\sigma}^{(i)}/2$. The Dicke states are the simultaneous eigenstates of $\mathbf{J}$ and J_z, so that $|g,n\rangle \to |J = N/2, M = n - N/2, g\rangle$. Similarly, the symmetric Rydberg

states can be mapped to an effective spin with $J = (N-1)/2$: setting aside the single Rydberg atom, we treat the remaining $N-1$ atoms as comprising another set of Dicke states, and we can say $|r,n\rangle \rightarrow |J = (N-1)/2, M = n-(N-1)/2, r\rangle$. Putting Eq. (5.14) in this basis, we find that the effect of the microwave is to rotate the pseudo-spin about the x- or y-axis, depending on its phase:

$$H_{\mu w}(t) = \Omega_{\mu w}(\cos(\phi(t))J_x + \sin(\phi(t))J_y) - \omega_{\mu w}(J_z + \frac{N}{2}). \tag{5.15}$$

Note that this Hamiltonian applies the same set of operators to both the ground and Rydberg pseudo-spins; the two manifolds undergo SU(2) rotations in parallel.

To see how such bosonic driving can be used with with the nonlinearity associated with the Rydberg blockade to create entanglement, consider the two-qubit scheme shown in Fig. 5.2c. Both qubits begin in the logical-$|0\rangle$ state, while logical-$|1\rangle$ is strongly dressed by the Rydberg laser. The microwave is tuned to resonance including the single-atom light shift (i.e. $\Delta_{\mu w} = (\Delta_r - \sqrt{\Omega_r^2 + \Delta_r^2})/2$), so it resonantly drives the $|g,0\rangle \leftrightarrow |\widetilde{g,1}\rangle$ transition. On the other hand, the $|\widetilde{g,1}\rangle \leftrightarrow |\widetilde{g,2}\rangle$ transition is off resonance by the two-body light shift κ. If $\kappa \gg \Omega_r$, the interaction creates a "spin-flip blockade", suppressing excitation to $|\widetilde{g,2}\rangle$. This is the dressed-ground analog of the optically induced Rydberg blockade. With a perfect spin-flip blockade, a π-pulse can take $|g,0\rangle$ to $|\widetilde{g,1}\rangle$; adiabatically ramping down the Rydberg laser then transfers this state to the bare $|g,1\rangle$, leaving maximal entanglement between ground-state atoms. This procedure was used by Jau *et al.* to generate a two-atom Bell state with fidelity $\geq 81\%$ [39]. For an arbitrary number of atoms, the equivalent procedure would generate a W-state, defined in Eq. 2.15.

While the spin-flip blockade provides a simple way to generate entanglement with a constant microwave phase, it has limitations. Firstly, it is slow, since the duration of the microwave pulse must be sufficiently long compared to $1/\kappa$ in order to avoid off-resonant excitation and thus induce a near perfect spin-flip blockade. In addition, we can achieve a much broader range of control tasks if ϕ is allowed to vary with time. In fact, an arbitrary $\phi(t)$ makes the system completely controllable; that is, for any states $|\Psi_{in}\rangle$ and $|\Psi_{out}\rangle$ in

the symmetric space of N atoms, there exists a phase as a function of time $\phi(t)$ such that the total Hamiltonian $H_{JC} + H_{\mu w}(t)$ generates a unitary mapping $|\Psi_{in}\rangle$ to $|\Psi_{out}\rangle$. In the weak-dressing limit of Eq. 5.10, the effective Hamiltonian acting on the dressed ground states takes the form of a "single-axis twisting" interaction on the collective spin [116],

$$H \approx \left(\frac{\Omega_r^2}{4\Delta_r^2} - \frac{N\kappa}{2}\right) J_z + \frac{\kappa}{2} J_z^2. \tag{5.16}$$

This nonlinear term is a well-known collective entangling Hamiltonian that allows for arbitrary control in the symmetric subspace with the addition of SU(2) rotations [96, 117]. We now outline a proof that a JC Rydberg ensemble with microwaves is controllable more generally, even with strong dressing; the full proof is given in Appendix A.

5.2.1 Outline of Controllability Proof

The conditions for controllability of a system can be understood in terms of the available set of Hamiltonians that can be manipulated, as initially laid out for finite dimensional Hilbert spaces in [118]. For a general control task, the total Hamiltonian consists of a constant part H_0 and one or more adjustable parts H_j,

$$H(t) = H_0 + \sum_j c_j(t) H_j, \tag{5.17}$$

where $c_j(t)$ are the time-dependent control parameters. A d-dimensional system described by such a Hamiltonian is controllable if we can choose $c_j(t)$ to generate any element of the Lie group SU(d). This, in turn, is true if and only if the operators $\{H_0, H_1, ..., H_n\}$ are a generating set for the Lie algebra $\mathfrak{su}(d)$. The algebra generated by a set of operators consists of all operators that can be reached by repeated commutations and linear combinations of the original set elements. Thus, the system is controllable if and only if we can create all elements of $\mathfrak{su}(d)$ through commutators and linear combinations of $\{H_0, H_1, ..., H_n\}$.

If d is fixed and finite, the controllability of a system can be checked algorithmically. One can calculate the commutators of all pairs of operators in $\{H_0, H_1, ..., H_n\}$, keeping track of which results are linearly independent of the original set. The new, independent operators are added to the set, and the process is repeated until the set spans $\mathfrak{su}(d)$ (meaning the system is controllable) or no more linearly independent operators can be generated (meaning it is not). In a system with variable d, like the N-atom ensemble considered here, the situation is more complicated; since there is no upper bound to the size of $\mathfrak{su}(d)$, we cannot generate all of its elements through brute force. Instead, we need some form of induction to guarantee that $\mathfrak{su}(d)$ can be generated regardless of d. Here, we rely on two theorems due to Seth Merkel [119], which together tell us that our entire system is controllable if we can generate J_x, J_z, and any irreducible, rank-two tensor, on the ground and Rydberg manifolds independently. This means that instead of having to generate all of $\mathfrak{su}(d)$, we need only generate six operators: two sets of $\{J_x, J_z, T\}$, projected onto the ground and Rydberg manifolds, where T is such a rank-two tensor.

We begin our proof with the system's full Hamiltonian, which is a combination of Eqs. 5.5 and 5.14: $H(t) = H_{JC} + H_{\mu w}(t)$. Fitting this to the form of Eq. (5.17), we find that

$$\begin{aligned} H_0 =& -\Delta_{\mu w}(J_z + \frac{N}{2}) + (E_{HF} - \Delta_r)P_r \\ &+ \sum_{n=1}^{N} \frac{\sqrt{n}\Omega_r}{2}(|g,n\rangle\langle r,n-1| + |r,n-1\rangle\langle g,n|), \\ H_1 =& J_x, \quad c_1(t) = \Omega_{\mu w}\cos(\phi(t)) \\ H_2 =& J_y, \quad c_2(t) = \Omega_{\mu w}\sin(\phi(t)), \end{aligned} \tag{5.18}$$

where $P_{r(g)} = \sum_n |n, r(g)\rangle\langle n, r(g)|$ is the projector onto the Rydberg (ground) manifold. Qualitatively, H_0 encapsulates the nonlinear couplings of H_{JC} and the effects of detuning, leaving J_x and J_y as our variable control Hamiltonians. Immediately, we have $[J_x, J_y] = iJ_z$, which acts symmetrically on the two manifolds. By twice commuting J_z with the nonlinear component of H_0, we obtain its antisymmetric counterpart; up to linear combinations with

previous operators,

$$[H_0,[H_0,J_z]] \rightarrow P_r J_z P_r - P_g J_z P_g. \tag{5.19}$$

Adding (subtracting) this with the original, symmetric J_z leaves J_z projected onto the Rydberg (ground) manifold. One more commutator allows us to spread the ground- and Rydberg-projections to J_x,

$$[P_{r(g)} J_z P_{r(g)}, J_y] = -iP_{r(g)} J_x P_{r(g)}. \tag{5.20}$$

Now that we have projected versions of J_x and J_z, we need to produce an irreducible, rank-two T, which we can do with a few more successive commutators. In Appendix A, we show each commutator individually; here, we write them as a single step for compactness. Again up to linear combinations with previous operators,

$$\Big[\big[[[H_0,J_z],P_g J_z P_g],[H_0,J_z]\big],P_g J_x P_g\Big] \rightarrow P_g\left(J_z J_y + J_y J_z\right) P_g, \tag{5.21}$$

which is an irreducible, rank-two tensor operator. The same formula holds with P_g replaced by P_r, giving us a T projected onto both manifolds. Combined with projected J_x and J_z and the theorems cited above, this shows that our system is completely controllable.

5.3 Finding Optimal Parameters

Given that the system is controllable, we know there is always some (non-unique) waveform $\phi(t)$ that will produce a given target state; our goal is to find such a $\phi(t)$. In general, $\phi(t)$ can be any function of time, but here we restrict it to a piecewise constant function to simplify analysis. Under this restriction, a control waveform consists of a sequence of s "phase steps" of length Δt, for a total run time of $T = s\Delta t$. The full range of possible control waveforms can thus be parameterized by an s-dimensional vector, $\vec{\phi}$. Our goal is to find a $\vec{\phi}$ such that the fidelity of the output state with some target state, $\mathcal{F}(\vec{\phi},\Psi_{tar})$, is sufficiently high. This procedure has been successfully employed to find optimal waveforms for control of hyperfine qudits [96].

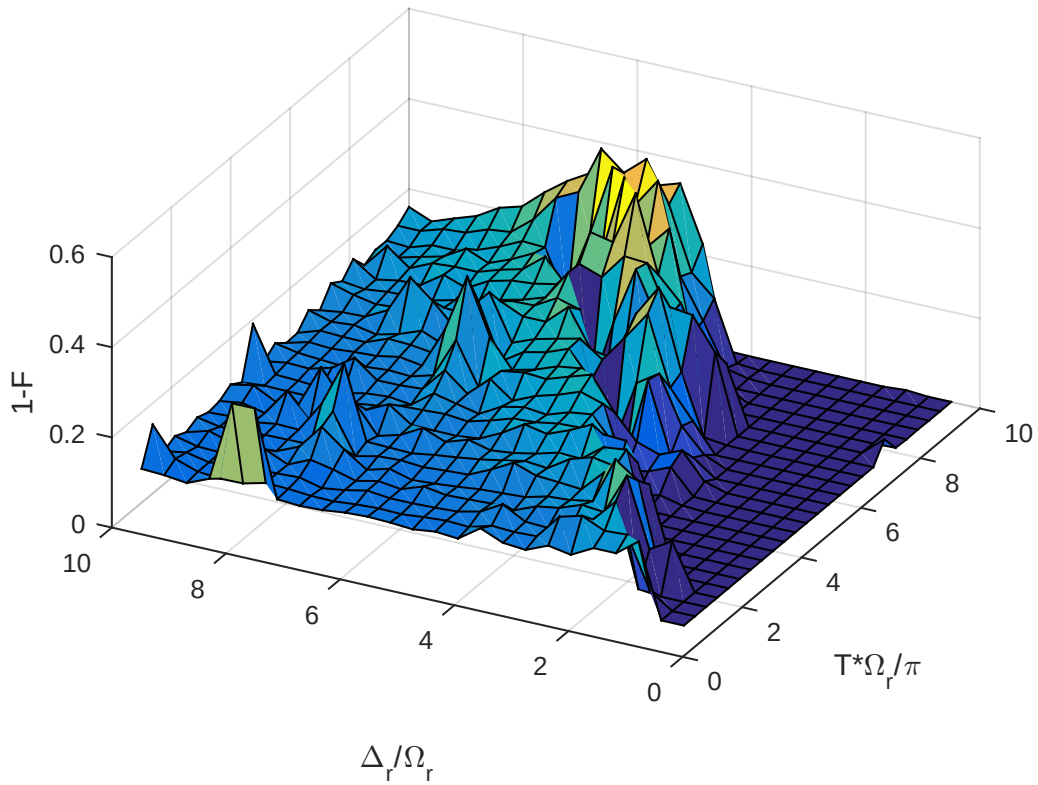

Figure 5.3: Simulated control fidelities to produce a six-atom cat state in the dressed basis, starting from $|g,0\rangle$. Plotted as a function of Rydberg laser detuning Δ_r and total run time T, using the minimum of $s = 25$ phase steps. For any given Δ_r, there is a well-delineated control time above which fidelity is arbitrarily close to one. As Δ_r increases, κ decreases and the minimum control time gets longer.

We accomplish this with a GRAPE gradient ascent algorithm [120], beginning with a random $\vec{\phi}$ (i.e. s random phases). We calculate the gradient of $\mathcal{F}$ at $\vec{\phi}$, which tells us the "direction" in parameter space in which fidelity is increasing most rapidly. We then adjust our vector of phases in this direction, updating it according to

$$\vec{\phi} \to \vec{\phi} + \delta \nabla \mathcal{F}|_{\vec{\phi}}, \tag{5.22}$$

where δ is a small parameter, chosen empirically to optimize run time. This procedure is repeated many times, and $\vec{\phi}$ "climbs" the fidelity landscape until $\mathcal{F}$ either exceeds some predetermined threshold or stops improving. If both T and s are sufficiently large, the

control landscape has no local maxima, and GRAPE can produce fidelities arbitrarily close to one [121]. The results are illustrated in Fig. 5.3 for a six-atom ensemble.

The choice of optimal parameters such as laser/microwave power and detuning will depend on fundamental sources of error such as decoherence as well as practical experimental concerns. In particular, it is desirable to minimize the runtime and complexity of our protocol, so we typically seek the minimum T and s needed for high-fidelity control. It takes $2d-1$ real numbers to specify a d-dimensional target state, so this puts a lower bound on s. For N atoms including both ground and Rydberg symmetric states, this gives $s \geq 4N+1$. In practice, we find that this inequality can often be saturated. More heuristically, we can predict that $\kappa T \gtrsim \pi$, the minimum time required to generate strong entanglement. Whether this bound can be saturated depends on the choice of experimental parameters, as detailed below.

To achieve optimal fidelities, we seek to perform control in the shortest possible time compared with our system's decoherence time. Decoherence due to photon scattering, occurring at rate γ, is of particular concern, so maximizing κ/γ is an important goal. Since κ is higher-order in Ω_r and Δ_r than the single-body light shift, scaling as Ω_r^4/Δ_r^3 in the weak dressing regime, it is highly sensitive to the power and detuning of the Rydberg laser. By contrast, γ scales as Ω_r^2/Δ_r^2, so $\kappa/\gamma \propto \Omega_r^2/\Delta_r$ increases with increased laser power and decreased detuning. Based on this, increasing our dressing strength — especially by increasing Ω_r — is a winning strategy in the fight against decoherence, and has the added benefit of reducing total run time. This suggests that maximum laser power, at or near resonance, is the best choice of parameters.

No matter how short the control time is in principle, though, we must still have s phase steps, and quickly switching a microwave's phase is not a trivial task. With resonant laser power that yields a Rabi frequency of a few MHz and ~ 10 atoms, the required Δt per phase step can easily shrink to tens of nanoseconds or less. Demands on the microwave switch time are even more strict, since the phase must change quickly enough to preserve the

piecewise-constant approximation of $\phi(t)$. The number of steps in the control waveform, then, is a primary limiting factor in the speed and feasibility of this protocol. Step quantity is also an important obstacle to the *scaling* of this type of control. κ is independent of N, so we do not expect the minimum T to depend strongly on the size of the ensemble; indeed, at least in the weak dressing regime described by Eq. (5.10), it is known that a cat state can be produced in time π/κ independent of atom number [106, 122]. On the other hand, s scales linearly with N, so fitting all the required steps into the available T is increasingly difficult with larger ensembles. Any speed limit on phase switching, no matter how small, will eventually limit the total control time beyond a certain N.

Once control time is limited by experimental restrictions on Δt rather than by κ, increasing κ is no longer beneficial; stronger dressing will only increase γ and other sources of error without any offsetting benefit. On the other hand, as long as κ is the limiting factor, increased dressing strength is advantageous as per the reasoning above. The optimal parameter regime, therefore, is highly dependent on the particulars of the experiment: Δ_r should be large enough to make the two speed limits match, if possible, but no higher.

5.4 Ground State Control

Having characterized some of the fundamental limitations of optimal microwave control, we can better understand its advantages and disadvantages compared to other entanglement generating protocols. In particular, we wish to compare optimal microwave control with the two other protocols described in Sec. 5.1: weakly-dressed spin squeezing in the quadratic κ regime, and Gea-Banacloche cat state generation through Rabi oscillation collapse and revival. Regardless of the protocol used, minimizing the run time to avoid decoherence is a primary goal, so we first compare speed limits. As noted above, weakly-dressed spin squeezing produces a maximally entangled state in exactly $t = \pi/\kappa$. Through simulations, we find that optimal microwave control also works in $t = \pi/\kappa$ for all

Scheme	Run Time	Regime	Target States	Control Steps
Weakly-dressed squeezing	π/κ	$\Delta_r \gg \Omega_r$	squeezed or cat states	1
Gea-Banacloche	$\sim .21\sqrt{N}\pi/\kappa$	$\Delta_r = 0$[1]	cat-like states only	1
Microwave control	π/κ[2]	any	any symmetric state	$4N+1$

Table 5.2: Quantum defects for low-ℓ Rydberg states of Alkali atoms, from [3]. At higher ℓ, so little of the valence electron's wavefunction penetrates the core that quantum defects become negligible.

but the smallest detunings; when $\Delta_r \lesssim \Omega_r/4$, symmetries in the control Hamiltonian make the control time somewhat longer [2] (see Fig. 5.4). The Gea-Banacloche protocol takes $t = \pi\sqrt{\bar{n}}/\Omega_r$; since it requires a resonant Rydberg laser, we can put this in terms of κ by solving Eq. (5.9) with $\Delta_r = 0$. Plugging in the result, and noting that $\bar{n} = N/2$ for a spin coherent state, we find $t = (\sqrt{2}-1)\sqrt{N}\pi/(2\kappa) \approx 0.21\sqrt{N}\pi/\kappa$.

Importantly, the run times for all three protocols scale as κ^{-1}. This supports our previous intuition that the rate of entanglement generation is generally linear in the strength of the Rydberg-dressing interaction. Despite this parallel, however, the three speed limits differ in significant ways. While weakly-dressed spin squeezing is limited only by κ, it requires Δ_r to be large enough for κ to be approximately quadratic. In this limit, κ itself will generally be small, resulting in slow entanglement generation compared with protocols that can work close to resonance. The Gea-Banacloche protocol, meanwhile, works on resonance (so κ is maximized), but its run time also scales with $\sqrt{N}$, which can be significant for large ensembles. Neglecting the phase step requirement, optimal microwave control works in $t = \pi/\kappa$ even with near-resonant dressing, making it the fastest of the three schemes. On the other hand, when N is high enough for phase switching time to be the limiting factor, the control time will increase linearly with N. This implies that the other, "single-step" protocols will be more effective for sufficiently large ensembles.

[1]The Gea-Banacloche protocol only works exactly in the large-N limit. For finite N, it produces a state with some residual entanglement between the system's spin and bosonic degrees of freedom.

[2]For very small detuning, $\Delta_r \lesssim \Omega_r/4$, microwave control time is increased due to Hamiltonian symmetries.

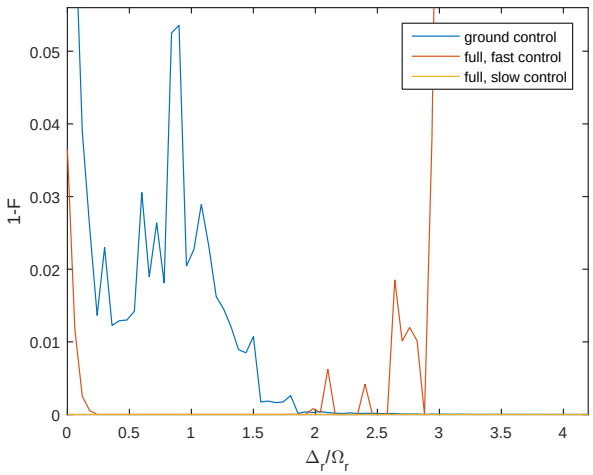

Figure 5.4: Simulated infidelities, $1-\mathcal{F}$, to produce a seven-atom cat state in the dressed basis, starting from $|g,0\rangle$, as a function of Rydberg laser detuning. The blue curve shows control with run time π/κ and only $2N+1=15$ phase steps, associated with control solely on the dressed-ground manifold; it fails at small Δ_r, but succeeds when Δ_r is large enough to suppress dressed Rydberg population. The red curve uses run time π/κ and the $4N+1=29$ phase steps needed for control on the full space of dressed-ground and dressed-Rydberg states, so it can succeed with smaller Δ_r. At the smallest detunings, the symmetries in our system's geometry make control more difficult [2], while at large detunings, the vast numerical mismatch between $\Omega_{\mu w}$ and κ becomes unwieldy; in both cases $T=\pi/\kappa$ is no longer sufficient. The yellow curve shows full Hilbert space control with a more generous $T=3\pi/\kappa$, and succeeds in all regimes.

Finally, both the weakly-dressed spin squeezing and Gea-Banacloche protocols can only generate a small subset of entangled states, so optimal control based on the JC Hamiltonian plus microwaves is the only protocol of the three that can generate arbitrary target states. These differences are summarized in Table 5.4.

Since phase switching requirements limit the speed of microwave control — both in absolute terms and relative to other entanglement protocols — control could be significantly accelerated by reducing the number of phase steps needed. At first glance this may seem impossible, since our system occupies a $2N+1$ dimensional Hilbert space and we need $4N+1$ parameters just to specify a target state. However, if our goal is to produce

an entangled *ground* state (i.e. a superposition of Dicke states), the Hilbert space of interest is practically cut in half, and we need only $2N+1$ parameters to specify a target in it. The dressed Rydberg states, while essential to producing the entangling interaction, are not in our target state subspace and thus correspond to extraneous degrees of freedom. If we can suppress population of these states, our control waveforms can be shortened to accommodate only the dressed ground states we are interested in controlling.

To see how this can be accomplished, we return to Eq. (5.14), describing the effect of coupling induced by the microwave or Raman transition. In the bare basis, the microwave couples $|0\rangle$ to $|1\rangle$ without acting on $|r\rangle$, so $\langle r,m|\, H_{\mu w}\, |g,n\rangle = 0$. By contrast, dressed Rydberg states $|\widetilde{r,n}\rangle$ have some $|g,n\rangle$ character, so the microwave coupling between dressed ground and Rydberg states is nonzero. The mixing angle in Eq. (2.18) gives us the rough magnitude of this coupling in the weak dressing regime:

$$\langle \widetilde{r,m}|\, H_{\mu w}\, |\widetilde{g,n}\rangle \sim \sin\left(\frac{1}{2}\arctan\left(\frac{\sqrt{n}\Omega_r}{\Delta_r}\right)\right) \langle g,m|\, H_{\mu w}\, |g,n\rangle \sim \frac{\sqrt{n}\Omega_r}{\Delta_r} \langle g,m|\, H_{\mu w}\, |g,n\rangle\,. \tag{5.23}$$

The effective Rabi rate is suppressed by an order of Ω_r/Δ_r for dressed ground-Rydberg compared to ground-ground couplings. Excitation is also suppressed by detuning; again in the weak dressing limit, the saturation parameter is on the order of $\Omega_{\mu w}^2/\Delta_r^2$. Combining these suppressing factors, we find that the microwave will approximately preserve dressed-ground population as long as

$$\frac{\sqrt{N}\Omega_r\Omega_{\mu w}^2}{\Delta_r^3} \ll 1. \tag{5.24}$$

Under this condition, we find that dressed ground control can be performed in $2N+1$ phase steps, as expected. Because this condition requires a large Δ_r, it goes hand in hand with a small κ, so ground manifold control is much slower than full Hilbert space control if phase steps are allowed to be arbitrarily short. Whether the tradeoff between κ and s is worthwhile will depend on the N and the minimum Δt in a given experiment.

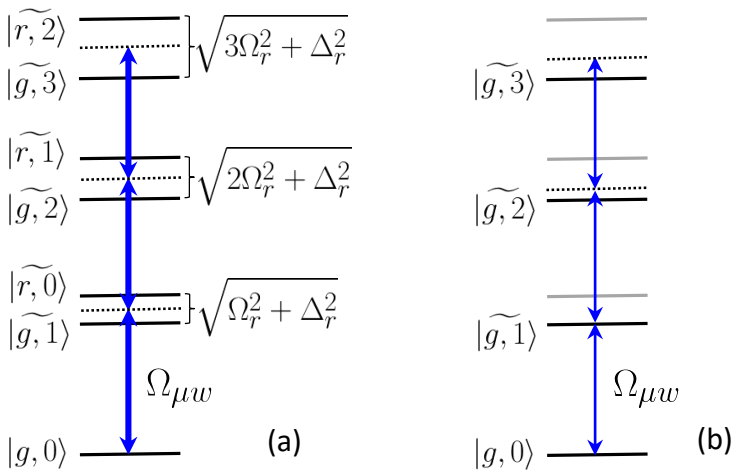

Figure 5.5: Optimal parameters for different control regimes. (a) For full Hilbert space control, both ground and Rydberg levels need to be strongly coupled. The microwave should be tuned between the two manifolds, and $\Omega_{\mu w}$ should be larger than the energy gap $\sqrt{n\Omega_r^2+\Delta_r^2}$. (b) For dressed ground control, ground-ground coupling should be much stronger than ground-Rydberg coupling. The microwave should be tuned near ground-ground resonance (including the single-atom light shift), and $\Omega_{\mu w}$ should be too small to overcome the energy gap.

Dressed ground and full Hilbert space control are optimized with qualitatively different choices of microwave and laser parameters. In full control, the system traverses all parts of Hilbert space to get to its destination, so all states must be coupled strongly to each other. Since the light shift provides a gap between the ground and Rydberg manifolds of order $\sim \sqrt{\Omega_r^2+\Delta_r^2}$, $\Omega_{\mu w}$ needs to be at least that large to strongly drive both transitions at once. Both to relax this condition and to maximize interaction strength, Δ_r should be kept small compared to Ω_r. The microwave resonance should also be tuned around halfway between the ground and Rydberg states in the rotating frame ($\omega_{\mu w} \approx E_{HF} + \Delta_R/2$), so that one manifold is not coupled much more strongly than the other. If these conditions are not met, population transfer between the ground and Rydberg manifolds will be slow compared to intra-manifold transfer, and control can be bottlenecked by population getting "stuck" in the Rydberg manifold for extended periods.

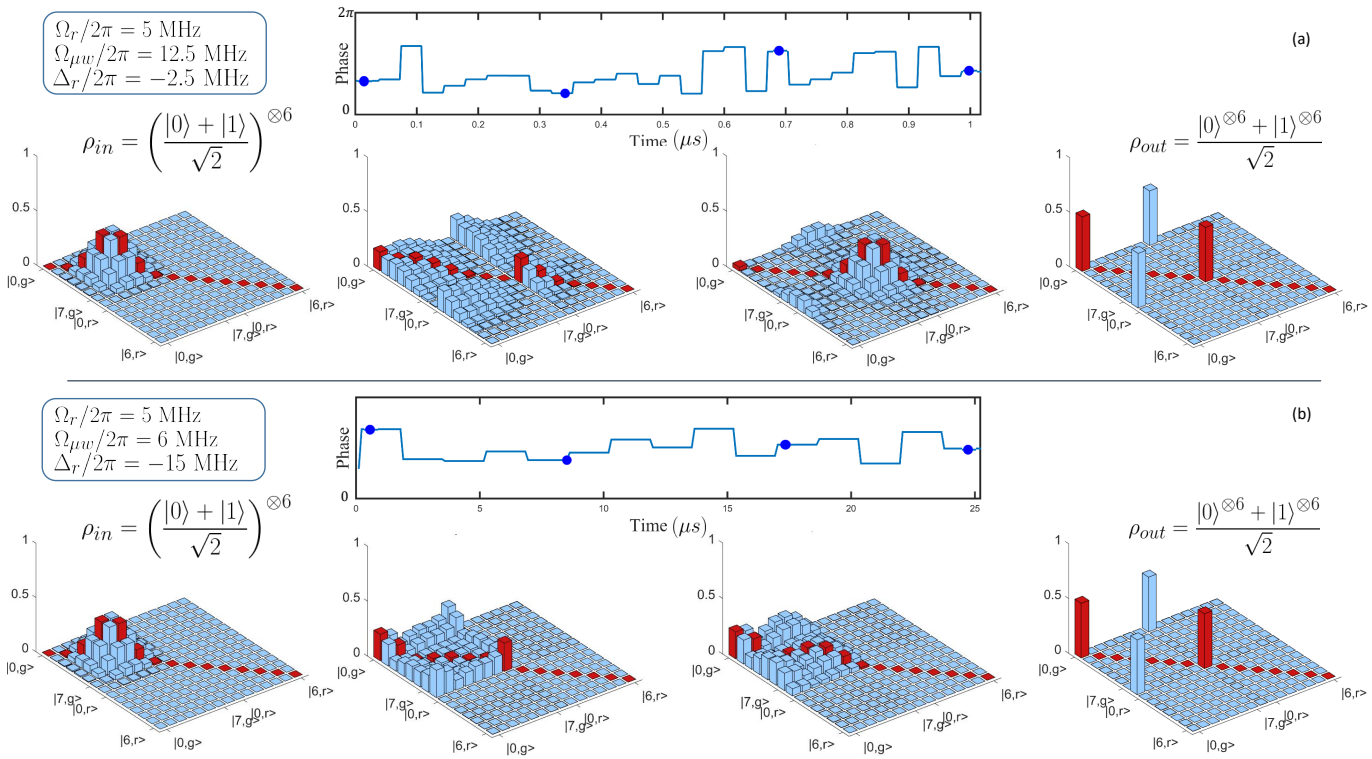

Figure 5.6: Producing a seven-atom cat state in the dressed ground basis. Line plots show the piecewise-constant microwave phase, $\phi(t)$. Bar charts show the real part of the 15×15 density matrix at various moments in time. (a) Full Hilbert space control. Microwave power is large compared to Rydberg laser detuning, so all 15 symmetric states are populated during control. Consequentially, $4N + 1 = 29$ phase steps are needed, and phase switching time must be on the order of nanoseconds to achieve κ-limited control speed. (b) Dressed ground control. Microwave power is small compared to Rydberg laser detuning, and only the 8 dressed-ground states are strongly coupled. Only $2N + 1 = 15$ phase steps are needed, so demands on phase switching time are less stringent. This comes at the price of maximum speed; weaker Rydberg coupling reduces κ by more than an order of magnitude, with a commensurate increase in run time.

On the other hand, dressed ground control relies on the assumption that population will never need to be dynamically de-excited from the Rydberg manifold, so parameters should be chosen to *minimize* coupling between manifolds. $\Omega_{\mu w}$ should be small compared to the light shift gap, and a large Δ_r makes this easier to accomplish. Likewise, the microwave should be tuned near resonance with the transitions between dressed ground

states ($\omega_{\mu w} \approx E_{HF} + E_{LS1}$) to allow strong ground-ground coupling with minimal ground-Rydberg coupling. The microwave power also needs to be on the order of κ in order for Eq. (5.24) to hold over the entire control time, so $\Omega_{\mu w}$ should scale inversely with Δ_r. If these conditions are not met, significant population can leak into the Rydberg manifold, where $2N+1$ free parameters are no longer enough to bring it back to ground. These parameter differences are outlined in Fig. 5.4. Dressed ground and full Hilbert space control provide two complimentary methods that function well in different regimes, as demonstrated in Fig. 5.4 for seven atoms. The two methods produce waveforms — each optimal for its respective parameter regime — that reach the same destination in Hilbert space but take qualitatively different paths to get there. This is illustrated in Fig. 5.6, which shows how both types of control can be used to produce a seven-atom cat state.

5.5 Conclusion

The isomorphism between symmetric, Rydberg blockaded ensembles of neutral atoms and the Jaynes-Cummings model provides a powerful framework for studying control in such ensembles. Many existing techniques for JC control can be borrowed from other platforms, for both specific and general control tasks. Symetrically controlled atomic ensembles also admit novel control techniques, based on SU(2) rotation of the "bosonic" degree of freedom, with no natural analogue in conventional cavity JC. With a time-varying phase, such rotation is sufficient to drive arbitrary control in the Dicke subspace.

The time required for this type of control is limited by two factors: the interaction strength between qubits, and the phase-switching speed required to produce a control waveform. The former depends on the available power and detuning of the Rydberg-coupling laser, while the latter depends on the size of the Hilbert space being controlled. To relax the limits set by phase-switching speed, we introduced the idea of dressed ground control, in which the system's dressed excited states are suppressed to remove extraneous

degrees of freedom. We showed how microwave parameters can be chosen to implement dressed-ground control in neutral atom ensembles, but the idea of control on a restricted Hilbert space could be a useful tool in any platform whose state space admits some partitioning.

All the analysis in this chapter assumed an ideal blockade and neglected experimental imperfections, so incorporating decoherence and other imperfections is a natural direction for future study. While symmetric control can in principle work for any number of atoms given sufficient time, noise sources such as photon scattering will put a time limit on high-fidelity control and determine the maximum ensemble size that can be realistically controlled. Assuming decoherence can be managed for at least a few μs, controlling several atoms should be viable with current technology. Errors due to imperfect Rydberg blockade and Hamiltonian asymmetry will be especially interesting to explore, as they couple the ground and single-Rydberg Dicke states to a larger Hilbert space. As such, their effects might be a source of not only decoherence, but richer dynamics.

Chapter 6

Summary and Outlook

In this work, we explored the flexible entangling power of the Rydberg-dressing interaction. Using this interaction, one can convert the Rydberg blockade effect — already a broadly useful tool in the neutral atom toolbox — into a direct interaction between dressed ground states. While the physics of Rydberg interactions is rich and complex, the Rydberg-dressing interaction works by *avoiding* simultaneous excitation of multiple Rydberg atoms, so many of these complexities need not be considered. In addition to simplifying analysis, this prevents some adverse effects of strong Rydberg excitation. Because the size of the interaction depends on dressing strength as well as the Rydberg blockade itself, it can be adjusted by changing the power and/or detuning of the Rydberg-exciting laser. Such a tunable interaction can be useful as a static parameter (choosing the best interaction strength for the task at hand) or a dynamic one (varying interaction strength over the course of a single experiment). In particular, by continuously sweeping the interaction from zero- to full-strength, one can map a bare ground input state to the dressed basis for straightforward interaction. When the interaction is done, one can sweep back to zero strength, leaving pure ground-state entanglement.

The structure of the Rydberg-dressing interaction lends itself to the adiabatic model

of quantum computing, in which an entire computation is in some sense performed by going into the dressed basis. An adiabatic computation begins with a Hamiltonian whose ground state is easy to prepare. By slowly ramping to a Hamiltonian whose ground state encodes the solution to a problem, one can transform the easy-to-prepare initial state into its solution-encoding counterpart. Rydberg-dressing can provide an interaction term in the final Hamiltonian, opening the door to NP hard problems such as the 2D Ising model. Since the final Hamiltonian must be ramped up smoothly, the tunability of the Rydberg-dressing interaction is essential to this protocol. To evaluate the experimental viability of this protocol, we modeled a sample computation for 2–4 qubits, with realistic laser parameters and including photon scattering. We found that fidelities of ~ 0.99 should be achievable, and we expect that fidelities will stay acceptably high up to 10–20 qubits where classically difficult simulation is accessible.

To obtain higher fidelities, in this or any adiabatic computation, future study could focus on optimizing the shape of the control functions that connects the initial and final Hamiltonians. To remain adiabatic, the ramp speed is limited by the energy gap between ground and excited states; a ramp whose speed tracks the changing gap could offer faster, higher-fidelity computation without sacrificing adiabaticity. Alternatively, one might consider modifying the details of the Rydberg-dressing to produce interaction types beyond the $\sigma_z \otimes \sigma_z$ terms we described. For example, a scheme that employs simultaneous σ_z and σ_x interactions in the same lattice is currently under development [123]. Given a sufficiently large set of interactions, Rydberg-based AQC could be applied to problems that offer a true quantum speedup. Grover's search algorithm provides an especially attractive target for this, as an adiabatic implementation is already known [124].

If the Rydberg-dressed interaction is applied to just two qubits at a time, it can generate an entangling logic gate, which can then be incorporated into larger circuits for universal, gate model computation. In the dressed basis, the nonlinear energy shift from the interaction gives rise to an "entangling phase" that accumulates over time; with properly chosen

dressing duration, this leads to a CPHASE gate. We modeled the effects of atomic thermal motion on such gates, and showed that a "Doppler-free" setup with counterpropagating lasers could suppress their impact by more than an order of magnitude. Using this technique, we found that gate infidelities of $\sim 2 \times 10^{-3}$ should be possible. Interestingly, the Doppler-free setup does not offer the same error suppression in resonant-pulse-based gates; it only works in tandem with the intrinsic robustness of adiabatic dressing.

Since gates in this scheme require adiabatic ramps into the dressed basis and back, optimally shaped Hamiltonian transformations could improve these gates in the same way they could improve AQC. Beyond this, the basic principles of the Doppler-free scheme could be generalized to other error sources. Any coherent error that takes the form of a coupling outside the computational subspace will be naturally suppressed through adiabatic following. By modifying the gate protocol to put as many errors as possible in this form, one could make it robust against a wide range of decoherence sources. Independent of fidelity concerns, the basic gate design could also be generalized to take advantage of the Rydberg-dressing interaction's many-body character. For instance, if three atoms are dressed simultaneously, they will experience a three-body entangling shift in addition to the 3κ that we would expect from a purely pairwise interaction. This shift could be harnessed to generate a doubly-controlled-PHASE gate which, up to local unitaries, is equivalent to a Toffoli gate.

Outside the context of quantum computing, the Rydberg-dressed interaction can be used to produce many-body entangled states. In the perfect blockade limit, a symmetrically dressed ensemble of neutral atoms is isomorphic to the widely studied Jaynes-Cummings model; they are thus amenable to a range of entangling protocols developed for other Jaynes-Cummings platforms. In addition, microwaves can drive rotations in the model's bosonic sector, offering an entanglement method unique to neutral atoms. We proved that together with the nonlinearity of the Rydberg-dressed interaction, driving the system with a microwave field with time-dependent phase is sufficient to generate arbitrary

symmetric states of the ensemble. We compared this control scheme with two other protocols for Jaynes-Cummings entanglement. We found that microwave control compares favorably in terms of its flexibility and dependence on laser parameters, but that demands on the phase switching rate present a major obstacle to achieving maximum control speeds. To ameliorate this, we propose a dressed ground control scheme, in which the microwave parameters are chosen to maximize ground-ground coupling while suppressing Rydberg excitation. This halves the effective size of the Hilbert space being controlled, and by extension the number of phase steps required.

Unlike with the two quantum computing protocols above, we have not modeled errors for this control scheme in any detail. Decoherence due to system inhomogeneities (whether in the laser, microwave, or Rydberg blockade) merits special attention, as it will break the assumed symmetries of the control task; properly addressing this type of error will likely require expanding the ideal JC Hilbert space to include some asymmetric states. Given the structural parallels between our microwave control and Rydberg-dressed gate schemes, it is likely that some variant of the Doppler-free laser setup could reduce control errors. The tools of optimal control can also be used to build robustness against errors into the control waveform itself [14], so addressing these types of imperfections is both important and non-trivial. A particularly interesting possibility is engineering robustness to variations in atom number; waveforms with this type of robustness could generate ensemble states of a particular class — such as cat states — even in ensembles whose size is not precisely known.

In summary, we have shown how the Rydberg-dressing interaction can be used in three distinct, but related, quantum information processing protocols. Beyond solving interesting problems in their own right, these protocols offer insight into questions of entanglement speed and adiabatic error suppression. They also illustrate the advantages of Rydberg-dressing as an interaction mechanism, especially in terms of its tunability and robustness. Ultimately, we hope that the principles explored here will inform the application

of Rydberg-dressing to a broader range of challenges in neutral atom physics.

Appendix A

Proof: H_{JC} With Microwaves is Controllable

To reiterate from Sec. 5.2.1, the total Hamiltonian for a general control task consists of a constant part H_0 and one or more adjustable parts H_j,

$$H(t) = H_0 + \sum_j c_j(t) H_j, \tag{A.1}$$

where $c_j(t)$ are the time-dependent control parameters. A d-dimensional system described by such a Hamiltonian is controllable if and only if the operators $\{H_0, H_1, ..., H_n\}$ are a generating set for the Lie algebra $\mathfrak{su}(d)$. Therefore, we can show that a system is controllable by generating all elements of $\mathfrak{su}(d)$ through nested commutators and linear combinations of $\{H_0, H_1, ..., H_n\}$. In the case we consider here, our full Hamiltonian is a combination of Eqs. 5.5 and 5.14: $H(t) = H_{JC} + H_{\mu w}(t)$. Splitting this into constant and variable portions

gives

$$\begin{aligned} H_0 =& -\Delta_{\mu w}(J_z+\frac{N}{2})+(E_{HF}-\Delta_r)P_r \\ &+\sum_{n=1}^{N}\frac{\sqrt{n}\Omega_r}{2}(|g,n\rangle\langle r,n-1|+|r,n-1\rangle\langle g,n|), \\ H_1 =& J_x, \quad c_1(t)=\Omega_{\mu w}\cos(\phi(t)) \\ H_2 =& J_y, \quad c_2(t)=\Omega_{\mu w}\sin(\phi(t)), \end{aligned} \tag{A.2}$$

where $P_{r(g)}=\sum_n |n,r(g)\rangle\langle n,r(g)|$ is the projector onto the Rydberg (ground) manifold. Our goal is to produce the full Lie algebra for our system through commutators and linear combinations of these three Hamiltonians. Before beginning, we take three steps to simplify subsequent notation. First, we define the "coupling" portion of H_0,

$$H_C \equiv \sum_{n=1}^{N}\frac{\sqrt{n}\Omega_r}{2}(|g,n\rangle\langle r,n-1|+|r,n-1\rangle\langle g,n|). \tag{A.3}$$

Second, without loss of generality, we switch to units of energy with $\Omega_r/2=1$, leaving

$$H_0 \to H_C-\Delta_{\mu w}(J_z+\frac{N}{2})+(E_{HF}-\Delta_r)P_r. \tag{A.4}$$

Third, because the trace of H_0 will at most contribute an overall phase which can be ignored, we subtract $-\Delta_{\mu w}\frac{N}{2}+\frac{E_{HF}-\Delta_r}{2}$ from the overall energy to leave H_0 traceless:

$$H_0 \to H_C-\Delta_{\mu w}J_z+\frac{E_{HF}-\Delta_r}{2}(P_r-P_g). \tag{A.5}$$

Note that H_1 and H_2 are entirely off-diagonal operators, and so are already traceless.

Immediately, we can commute J_x and J_y to get

$$\begin{aligned} J_z &= \sum_{n=1}^{N}\Big(n|g,n\rangle\langle g,n|+(n-1)|r,n-1\rangle\langle r,n-1|\Big)-\frac{N}{2}P_g-\frac{N-1}{2}P_r \\ &= H_C^2-\frac{1}{2}P_r-\frac{N}{2}\mathbb{1}. \end{aligned} \tag{A.6}$$

Because J_z is diagonal in the $\{|g,n\rangle,|r,n\rangle\}$ basis, it commutes with the projector and iden-

tity in H_0, and their commutator is greatly simplified,

$$\begin{aligned}[H_0, J_z] &= [H_C, J_z] = [H_C, H_C^2 - \frac{1}{2}P_r - \frac{N}{2}\mathbb{1}] = -\frac{1}{2}[H_C, P_r] \\ &= \frac{1}{2}\sum_{n=1}^{N}\sqrt{n}\Big(\,|r,n-1\rangle\langle g,n| - |g,n\rangle\langle r,n-1|\,\Big) \equiv \frac{i}{2}\bar{H}_C.\end{aligned} \tag{A.7}$$

Commuting with J_z again,

$$\begin{aligned}[\bar{H}_C, J_z] =& i\sum_{n=1}^{N}\sqrt{n}\Big((n-1-\frac{N-1}{2})\,|g,n\rangle\langle r,n-1| - (n-\frac{N}{2})\,|r,n-1\rangle\langle g,n| \\ &- (n-\frac{N}{2})\,|g,n\rangle\langle r,n-1| + (n-1-\frac{N-1}{2})\,|r,n-1\rangle\langle g,n|\Big) \\ =& -\frac{1}{2}i\sum_{n=1}^{N}\sqrt{n}\Big(\,|g,n\rangle\langle r,n-1| + |r,n-1\rangle\langle g,n|\,\Big) = -\frac{1}{2}iH_C.\end{aligned} \tag{A.8}$$

We can now use H_C directly in subsequent steps, which will avoid complicating terms from the microwave and laser detunings. Our next step is to commute H_C with $\bar{H}_C$, giving

$$\begin{aligned}[H_C, \bar{H}_C] &= 2i\sum_{n=1}^{N} n\Big(\,|r,n-1\rangle\langle r,n-1| - |g,n\rangle\langle g,n|\,\Big) \\ &= 2i\Big(P_r(J_z + \frac{N-1}{2} + 1)P_r - P_g(J_z + \frac{N}{2})P_g\Big) \\ &\equiv 2i\bar{J}_z.\end{aligned} \tag{A.9}$$

This operator breaks the symmetry between the manifolds, and we can combine it with the original J_z to get operators projected onto each manifold individually,

$$J_z - \bar{J}_z = 2P_gJ_zP_g + \frac{N}{2}P_g - \frac{N+1}{2}P_r, \tag{A.10}$$

$$J_z + \bar{J}_z = 2P_rJ_zP_r - \frac{N}{2}P_g + \frac{N+1}{2}P_r. \tag{A.11}$$

Note that the projectors commute with any operator that does not couple the two manifolds, so we can ignore them when commuting these projected J_z's with other J_i's. The resulting commutators allow us to spread the ground- and Rydberg-projections to J_x and J_y,

$$[J_z - \bar{J}_z, J_j] = 2\varepsilon_{zjk}P_gJ_kP_g, \tag{A.12}$$

$$[J_z + \bar{J}_z, J_j] = 2\varepsilon_{zjk}P_rJ_kP_r, \tag{A.13}$$

where ε_{zjk} is the Levi-Civita symbol with its first index fixed as z. This gives us independent SU(2) rotations of the two manifolds.

To get from SU(2) rotation to complete control, we invoke a theorem due to Seth Merkel [119]:

Theorem 1. *Consider a manifold M that is describable by a collective pesudo-spin. Let T be an operator that has nonzero overlap with at least one irreducible, rank-two tensor operator on said spin. Then M is controllable with the Hamiltonians* $\{J_x, J_y, T\}$.

Based on this, we need to generate a rank-2 irreducible Hamiltonian for each manifold to make it controllable. This can be accomplished by commuting the projected J_z with $\bar{H}_C$:

$$\begin{aligned}
[\bar{H}_C, P_g J_z P_g] &= -i\sum_{n=1}^{N} n\sqrt{n}\Big(\,|g,n\rangle\langle r,n-1| + |r,n-1\rangle\langle g,n|\,\Big) \\
&\quad + \frac{N}{2} i\sum_{n=1}^{N}\sqrt{n}\Big(\,|g,n\rangle\langle r,n-1| + |r,n-1\rangle\langle g,n|\,\Big) \\
&\equiv -iH_C' + \frac{N}{2} iH_C
\end{aligned} \tag{A.14}$$

$$\begin{aligned}
[H_C', \bar{H}_C] &= 2i\sum_{n=1}^{N} n^2\Big(\,|r,n-1\rangle\langle r,n-1| - |g,n\rangle\langle g,n|\,\Big) \\
&= 2i\Big(P_r(J_z + \frac{N-1}{2} + 1)^2 P_r - P_g(J_z + \frac{N}{2})^2 P_g\Big) \\
&= 2i\Big(P_r J_z^2 P_r - P_g J_z^2 P_g + (N-1)P_r J_z P_r \\
&\quad - NP_g J_z P_g + \left(\frac{N+1}{2}\right)^2 P_r - \left(\frac{N}{2}\right)^2 P_g\Big).
\end{aligned} \tag{A.15}$$

This Hamiltonian has terms quadratic in n; we now condense it before commuting it with J_x to obtain a nonlinearity in the ground manifold alone. The third and fourth terms of the Hamiltonian are J_z on the ground and Rydberg manifolds, respectively, which we have already generated and can subtract away. The first, fifth, and sixth terms, meanwhile, commute with J_x, so we need only consider the second (J_z^2) term, which produces the commutator,

$$[P_g J_z^2 P_g, P_g J_x P_g] = iP_g\Big(J_z J_y + J_y J_z\Big)P_g. \tag{A.16}$$

This is an anti-commutator between two J's, so it is an irreducible rank-2 operator. The same procedure with $P_r J_z P_r$ gives a comparable operator for the Rydberg manifold, so we now have SU(2) rotations plus a rank-2 operator for both manifolds. This means that they are independently controllable.

All that remains is to join the two manifolds together, and to show that they are controllable as a whole as well as separately. For this, we invoke another theorem due to Seth Merkel [119]:

Theorem 2. *Consider two subspaces, L and M. Let $|\ell\rangle$ and $|m\rangle$ be particular states in each of these spaces, respectively. If L, M, and the subspace spanned by $\{|\ell\rangle, |m\rangle\}$ are each independently controllable, then the full space $L \oplus M$ is controllable.*

We have already shown the controllability of the two subspaces, so we just need to show controllability of any subspace consisting of one state from each. We arbitrarily choose $\{|g1\rangle, |r0\rangle\}$. Since both manifolds are controllable, we can generate any traceless Hamiltonians within them. In particular, we can generate $|g0\rangle\langle g0| - |g2\rangle\langle g2|$ on the ground manifold and $|r0\rangle\langle r0| - |r1\rangle\langle r1|$ on the Rydberg manifold. Summing these and commuting with H_C gives

$$\begin{aligned}\Big[H_C, |g0\rangle\langle g0| - (|g2\rangle\langle g2| + |r1\rangle\langle r1|) + |r0\rangle\langle r0|\Big] &= [H_C, |r0\rangle\langle r0|] \\ &= 2\Big(|g1\rangle\langle r0| - |r0\rangle\langle g1|\Big) = 2i\sigma_y\end{aligned} \tag{A.17}$$

where σ_i denotes a Pauli operator on the two-state subspace. Commuting this with the laser coupling Hamiltonian one last time,

$$[H_C, \sigma_y] = 2i\Big(|g1\rangle\langle g1| - |r0\rangle\langle r0|\Big) = 2i\sigma_z. \tag{A.18}$$

Two Pauli operators give us control over the two-state subspace, and therefore over the entire space. □

Appendix B

Boson Sampling with Distinguishable Photons

B.1 Introdution

A universal quantum computer could solve a number of important problems – such as factoring large numbers – thought to be intractable on classical devices. At present, however, building such a device is not experimentally feasible, and significant advancements are required before this changes. In the nearer term, it may be possible to build more narrowly tailored quantum devices, less flexible than a universal computer but still capable of efficiently solving one or more classically difficult problems. Aaronson and Arkhipov recently investigated one such device: the boson sampling device, or boson sampler [125]. Under ideal conditions, a boson sampler uses only linear optics and photon detection to efficiently solve a sampling problem that is classically difficult (up to widely accepted complexity-theory conjectures). Beyond potential applications to practical problems (e.g. [126]), such a device would be of theoretical interest in that it would provide experimental evidence against the Extended Church-Turing Thesis, and for the power of quantum

computing more generally.

In a real experiment, however, no boson sampler will be ideal. At best, we can hope for a boson sampler that is *close* to ideal, with imperfections small enough that its output distribution is still classically difficult to sample from. More precisely, if the magnitude of noise is characterized by some small parameter ε, there will be bounds on how large ε can be while still solving a hard problem. If these bounds depend on the size of the system, they must be taken into account when determining the scalability of the boson sampling algorithm. After all, algorithm demanding exponentially high experimental precision is no more scalable than one requiring exponential run time.

Several recent works have explored the effects of various types of noise on boson sampling, and have generally found that polynomial precision (i.e. inverse polynomial scaling of ε) is sufficient to maintain the classical hardness of the sampling problem. Specifically, polynomially small errors are known to be sufficient for unitary imperfections in the linear optical network [127], photon loss rates [128], and coherent displacements of the single-photon input states [129]. More recently, Shchesnovich showed that photon distinguishability does not interfere with the scaling of the boson sampling problem as long as the photons' wavefunction non-overlap is polynomially small [130]. In all of these works, polynomial precision is treated as an "efficient" demand in the computer science sense, analogous to the polynomial time/space requirements of any scalable algorithm. From this, it is suggested that boson sampling scales efficiently in the face of noise, or at least in the face of the specific noise types analyzed. However, we show here that polynomial precision requirements are not an unusual feature of the boson sampler; rather, polynomially small error is adequate for a broad range of quantum information tasks, including universal quantum computation. A realistic boson sampler, then, is likely to be no more scalable than a universal quantum computer without error correction.

The remainder of this appendix is organized as follows. In section B.2, we set up a per-component model of errors and use this model to analyze the classical difficulty of

simulating a noisy boson sampler. We find that in general, the sampling problem remains classically hard if the error per component scales inversely with the total number of components. In section B.3, we consider an alternative error metric, based on the probability distributions of noisy variables, and show that it likewise requires at most polynomial precision. Finally, in section B.4, we interpret these results in the context of boson sampling scalability.

B.2 Error Bounds for Scalable Boson Sampling

We begin by considering the structure of an ideal boson sampler, following [131]. Such a device takes as input a state consisting of N indistinguishable photons distributed among M modes,

$$|\Psi_{in}\rangle = \prod_{i=1}^{N} \hat{a}_i^\dagger \, |0\rangle^{\otimes M} . \tag{B.1}$$

This state is sent through a network of linear optics that transforms the photon creation operators $a_i^\dagger$ according to

$$\hat{a}_i^\dagger \rightarrow \sum_{i,j} \Lambda_{i,j} \hat{a}_j^\dagger . \tag{B.2}$$

The mode transformation matrix, Λ, is $M \times M$ and can be found efficiently for a given physical configuration of the boson sampler [132]. The full action of the sampler on all modes can be described by a unitary applied to the input state, $U\,|\Psi_{in}\rangle = |\Psi_{out}\rangle$. The output state is finally measured in each mode's number basis, giving some sorting of N photons into M modes with probabilities depending on the sampler settings. Each $|\Psi_{out}\rangle$ is thus associated with a probability distribution $\widetilde{\mathcal{D}}$ over the $\binom{N+M-1}{N}$-dimensional space of photon sortings. The probabilities in $\widetilde{\mathcal{D}}$ are in turn proportional to permanents of submatrices of Λ; calculating these permanents is in the complexity class **#P-Complete**, which is strongly believed to not be efficiently solvable by classical devices. Even sampling from

such a probability distribution is thought to be classically difficult, so measuring outputs from an ideal boson sampler would demonstrate an exponential quantum speedup over any classical algorithm [125].

A realistic boson sampler will likewise generate N-photon sortings according to some $\mathcal{D}$, but any imperfections will cause the probabilities in $\mathcal{D}$ to vary from their ideal values. If these imperfections are large enough, $\mathcal{D}$ can become classically easy to sample from, and the boson sampler will no longer demonstrate an exponential speedup. For example, if a boson sampler's input photons are completely distinguishable from one another, their output statistics can be efficiently simulated by treating them as independent, classical particles. Our goal is to determine under what conditions sampling from a realistic $\mathcal{D}$ remains hard, and whether these conditions interfere with the boson sampler's scalability.

Since any boson sampler is built up from a few, basic components — single photon generators, phase shifters, beam splitters, and detectors — it is natural to consider errors in "per-component" terms. That is, each component may have imperfections that cause it to behave differently from its ideal counterpart, but errors in any two components are considered independent from one another. We model each realistic phase shifter and beam splitter as applying a unital map, i.e. a probabilistic sum of unitary operators, so that the k^{th} such component modifies the system's density matrix according to

$$\rho_k = \int d\alpha P(\alpha) U_k(\alpha) \rho_{k-1} U_k(\alpha)^\dagger, \tag{B.3}$$

where $P(\alpha)$ is some probability distribution over the classical random variable α. This map is in contrast to the single unitary operator, $\widetilde{U}_k$, that the k^{th} component would apply in an ideal sampler. Photon generators can be modeled similarly by treating errors as maps that act immediately following ideal single-photon generation; in this case, $\widetilde{U}_k$ is simply the identity. For instance, if our first realistic component is a photon generator that produces

a photon with a random time delay, this effect transforms the ideal state according to

$$\begin{aligned}\rho_0 &= |\Psi_{in}\rangle \langle\Psi_{in}|, \\ \rho_1 &= \int d\alpha P(\alpha) e^{-i\omega\alpha} \rho_0 e^{i\omega\alpha},\end{aligned} \tag{B.4}$$

where ω is the frequency of the first photon and $|\Psi_{in}\rangle$ is the ideal input state from Eq. (B.1). Likewise, realistic detectors can be modeled as imperfect maps acting immediately before ideal detection.

The full, realistic process is thus described by a number-basis measurement of the output state,

$$\rho_{out} = \int d\alpha P(\alpha) \left(\prod_{k=1}^{K} U_k(\alpha) \right) |\Psi_{in}\rangle \langle\Psi_{in}| \left(\prod_{k=1}^{K} U_k(\alpha)^\dagger \right), \tag{B.5}$$

where K is the total number of components. The probability to find a given output state, $|\psi\rangle$, is then

$$\langle\psi| \rho_{out} |\psi\rangle = \int d\alpha P(\alpha) \left| \langle\psi| \prod_{k=1}^{K} U_k(\alpha) |\Psi_{in}\rangle \right|^2. \tag{B.6}$$

In an ideal sampler, the probability to find $|\psi\rangle$ is given by the simpler expression,

$$\langle\psi| \widetilde{\rho}_{out} |\psi\rangle = \left| \langle\psi| \prod_{k=1}^{K} \widetilde{U}_k |\Psi_{in}\rangle \right|^2. \tag{B.7}$$

The realistic and ideal equations give two probability distributions over all $|\psi\rangle$, which we denote $\mathcal{D}$ and $\widetilde{\mathcal{D}}$, respectively; a good boson sampler will sample from a $\mathcal{D}$ that is close enough to $\widetilde{\mathcal{D}}$ to retain the computational hardness of the ideal case.

Since the difference between realistic and ideal boson samplers is captured by the imperfect unitary operators U_k, we would like to find restrictions on U_k to insure that the output distribution is still difficult to sample from. Finding necessary conditions for sampling difficulty is a complex problem, and beyond the scope of this dissertation. However, one *sufficient* condition for difficulty is to demand output states that stay close to the ideal

case for all N; that is, $||\mathcal{D} - \widetilde{\mathcal{D}}|| \in O(1)$ in the number of photons N. In order to relate this global requirement to the error tolerances on individual components, we make use of the following theorem. It is due to Bernstein and Vazirani[133] but has been modified to suit the present context.

Theorem 3 (Unitary Errors Add)**.** *Let $U_1(\alpha), \ldots, U_N(\alpha)$ be distributions over α of unitary operators. Suppose an ideal sequence of operators would transform an initial state $|\widetilde{\psi}_0\rangle$ according to $\widetilde{U}_k |\widetilde{\psi}_{k-1}\rangle = |\widetilde{\psi}_k\rangle$, but the actual operators are incorrect such that*

$$\begin{aligned} &U_k(\alpha)\,|\widetilde{\psi}_{k-1}\rangle = |\psi_k(\alpha)\rangle\,, \text{ where} \\ &\int d\alpha P(\alpha) || \,|\widetilde{\psi}_k\rangle - |\psi_k(\alpha)\rangle\,|| = \varepsilon_k. \end{aligned} \tag{B.8}$$

Then $||\widetilde{\mathcal{D}} - \mathcal{D}|| \leq \sum_{k=1}^{K} \varepsilon_k = K\bar{\varepsilon}$, where $\bar{\varepsilon}$ is the average error per unitary.

Proof. Let $|\Upsilon_k(\alpha)\rangle = |\widetilde{\psi}_k\rangle - |\psi_k(\alpha)\rangle$, the orthogonal (non-normalized) "error" component of $|\psi_k(\alpha)\rangle$. Then

$$|\widetilde{\psi}_K\rangle = |\psi_K(\alpha)\rangle + |\Upsilon_K(\alpha)\rangle \text{ by definition} \tag{B.9}$$

$$= U_K(\alpha)\,|\widetilde{\psi}_{K-1}\rangle + |\Upsilon_K(\alpha)\rangle \text{ by hypothesis} \tag{B.10}$$

$$= U_K(\alpha)\cdots U_1(\alpha)\,|\widetilde{\psi}_0\rangle + U_K(\alpha)\cdots U_2(\alpha)\,|\Upsilon_1(\alpha)\rangle + \ldots + |\Upsilon_K(\alpha)\rangle\,. \tag{B.11}$$

Subtracting the first term on the right and applying the triangle inequality we have

$$||\,|\widetilde{\psi}_K\rangle - U_K(\alpha)\cdots U_1(\alpha)\,|\widetilde{\psi}_0\rangle\,|| \leq ||\,|\Upsilon_1(\alpha)\rangle\,|| + \ldots + ||\,|\Upsilon_K(\alpha)\rangle\,||, \tag{B.12}$$

where we have made use of the fact that unitaries do not affect the norms of any $|\Upsilon_k\rangle$. Finally, following [127] we show that the 2-norm distance between two states $|\psi\rangle$ and $|\widetilde{\psi}\rangle$ is an upper bound on the trace norm of the same quantity.

$$\begin{aligned} ||\,|\psi\rangle - |\widetilde{\psi}\rangle\,||_{\text{tr}} &= \sqrt{1 - \left|\,\langle\psi|\widetilde{\psi}\rangle\,\right|^2} \\ &\leq \sqrt{1 - \left(\text{Re}\,\langle\psi|\widetilde{\psi}\rangle\,\right)^2} \\ &= \sqrt{1 - \left(1 - \frac{1}{2}\left\||\psi\rangle - |\widetilde{\psi}\rangle\right\|\right)^2} \\ &\leq \left\||\psi\rangle - |\widetilde{\psi}\rangle\right\|. \end{aligned} \tag{B.13}$$

As noted in [127], the trace norm distance between two states upper bounds the variation distance between their respective output distributions, so

$$||\mathcal{D} - \widetilde{\mathcal{D}}|| \leq \int d\alpha P(\alpha) \sum_{k=1}^{K} || \, |\Upsilon_k(\alpha)\rangle \, || = \sum_{k=1}^{K} \varepsilon_k. \tag{B.14}$$

This theorem implies that errors in a boson sampler — as quantified in Eq. (B.8) — are at worst additive over components. Therefore, if the average error per component decreases as $\bar{\varepsilon} \propto 1/K$ or faster with increasing K, then a boson sampler remains classically hard to simulate as its size increases. The additivity of errors further allows us to divide the components into subgroups and consider error bounds on each subgroup independently. In particular, an N-photon boson sampler needs only N single photon generators, so photon generator error can scale as $1/N$ without interfering with the classical difficulty of the sampling problem. Error in other groups of components will generally need to scale inversely with higher-order polynomials of N, but insofar as the total number of components is polynomial in N, difficult boson sampling can be achieved with polynomially small error in all components.

B.3 Bounds on the Form of $P(\alpha)$

The above discussion quantifies errors via the average trace-norm distance between unitary outputs, $\bar{\varepsilon}$, but error magnitude could be measured in other ways. One physically motivated option would be to look at bounds on $P(\alpha)$, the distribution of classical random variables that change the system's behavior from shot to shot. For instance, returning to the example of time delayed input photons, bounds on $P(\alpha)$ would translate to requirements on how narrow the distribution of firing times must be. Here, we show that the means and widths of any $P(\alpha)$ need only scale polynomally in $\frac{1}{N}$ to achieve the desired bounds on $\bar{\varepsilon}$.

B.3.1 Integral of $P(\alpha)$

We begin by expanding out the definition of ε from Eq. (B.8),

$$\varepsilon_k = \int_{-\infty}^{\infty} d\alpha P(\alpha) D(\alpha), \tag{B.15}$$

$$D(\alpha) \equiv 1 - \left| \langle \Psi_k(\alpha) | \widetilde{\Psi}_k \rangle \right|^2, \tag{B.16}$$

such that $\langle \Psi_k(\alpha) | \widetilde{\Psi}_k \rangle$ is a continuous function of α. Without loss of generality, we assume $\alpha = 0$ corresponds to the ideal case, so $\langle \Psi_k(0) | \widetilde{\Psi}_k \rangle = 1$. Note that $D(\alpha)$ depends only on the overlap between the actual and ideal outputs of a single component, and so is independent of N. On the other hand, we expect that the tolerable noise will shrink as N increases, meaning that $P(\alpha)$ will get narrower. In the large-N limit, $P(\alpha)$ will be very narrow compared to $D(\alpha)$, and we can Taylor expand $D(\alpha)$ to lowest nonvanishing order. (More formally, if $1 - A\alpha^\ell$ is the lowest nonvanishing order expansion of D, we can always choose some $B > A$ such that $\forall \alpha \; 1 - B\alpha^\ell \leq D(\alpha)$ and use this lower bound for all subsequent steps.) Since $\alpha = 0$ gives maximum overlap by definition, $D(0) = D'(0) = 0$, meaning $D(\alpha) \in O(\alpha^2)$ for small α.

To simplify analysis, we define a radius $R(N)$ such that

$$D(R(N)) \in O\left(\frac{1}{N}\right) \; \forall x \in [-R(N), R(N)]. \tag{B.17}$$

In words, $R(N)$ is the radius within which the photons are "close enough" to their ideal states for our purposes. From the scaling argument above, we know that $D(R(N)) \in O(R(N)^2)$, which implies

$$R(N) \in O\left(\frac{1}{N^{1/2}}\right). \tag{B.18}$$

Applying this bound to Eq. (B.15) gives

$$\begin{aligned} \varepsilon_k &\leq \left(1 - \int_{-R(N)}^{R(N)} d\alpha P(\alpha)\right) + \max_{\alpha \in [-R(N), R(N)]} D(\alpha) \\ &\leq \left(1 - \int_{-R(N)}^{R(N)} d\alpha P(\alpha)\right) + O\left(\frac{1}{N}\right) \end{aligned} \tag{B.19}$$

or, for ε_k as a whole to scale as $\frac{1}{N}$,

$$1 - \int_{-R(N)}^{R(N)} d\alpha P(\alpha) \in O\left(\frac{1}{N}\right). \tag{B.20}$$

B.3.2 Mean and Width of $P(\alpha)$

There are a number of ways in which one could quantify the precision of a distribution $P(\alpha)$, and each could be given bounds using Eq. (B.20). One intuitive way is to fix the functional form of $P(\alpha)$ while allowing its mean and width to vary with N:

$$P(\alpha) = \frac{1}{\Delta(N)} \mathbf{P}_k \left(\frac{\alpha - \bar{\alpha}(N)}{\Delta(N)}\right) \tag{B.21}$$

where $\mathbf{P}_k$ is an N-independent probability distribution, $\bar{\alpha}(N)$ and $\Delta(N)$ are the N-dependent mean and characteristic width of the original $P(\alpha)$, respectively, and the overall factor of $\frac{1}{\Delta(N)}$ allows both distributions to be normalized. Plugging this form into Eq. (B.20) and performing a change of variables, we get

$$1 - \frac{1}{\Delta(N)} \int_{-R(N)}^{R(N)} d\alpha \mathbf{P}_k \left(\frac{\alpha - \bar{\alpha}(N)}{\Delta(N)}\right) \in O\left(\frac{1}{N}\right) \tag{B.22}$$

$$u \equiv \frac{\alpha - \bar{\alpha}(N)}{\Delta(N)} \tag{B.23}$$

$$1 - \int_{(-R(N)-\bar{\alpha}(N))/\Delta(N)}^{(R(N)-\bar{\alpha}(N))/\Delta(N)} du \mathbf{P}_k(u) \in O\left(\frac{1}{N}\right). \tag{B.24}$$

Because our goal is to find each photon somewhere in $\alpha \in [-R(N), R(N)]$ with high probability, we can assume that $\bar{\alpha}(N)$ must stay well within that interval for all N. Formally, we require that $\lim_{N\to\infty} R(N)/|\bar{\alpha}(N)| > 1$, which can only hold true if

$$\bar{\alpha}(N) \in O\left(\frac{1}{\sqrt{N}}\right). \tag{B.25}$$

Assuming this condition is met, we can define

$$R'(N) \equiv R(N) - |\bar{\alpha}(N)| \tag{B.26}$$

as the radius such that if α is within $R'(N)$ of its mean, it is within $R(N)$ of zero. For any $\bar{\alpha}(N)$ that meets our requirements, $R'(N) \leq R(N)$ and $O(R'(N)) \in O(R(N))$, so we can use R' to simplify Eq. (B.24) without changing any of its scaling properties:

$$1 - \int_{(-R(N)-\bar{\alpha}(N))/\Delta(N)}^{(R(N)-\bar{\alpha}(N))/\Delta(N)} du \mathbf{P}_k(u) \leq 1 - \int_{-R'(N)/\Delta(N)}^{R'(N)/\Delta(N)} du \mathbf{P}_k(u) \tag{B.27}$$

$$= \int_{-\infty}^{-R'(N)/\Delta(N)} du \mathbf{P}_k(u) + \int_{R'(N)/\Delta(N)}^{\infty} du \mathbf{P}_k(u) \in O\left(\frac{1}{N}\right). \tag{B.28}$$

Qualitatively, this expression tells us that the total probability in the "tails" of $\mathbf{P}_k$, outside the growing interval $[\frac{-R'(N)}{\Delta(N)}, \frac{R'(N)}{\Delta(N)}]$, must drop off as $\frac{1}{N}$ or faster. We can describe the behavior of $\mathbf{P}_k$ in these tails by its asymptotic polynomial order m, defined by

$$\lim_{u \to \infty} \mathbf{P}_k(u) \propto u^{-m}. \tag{B.29}$$

(We have assumed, without loss of generality, that the order of $\mathbf{P}_k$ as $u \to \infty$ is $\leq$ its order as $u \to -\infty$.) Because $\mathbf{P}_k$ is a bounded function, $m > 1$, but there are no other restrictions on its value; m need not be an integer, and can be infinite if $\mathbf{P}_k$ is asymptotically sub-polynomial. This asymptotic behavior determines the large-N scaling of Eq. (B.28), so we can plug it in to make the equation integrable:

$$O\left(\int_{\pm R'(N)/\Delta(N)}^{\pm\infty} du \mathbf{P}_k\right) = O\left(\int_{\pm R'(N)/\Delta(N)}^{\pm\infty} du\, u^{-m}\right) \tag{B.30}$$

$$= O\left(\left(\sqrt{N}\Delta(N)\right)^{m-1}\right) \in O\left(\frac{1}{N}\right) \tag{B.31}$$

$$\Delta(N) \in O\left(n^{-\frac{m+1}{2(m-1)}}\right). \tag{B.32}$$

This expression gives bounds on the width of our probability distribution for any asymptotic behavior of $\mathbf{P}_k$. A few values of m offer especial insight:

- If $\mathbf{P}_k$ drops off exponentially (m is infinite), $\Delta(N)$ need only scale as $\frac{1}{\sqrt{N}}$.
- If we want $\Delta(N)$ to scale linearly in $\frac{1}{N}$, $\mathbf{P}_k$ must drop off cubically or faster ($m \geq 3$).

- For any bounded $\mathbf{P}_k$, it is sufficient for $\Delta(N)$ to scale polynomially in $\frac{1}{N}$, although the necessary polynomial may be very high-order if m is close to 1.

Combining this with Eq. (B.25), we can say that the mean and width of our probability distributions $P(\alpha)$ can shrink polynomially to ensure classically difficult sampling, similar to $\bar{\varepsilon}$.

B.4 Analysis

Both results above were framed in terms of boson samplers, but they apply equally well to any quantum information process that can be described as a sequence of ideally-unitary components followed by measurement. Such processes form a broad category that includes universal, circuit model quantum computation. For any of these processes, we have shown that realistic output statistics can be kept close to the ideal case if the unital error per component shrinks as one over the total number of components. How this should be interpreted is up for debate. If one is willing to treat experimental imperfections as a resource, like memory or run time, which must be steadily improved to accommodate larger problems, then this result is good news; it implies that error considerations will never place exponentially stringent demands on an otherwise scalable problem. On the other hand, it is widely believed that quantum error correction will be necessary for scalable, universal quantum computation [134], a belief which is incompatible with the "precision as resource" model. Quantum error correction is only a necessity if we require devices to work scalably with sub-polynomial error reduction, and it is unlikely that boson samplers meet this stricter condition. In particular, if neither total photon loss nor dark counts can be constrained with increasing system size, the two combined can cause serious problems for classical simulation difficulty [135]. Because of this, care must be taken when comparing the power of a boson sampler to that of a universal quantum computer, and more generally when considering boson sampling as a demonstration of scalable quantum supremacy.

References

[1] T. Keating *et al.*, Phys. Rev. A **87**, 052314 (2013).

[2] S. T. Merkel, P. S. Jessen, and I. H. Deutsch, Phys. Rev. A **78**, 023404 (2008).

[3] C. E. Burkhardt and J. J. Leventhal, The quantum defect, in *Topics in Atomic Physics*, pp. 214–229, Springer New York, 2006.

[4] A. Steane, Reports on Progress in Physics **61**, 117 (1998).

[5] C. Monroe, D. M. Meekhof, B. E. King, W. M. Itano, and D. J. Wineland, Phys. Rev. Lett. **75**, 4714 (1995).

[6] C. A. Sackett *et al.*, Nature **404**, 256 (2000).

[7] H. Häffner *et al.*, Nature **438**, 643 (2005).

[8] D. L. Moehring *et al.*, Nature **449**, 68 (2007).

[9] L. DiCarlo *et al.*, Nature **467**, 574 (2010).

[10] M. Bayer *et al.*, Science **291**, 451 (2001).

[11] C. Barthel, D. J. Reilly, C. M. Marcus, M. P. Hanson, and A. C. Gossard, Phys. Rev. Lett. **103**, 160503 (2009).

[12] P. Kok *et al.*, Rev. Mod. Phys. **79**, 135 (2007).

[13] D. Schrader *et al.*, Phys. Rev. Lett. **93**, 150501 (2004).

[14] B. E. Anderson, H. Soza-Martinez, C. A. Riofrío, I. H. Deutsch, and P. S. Jessen, Phys. Rev. Lett. **114**, 240401 (2015).

[15] M. Anderlini *et al.*, Nature **448**, 452 (2007).

[16] T. Pellizzari, S. A. Gardiner, J. I. Cirac, and P. Zoller, Phys. Rev. Lett. **75**, 3788 (1995).

[17] G. K. Brennen, C. M. Caves, P. S. Jessen, and I. H. Deutsch, Phys. Rev. Lett. **82**, 1060 (1999).

[18] T. F. Gallagher, *Rydberg Atoms* (Cambridge University Press, 2005).

[19] S. D. Hogan and F. Merkt, Phys. Rev. Lett. **100**, 043001 (2008).

[20] M. Brune, S. Haroche, V. Lefevre, J. M. Raimond, and N. Zagury, Phys. Rev. Lett. **65**, 976 (1990).

[21] M. Brune *et al.*, Phys. Rev. Lett. **76**, 1800 (1996).

[22] C. Boisseau, I. Simbotin, and R. Côté, Phys. Rev. Lett. **88**, 133004 (2002).

[23] D. Booth, S. T. Rittenhouse, J. Yang, H. R. Sadeghpour, and J. P. Shaffer, Science **348**, 99 (2015).

[24] D. Jaksch *et al.*, Phys. Rev. Lett. **85**, 2208 (2000).

[25] M. D. Lukin *et al.*, Phys. Rev. Lett. **87**, 037901 (2001).

[26] M. H. Devoret, D. Esteve, and C. Urbina, Nature **360**, 547 (1992).

[27] N. Schlosser, G. Reymond, I. Protsenko, and P. Grangier, Nature **411**, 1024 (2001).

[28] L. Isenhower *et al.*, Phys. Rev. Lett. **104**, 010503 (2010).

[29] M. D. Lukin, M. Fleischhauer, and R. Cote, Phys. Rev. Lett. **87**, 037901 (2001).

[30] T. Amthor, C. Giese, C. S. Hofmann, and M. Weidemüller, Phys. Rev. Lett. **104**, 013001 (2010).

[31] I. I. Beterov *et al.*, Phys. Rev. A **88**, 010303 (2013).

[32] S. Sevinçli and T. Pohl, New Journal of Physics **16**, 123036 (2014).

[33] D. Petrosyan, M. Höning, and M. Fleischhauer, Phys. Rev. A **87**, 053414 (2013).

[34] J.-F. Huang, J.-Q. Liao, and C. P. Sun, Phys. Rev. A **87**, 023822 (2013).

[35] T. Peyronel *et al.*, Nature **488**, 57 (2012).

[36] R. Boddeda *et al.*, Rydberg-induced optical nonlinearities from a cold atomic ensemble trapped inside a cavity, arXiv:1512.08480v1, 2015.

[37] T. Wilk *et al.*, Phys. Rev. Lett. **104**, 010502 (2010).

[38] K. M. Maller *et al.*, Phys. Rev. A **92**, 022336 (2015).

[39] Y.-Y. Jau, A. M. Hankin, T. Keating, I. H. Deutsch, and G. W. Biedermann, Nature Physics **12**, 71 (2016).

[40] A. M. Steane, Phys. Rev. A **68**, 042322 (2003).

[41] T. Opatrný and K. Mølmer, Phys. Rev. A **86**, 023845 (2012).

[42] M. Ebert, M. Kwon, T. G. Walker, and M. Saffman, Phys. Rev. Lett. **115**, 093601 (2015).

[43] M. M. Müller *et al.*, Phys. Rev. A **89**, 032334 (2014).

[44] D. Barredo *et al.*, Phys. Rev. Lett. **114**, 113002 (2015).

[45] K. Bergmann, H. Theuer, and B. W. Shor, Rev. Mod. Phys. **70**, 1003 (1998).

[46] J. E. Johnson and S. L. Rolston, Phys. Rev. A **82**, 033412 (2010).

[47] R. F. Stebbings and F. B. Dunning, *Rydberg States of Atoms and Molecules* (Cambridge University Press, 2011).

[48] W. Happer, Y.-Y. Jau, and T. G. Walker, *Optically Pumped Atoms* (Wiley-VCH, 2010).

[49] L. Béguin, A. Vernier, R. Chicireanu, T. Lahaye, and A. Browaeys, Phys. Rev. Lett. **110**, 263201 (2013).

[50] A. Schwettmann, J. Crawford, K. R. Overstreet, and J. P. Shaffer, Phys. Rev. A **74**, 020701 (2006).

[51] L. Santos, G. V. Shlyapnikov, P. Zoller, and M. Lewenstein, Phys. Rev. Lett. **85**, 1791 (2000).

[52] T. G. Walker and M. Saffman, Phys. Rev. A **77**, 032723 (2008).

[53] T. Amthor, C. Giese, C. S. Hoffmann, and M. Weidemüller, Phys. Rev. Lett. **104**, 013001 (2010).

[54] M. Saffman, T. G. Walker, and K. Mølmer, Rev. Mod. Phys. **82**, 2313 (2010).

[55] A. Derevianko, P. Kómár, T. Topcu, R. M. Kroeze, and M. D. Lukin, Effects of molecular resonances on rydberg blockade, arXiv:1508.02480v1, 2015.

[56] G. E. Santoro and E. Tosatti, J. Phys. A: Math. Gen. **39**, R393 (2006).

[57] A. B. Finnila, M. A. Gomez, C. Sebenik, C. Stenson, and J. D. Doll, Chem. Phys. Lett. **219**, 343 (1994).

[58] T. Kadowaki and H. Nishimori, Phys. Rev. E **58**, 5355 (1998).

[59] A. Das and B. K. Chakrabarti, Rev. Mod. Phys. **80**, 1061 (2008).

[60] A. A. Houck, H. E. Türeci, and J. Koch, Nat. Phys. **8**, 292 (2012).

[61] M. W. Johnson *et al.*, Nature **473**, 194 (2011).

[62] S. Boixo *et al.*, Nat. Phys. **10**, 218 (2014).

[63] E. Farhi *et al.*, Science **292**, 472 (2000).

[64] A. M. Childs, E. Farhi, and J. Preskill, Phys. Rev. A **65**, 012322 (2002).

[65] E. Urban *et al.*, Nat. Phys. **5**, 110 (2009).

[66] A. Gaëtan *et al.*, New Journal of Physics **12**, 065040 (2010).

[67] T. Pohl, E. Demler, and M. D. Lukin, Phys. Rev. Lett. **104**, 043002 (2010).

[68] K. Kim *et al.*, Nature **465**, 590 (2010).

[69] J. Simon *et al.*, Nature **472**, 307 (2011).

[70] T. Kadowaki and H. Nishimori, Phys. Rev. E **58**, 5355 (1998).

[71] F. Barahona, J. Phys. A: Math. Gen. **15**, 3241 (1982).

[72] K. Karimi *et al.*, Quant. Inf. Proc. **11**, 77 (2012).

[73] D. Leibfried, Nature **463**, 608 (2010).

[74] S. A. Kemme *et al.*, Proc. SPIE **8249**, 82490E (2012).

[75] C. Knoernschild *et al.*, Appl. Phys. Lett. **97**, 134101 (2010).

[76] L. Isenhower, W. Williams, A. Dally, and M. Saffman, Optics Letters **34**, 1159 (2009).

[77] T. Pohl and P. R. Berman, Phys. Rev. Lett. **102**, 013004 (2009).

[78] M. Müller, L. Liang, I. Lesanovsky, and P. Zoller, New J. Phys. **10**, 093009 (2008).

[79] X. L. Zhang, L. Isenhower, A. T. Gill, T. G. Walker, and M. Saffman, Phys. Rev. A **82**, 030306 (2010).

[80] A. M. Hankin *et al.*, Phys. Rev. A **89**, 033416 (2014).

[81] M. Saffman, X. L. Zhang, A. T. Gill, L. Isenhower, and T. G. Walker, J. Phys.: Conf. Ser. **264**, 012023 (2011).

[82] D. Møller, L. B. Madsen, and K. Mølmer, Phys. Rev. Lett. **100**, 170504 (2008).

[83] E. Brion, L. H. Pedersen, K. Mølmer, S. Chutia, and M. Saffman, Phys. Rev. A **75**, 032328 (2007).

[84] E. Brion, L. H. Pedersen, and K. Mølmer, Journal of Physics B: Atomic, Molecular and Optical Physics **40**, S159 (2007).

[85] D. D. B. Rao and K. Mølmer, Phys. Rev. A **89**, 030301 (2014).

[86] A. Aspect, E. Arimondo, R. Kaiser, N. Vansteenkiste, and C. Cohen-Tannoudji, Phys. Rev. Lett. **61**, 826 (1988).

[87] J. M. Martinis and M. R. Geller, Phys. Rev. A **90**, 022307 (2014).

[88] J. Migdalek and Y.-K. Kim, J. Phys. B: At. Mol. Opt. Phys. **31**, 1947 (1998).

[89] W. Li, C. Ates, and I. Lesanovsky, Phys. Rev. Lett. **110**, 213005 (2013).

[90] R. Heidemann *et al.*, Phys. Rev. Lett. **99**, 163601 (2007).

[91] T. Topcu and A. Derevianko, Phys. Rev. A **88**, 043407 (2013).

[92] R. Raussendorf, D. E. Browne, and H. J. Briegel, Phys. Rev. A **68**, 022312 (2003).

[93] S. Bravyi and A. Kitaev, Phys. Rev. A **71**, 022316 (2005).

[94] J. Appel *et al.*, Proc. Natl. Acad. Sci. USA **106**, 10960 (2009).

[95] A. Steane, Proc. Roy. Soc. Lond. A **452**, 2551 (1954).

[96] S. Chaudhury *et al.*, Phys. Rev. Lett. **99**, 163002 (2007).

[97] I. H. Deutsch and P. S. Jessen, Optics Communications **283**, 681 (2010).

[98] A. Smith *et al.*, Phys. Rev. Lett. **111**, 170502 (2013).

[99] N. Kiesel, C. Schmid, G. Tóth, E. Solano, and H. Weinfurter, Phys. Rev. Lett. **98**, 063604 (2007).

[100] S. Raghavan, H. Pu, P. Meystre, and N. P. Bigelow, Optics Communications **188**, 149 (2001).

[101] R. H. Dicke, Phys. Rev. **93**, 99 (1954).

[102] F. W. Cummings, Phys. Rev. **140**, A1051 (1965).

[103] D. Møller, L. B. Madsen, and K. Mølmer, Phys. Rev. Lett. **100**, 170504 (2008).

[104] S. Sachdev, *Quantum Phase Transitions* (Cambridge University Press, 2011).

[105] J. H. Eberly, N. B. Narozhny, and J. J. S. Mondragon, Phys. Rev. Lett. **44**, 1323 (1980).

[106] J. Gea-Banacloche, Phys. Rev. A **44**, 5913 (1991).

[107] I. I. Beterov *et al.*, Phys. Rev. A **90**, 043413 (2014).

[108] V. Jurdjevic and H. J. Sussmann, J. Differ. Equations **12**, 313 (1972).

[109] S. G. Schirmer, J. V. Leahy, and A. I. Solomon, J. Phys. A **35**, 4125 (2002).

[110] S. Haroche and J.-M. Raimond, J. Phys. B: At. Mol. Opt. Phys. **38**, 551 (2005).

[111] D. Leibfried, R. Blatt, C. Monroe, and D. Wineland, Rev. Mod. Phys. **75**, 281 (2003).

[112] J. M. Fink *et al.*, Nature **454**, 315 (2008).

[113] C. K. Law and J. H. Eberly, Phys. Rev. Lett. **76**, 1055 (1996).

[114] A. Ben-Kish *et al.*, Phys. Rev. Lett. **90**, 037902 (2003).

[115] M. Hofheins *et al.*, Nature **459**, 546 (2009).

[116] M. Kitegawa and M. Ueda, Phys. Rev. A **47**, 5138 (1993).

[117] P. Giorda, P. Zanardi, and S. Lloyd, Phys. Rev. A **68**, 062320 (2003).

[118] V. Jurdjevic and H. J. Sussmann, J. Differ. Equations **12**, 313 (1972).

[119] S. Merkel, *Quantum control of d-dimensional quantum systems with application to alkali atomic spins*, PhD thesis, University of New Mexico, 2003.

[120] N. Khaneja, T. Reiss, C. Kehlet, T. Schulte-Herbrüggen, and S. J. Glaser, J. Mag. Res. **172**, 296 (2005).

[121] H. Rabitz, M. Hsieh, and C. Rosenthal, Phys. Rev. A **72**, 052337 (2005).

[122] V. Bužek, H. Moya-Cessa, P. L. Knight, and S. J. D. Phoenix, Phys. Rev. A **45**, 8190 (1992).

[123] V. Borish, O. Markovic, and M. Schleier-Smith, Towards quantum simulations of frustrated spin models with rydberg-dressed atoms, 2016, Poster presented at Southwest Quantum Information and Technology (SQuInT), Feb 18, Albuquerque, NM.

[124] J. Roland and N. J. Cerf, Phys. Rev. A **65**, 042308 (2002).

[125] S. Aaronson and A. Arkhipov, The computational complexity of linear optics, in *Proceedings of the Forty-third Annual ACM Symposium on Theory of Computing*, STOC '11, pp. 333–342, New York, NY, USA, 2011, ACM.

[126] J. Huh, G. G. Guerreschi, B. Peropadre, J. R. McClean, and A. Aspuru-Guzik, Boson sampling for molecular vibronic spectra, arXiv:1412.8427v1, 2014.

[127] A. Arkhipov, Boson sampling is robust to small errors in the network matrix, arXiv:1412.2516v1, 2014.

[128] P. P. Rohde and T. C. Ralph, Phys. Rev. A **85**, 022332 (2012).

[129] K. P. Seshadreesan, J. P. Olson, K. R. Motes, P. P. Rohde, and J. P. Dowling, Phys. Rev. A **91**, 022334 (2015).

[130] V. S. Shchesnovich, Phys. Rev. A **91**, 063842 (2015).

[131] P. P. Rhode, Phys. Rev. A **86**, 052321 (2012).

[132] M. Reck, A. Zeilinger, H. J. Bernstein, and P. Bertani, Phys. Rev. Lett. **73**, 58 (1994).

[133] E. Bernstein and U. Vazirani, Siam J. Comput. **26**, 1411 (1997).

[134] D. Gottesman, An introduction to quantum error correction and fault-tolerant quantum computation, in *Quantum Information Science and Its Contributions to Mathematics, Proceedings of Symposia in Applied Mathematics*, pp. 15–58, Amer. Math. Soc., 2010.

[135] S. Rahimi-Keshari, T. C. Ralph, and C. M. Caves, Efficient classical simulation of quantum optics, arXiv:1511.06526v1, 2015.